2016-12

Closed-loop optimal control implementations for space applications

Monk, Colin S.

Monterey, California: Naval Postgraduate School

NAVAL POSTGRADUATE SCHOOL

MONTEREY, CALIFORNIA

THESIS

CLOSED-LOOP OPTIMAL CONTROL IMPLEMENTATIONS FOR SPACE APPLICATIONS

by

Colin S. Monk

December 2016

Thesis Advisor: Mark Karpenko
Second Reader: I. M. Ross

THIS PAGE INTENTIONALLY LEFT BLANK

REPORT DOCUMENTATION PAGE			Form Approved OMB No. 0704-0188

1. AGENCY USE ONLY *(Leave blank)*	2. REPORT DATE	3. REPORT TYPE AND DATES COVERED
	December 2016	Master's thesis, Jan-Dec 2016

4. TITLE AND SUBTITLE

CLOSED-LOOP OPTIMAL CONTROL IMPLEMENTATIONS FOR SPACE APPLICATIONS

5. FUNDING NUMBERS

6. AUTHOR(S) Colin S. Monk

7. PERFORMING ORGANIZATION NAME(S) AND ADDRESS(ES)
Naval Postgraduate School
Monterey, CA 93943-5000

8. PERFORMING ORGANIZATION REPORT NUMBER

9. SPONSORING /MONITORING AGENCY NAME(S) AND ADDRESS(ES)
N/A

10. SPONSORING / MONITORING AGENCY REPORT NUMBER

11. SUPPLEMENTARY NOTES The views expressed in this thesis are those of the author and do not reflect the official policy or position of the Department of Defense or the U.S. Government. IRB number ____N/A____.

12a. DISTRIBUTION / AVAILABILITY STATEMENT
Approved for public release. Distribution is unlimited.

12b. DISTRIBUTION CODE

13. ABSTRACT (maximum 200 words)

This thesis explores concepts for a closed-loop optimal control implementation of minimum-time attitude maneuvers of spacecraft. The most common implementation of optimal control solutions is via open-loop commands. However, ignorance of the true system parameters can undermine the open-loop optimal control solution. While traditional closed-loop control methods can compensate for significant levels of uncertainty, this comes at the cost of optimality.

This work focuses on optimization of eigenaxis maneuvers, but the concepts are not limited to this constraint. The study begins with an examination of candidate control architectures, weighing the advantages of various closed-loop feedback architectures. A control architecture consisting of a traditional proportional-derivative (or quaternion error) feedback loop and a feed-forward control torque signal is deemed to have the best performance and is then selected for further study.

Next, through the analyses of a series of optimal control problems, several real-time optimal control algorithms are developed that continuously adapt to feedback on the system's actual states throughout the maneuver. These algorithms demonstrate significant performance improvements over conventional open-loop implementations, most notably shorter overall maneuver times. The results of this work, therefore, provide an algorithmic enhancement of spacecraft agility.

14. SUBJECT TERMS
optimal control, closed-loop control, real-time optimal control, eigenaxis, state prediction

15. NUMBER OF PAGES
209

16. PRICE CODE

17. SECURITY CLASSIFICATION OF REPORT	18. SECURITY CLASSIFICATION OF THIS PAGE	19. SECURITY CLASSIFICATION OF ABSTRACT	20. LIMITATION OF ABSTRACT
Unclassified	Unclassified	Unclassified	UU

NSN 7540-01-280-5500

Standard Form 298 (Rev. 2-89)
Prescribed by ANSI Std. 239-18

THIS PAGE INTENTIONALLY LEFT BLANK

Approved for public release. Distribution is unlimited.

CLOSED-LOOP OPTIMAL CONTROL IMPLEMENTATIONS FOR SPACE APPLICATIONS

Colin S. Monk
Lieutenant Commander, United States Navy
B.S., Tulane University, 2003

Submitted in partial fulfillment of the
requirements for the degree of

MASTER OF SCIENCE IN ASTRONAUTICAL ENGINEERING

from the

NAVAL POSTGRADUATE SCHOOL
December 2016

Approved by: Mark Karpenko
Thesis Advisor

I. M. Ross
Second Reader

Garth V. Hobson
Chair, Department of Mechanical and Aerospace Engineering

THIS PAGE INTENTIONALLY LEFT BLANK

ABSTRACT

This thesis explores concepts for a closed-loop optimal control implementation of minimum-time attitude maneuvers of spacecraft. The most common implementation of optimal control solutions is via open-loop commands. However, ignorance of the true system parameters can undermine the open-loop optimal control solution. While traditional closed-loop control methods can compensate for significant levels of uncertainty, this comes at the cost of optimality.

This work focuses on optimization of eigenaxis maneuvers, but the concepts are not limited to this constraint. The study begins with an examination of candidate control architectures, weighing the advantages of various closed-loop feedback architectures. A control architecture consisting of a traditional proportional-derivative (or quaternion error) feedback loop and a feed-forward control torque signal is deemed to have the best performance and is then selected for further study.

Next, through the analyses of a series of optimal control problems, several real-time optimal control algorithms are developed that continuously adapt to feedback on the system's actual states throughout the maneuver. These algorithms demonstrate significant performance improvements over conventional open-loop implementations, most notably shorter overall maneuver times. The results of this work, therefore, provide an algorithmic enhancement of spacecraft agility.

THIS PAGE INTENTIONALLY LEFT BLANK

TABLE OF CONTENTS

LIST OF FIGURES

ACKNOWLEDGMENTS

I would like to thank all my professors at the Naval Postgraduate School; you have had endless patience for my endless questions. I would like to especially thank my advisors, Dr. Mark Karpenko and Dr. Mike Ross, who introduced me to the potential for optimization; my perspective on the world will never be the same.

And, most of all, I would like to thank my wife, Jamie, who has given me so much support as I have worked on this thesis.

THIS PAGE INTENTIONALLY LEFT BLANK

I. INTRODUCTION, MOTIVATIONS AND OBJECTIVES

Optimal control solutions are commonly thought of—and therefore implemented—in open-loop. The engineer will develop an optimal trajectory of the control variable (or variables) in a given problem which, when applied to the system or plant whose performance is being optimized, produces the desired results. For example, in a spacecraft attitude maneuver problem, torque could be considered as the control variable; an optimal torque trajectory applied to the spacecraft would produce an optimal reorientation maneuver (i.e., minimum time maneuver or minimum effort, etc.). However, as with many engineering problems, some amount of uncertainty is always present in the definition of the nominal system and its parameters that form the basis of the optimal solution. To continue the example of the spacecraft attitude maneuver, the spacecraft rotational inertia is a fundamental system parameter that influence the nature of the optimal torque trajectory; errors in the inertia estimate will propagate into the solution for the torque trajectory, ultimately resulting in the actual spacecraft not following the expected attitude trajectory. Other sources of uncertainty, such as errors in the actual torque application, external disturbance forces/torques and sensor and processing noise, etc., can also negatively impact the practical implementation of an optimal control solution.

Classical control techniques solve the challenge of uncertainty with feedback. Feedback control loops measure the state of the system, such as attitude or position, and produce a control signal based on those state measurements to drive the system to the desired end-state (i.e., to reduce or eliminate the error). Closed-loop control methods are used in nearly all control systems across all engineering disciplines. Thus, integrating the behavior of existing feedback control loops within an optimal control solution presents an opportunity to improve the practical performance of optimal control solutions in the presence of uncertainty and feedback system dynamics.

Another important motivation in developing optimal control solutions compatible with feedback relates to solution implementation. Optimal control is frequently applied to existing systems, which may not have been designed to accommodate alternative control methods. Existing systems can have a variety of access points and adjustable parameters through which an optimal control solution can potentially be implemented. These access points and parameters will vary from system to system depending on the particular design implementation of the feedback controller and can affect the overall performance of the system. In consideration of this fact, there may be cases in which optimal control solutions must be implemented in the presence of closed feedback loops.

A. GENERAL CONTROL ARCHITECTURES

The fundamental difference between open-loop and closed-loop control is the presence of feedback. In closed-loop control, some aspect of system state is measured and incorporated into the actuating signals. Examples of closed-loop and open-loop systems are presented in Figures 1–3. The assumed system model is based on a double integrator model in which the position trajectory of the system can be calculated by integrating the applied torque trajectory and then integrating the resulting velocity trajectory. This is explained in more detail in equations (1.1), (1.2), and (1.3).

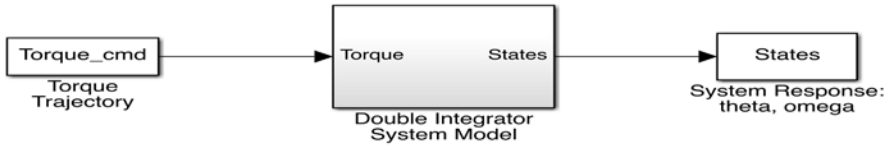

Figure 1. Example of open-loop control

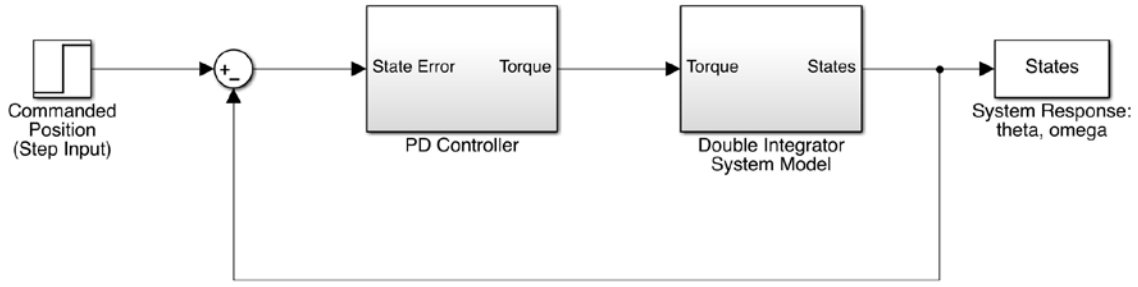

Figure 2. Example of closed-loop control

In the open-loop control system of Figure 1, a time varying torque trajectory is the control variable. This torque profile is applied to the plant, in this case a simple double-integrator model, and the output is a trajectory of system states. The states of interest are usually the position and velocity of the system.

In contrast, the closed-loop system of Figure 2 has a trajectory of commanded states as the input variable(s). The difference between the commanded state and the actual state is determined and used to compute a proportional-derivative (PD) control action. The controller produces a torque signal based on the state error and the gains of the PD controller. The details of how a PD controller works will be discussed further in the following section. Closed-loop control differs from the open-loop implementation in that the feedback of the actual, current state of the system is constantly informing the torque applied to the plant model. This feedback provides some measure of assurance that the system will actually reach the desired end state at some point in time, in spite of either internal uncertainties or external disturbances. The open-loop control, on the other hand, has no means of correction if the system does not reach the desired end state.

Optimal control solutions can be implemented in either open-loop or closed-loop architectures, although they are most commonly implemented in the context of open-loop. In either case, the objective of optimal control is to determine a control trajectory that achieves the desired end state in an optimal

manner. These techniques are commonly used to minimize the maneuver time or the energy expended in the maneuver. The majority of this study will focus on minimum time maneuvers, which are relevant for agile satellite systems.

In both open- and closed-loop control approaches for satellite attitude control, the plant is modeled as a rigid body, and the classical rotational kinematics equations apply. For single degree of freedom systems (and spacecraft under the assumption of an eigenaxis constraint), the basic kinematic equation is:

$$\tau(t) = J \cdot \alpha(t) \tag{1.1}$$

In (1.1), τ is the time varying torque input; J is the rotational inertia of the system; and α is the angular acceleration. The variable α is simply the time derivative of angular velocity, ω; and ω is the time derivative of θ, the angular position, as shown in (1.2).

$$\alpha(t) = \dot{\omega}(t) = \ddot{\theta}(t) \tag{1.2}$$

Given τ and J, or, equivalently, α, the position and velocity trajectory of the system can be determined through simple integration:

$$\begin{aligned} \omega(t) &= \frac{1}{J}\int_0^t \tau(t)dt + \omega_0 \\ \theta(t) &= \int_0^t \omega(t)dt + \theta_0 \end{aligned} \tag{1.3}$$

B. THE BASELINE SYSTEM AND CLASSICAL CONTROLS

The one-dimensional closed-loop control architectures examined in this thesis use a proportional-derivative feedback control law. In a PD controller, the output torque is a function of the state error, the difference between the commanded state(s) and the current, actual state. It is important to note that in

models discussed in this thesis, the component dubbed “PD controller” is a mathematical model of both the control law as well as the actuator and associated components. In real world systems, the control law would exist in a microprocessor, but its output could be a voltage, current or other signal directed to a motor-controller for a torque-producing actuator such as a reaction wheel, CMG, etc. In these simple models, the PD controller encompasses multiple components and makes the simplifying assumption that all such components operate without error and with perfect dynamics.

The PD control law produces torque based on the state error, in accordance with the following equation [1]:

$$\tau_{PD} = k_p\left(\theta_{cmd} - \theta\right) + k_v\left(\omega_{cmd} - \omega\right) \tag{1.4}$$

In (1.4), k_p and k_v are the proportional and derivative gains, respectively; and θ_{cmd} and ω_{cmd} are the commanded state trajectories for both position and velocity, respectively. A common approach in control engineering is to use an input command that follows a step function trajectory. In other words, at the starting time of the maneuver, the commanded position will instantly jump to the final desired position, and the commanded velocity will, thus, remain at zero. In this case, the control law simplifies to the following:

$$\tau = k_p\left(\theta_{cmd} - \theta\right) - k_v\omega \tag{1.5}$$

Analytically determining the output state trajectories of a closed-loop system in the time domain can be cumbersome, but transforming the system equations into the frequency domain, sometimes called the s-domain, using Laplace transforms simplifies the problem [1]. A block diagram of a PD control loop in the s-domain is shown in Figure 3.

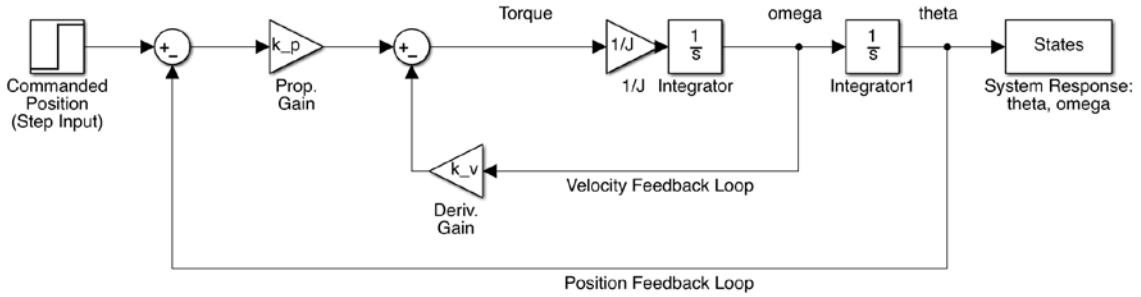

Figure 3. Block diagram of PD controller in the s-domain

An advantage of viewing a system as a block diagram in the s-domain is that it facilitates development of the overall system transfer function. This is because convolution in the time domain becomes multiplication and division in the s-domain. The overall transfer function is an expression that describes the output of the system for any given input in the frequency domain. Having developed the block diagram, the overall transfer function of the PD controller system can be derived using standard block diagram reduction.

$$\frac{\theta(s)}{\theta_{cmd}(s)} = \frac{\frac{k_p}{J}}{s^2 + \left(\frac{k_v}{J}\right)s + \frac{k_p}{J}} \tag{1.6}$$

For convenience, the model considered in this study has a nominal rotational inertia of $J = 1\,N \cdot m^2$. The transfer function of (1.6) is called a quadratic transfer function with a constant numerator, and is typical of a second order system [1]. The canonical quadratic transfer function has the form shown in (1.7).

$$G(s) = \frac{\omega_n^2}{s^2 + 2\zeta\omega_n s + \omega_n^2} \tag{1.7}$$

In (1.7), $\omega_n = \sqrt{k_p / J}$ is the known as the natural frequency and $\zeta = \frac{k_v}{2J\omega_n}$ as the damping ratio. The denominator of a transfer function gives the system's

characteristic equation. The roots of the characteristic equation are called poles; the poles determine the speed and shape of a system's response [1]. Classical control techniques focus on manipulating the transfer function in some fashion to achieve the desired performance. To develop a baseline classical control system, the PD controller's gains are manipulated to achieve the desired natural frequency and damping ratio, which are related to the characteristics of the transient response.

In classical control design, systems are typically built around the response to a unit step input for a second order system. Depending on the natural frequency and damping ratio, the system response may overshoot the commanded position and then oscillate about the final position with exponentially decaying magnitude; this is known as an underdamped response. Alternatively, the system response may approach the final commanded position monotonically; this is known as an overdamped response. A critically damped system will approach the final commanded position as quickly as possible with no oscillations. Each of these response types have advantages and disadvantages. Overdamped systems will take longer to reach the final position, but will do so without overshoot; underdamped systems can reach the final position more quickly, but in some applications, any amount of overshoot is undesirable. Proper controller design, therefore, requires careful system requirements considerations.

The system studied in this work will be designed to have a 5% overshoot and a settling time of 0.9 seconds. The percent overshoot (M_p) and 2% settling time (t_s) are related to the canonical parameters by the following equations:

$$M_p = e^{-\frac{\pi\zeta}{\sqrt{1-\zeta^2}}} \tag{1.8}$$

$$t_s = \frac{4}{\zeta\omega_n} \tag{1.9}$$

Solving (1.8) and (1.9) with for an overshoot of 5% and settling time of 0.9 sec yields a damping coefficient of $\zeta = 0.69$ and natural frequency of $\omega_n = 6.441$. Given these system characteristic values, the relationship between natural frequency, damping ratio and the PD controller transfer function, (1.6) and (1.7), and nominal inertia of $J = 1\,N \cdot m^2$, the PD controller gains can now be determined as $k_v = 8.89$ and $k_p = 41.5$.

A closed-loop system with these PD controller gains will be the baseline system for this study. All optimal control architectures considered herein will be based on manipulations of this system.

Now that the baseline system has been fully defined, the system response to a unit step input can be determined. The model simulation results, presented in Figure 4 and Figure 5, are produced using an ODE45 propagator in MATLAB.

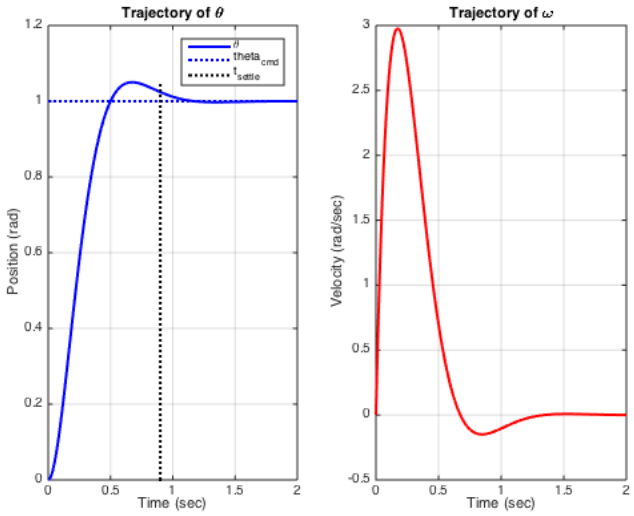

Figure 4. Time response of the baseline PD controller system

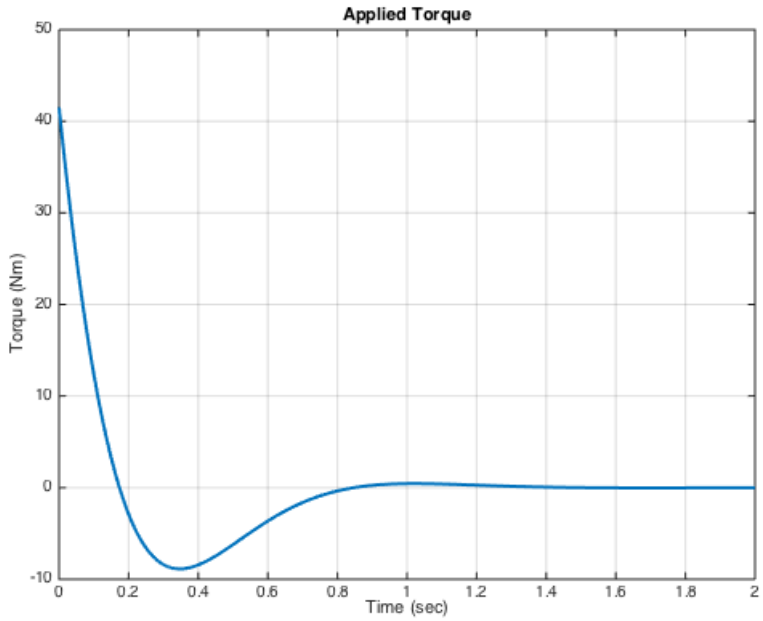

Figure 5. Total torque trajectory of baseline PD controller system

C. INTRODUCTION TO OPTIMAL CONTROL

Optimal control is a system design technique that seeks to determine the optimal control trajectory to achieve a particular end state at the lowest "cost." Optimal control takes a completely different approach from classical control theory. Unlike classical control theory, which is limited to linear (or linearized), and primarily single input / single output systems, optimal control can be applied to non-linear, multi-input / multi-output systems by considering the entire system dynamics and evaluating the implications of those dynamics to develop an optimal control input.

A good reference on optimal control theory can be found in [2]. While it is not the intent of this thesis to delve into a detailed explanation of how any general optimal control problem can be solved, many of the conclusions in this work are based on sound optimal control analysis. To facilitate a complete explanation of the progression of this study from classical closed-loop control

techniques to real-time optimal control concepts, a brief summary of the optimal control analysis techniques is warranted.

One of the first steps in setting up an optimal control problem is to define the system's dynamics. This is done in the time domain using the state space approach, and defining the system dynamics as a controlled set of first order differential equations that are a function of system states and controls:

$$\dot{\vec{x}} = f\left(\vec{x}, \vec{u}\right) \tag{1.10}$$

Naturally, an important step in optimal control is to define what is to be optimized. This depends on the goals of the designer and can include minimizing the time to reach an end state, minimizing energy consumption, maximizing altitude, etc. Whatever the desired goal, it must be articulated mathematically; this concept is embedded in the cost functional and its general form is:

$$J\left[\vec{x}(\bullet), \vec{u}(\bullet), t_f\right] = E\left(\vec{x}_f, t_f\right) + \int_{t_0}^{t_f} F\left(\vec{x}(t), \vec{u}(t)\right) dt \tag{1.11}$$

In (1.11), $\vec{x}(\bullet)$ is the state trajectory; $\vec{u}(\bullet)$ is the control trajectory; $E\left(\vec{x}_f, t_f\right)$ is the endpoint cost, which is a function of one or more final states or time. Functional $F\left(\vec{x}(t), \vec{u}(t)\right)$ is the running cost which is a function of one or more states and/or controls; and t_0 and t_f are the initial and final times, respectively. Not all cost functionals will have both an endpoint cost and a running cost; in fact, many optimal control problems will only have one or the other.

Other important parameters in the problem definition are the initial and final states and times. Depending on the optimal control problem, these parameters may not be specified, but it is important to capture them as best as they are known. An initial time is usually taken to be zero, but that need not necessarily be the case. Some problems will have a particular end time, but that is also not always the case, especially in problems where the final time is the

variable being optimized. Additionally, the end state may or may not take the form of prescribed points; it may, instead be a function. For example, an orbital problem may require that the final position and velocity satisfy mathematically defined orbital mechanics relationships. Regardless of whether the desired end state consists of a particular point or a locus of points (i.e., a function), the mathematical definition of the end state is called the end point function (not to be confused with the end point cost, contained in the cost function).

The final piece of the optimal control problem formulation is the definition of any constraints in the problem. Nearly all real-world engineering problems have constraints of some sort. These may include limits on the applied forces or torques (e.g., the maximum torque capacity of a reaction wheel), attitude orientation keep-out zones (e.g., the solar keep-out zone for an optical payload), or attitude orientation keep-in zones (e.g., minimum illumination of solar panels), etc.

The complete optimal control problem formulation includes the definition of the state vector, the control vector, the cost function, the system dynamics, the boundary values and endpoint function and all relevant constraints. A general optimal control problem formulation is:

$$
\begin{aligned}
&\underline{\text{States}}: \quad \vec{x} = \begin{bmatrix} x_1 \\ x_2 \\ \vdots \\ x_n \end{bmatrix} \qquad \underline{\text{Controls}}: \quad \vec{u} = \begin{bmatrix} u_1 \\ u_2 \\ \vdots \\ u_m \end{bmatrix} \\
&\underline{\text{minimize}}: \quad J\left[\vec{x}(\bullet), \vec{u}(\bullet), t_f\right] = E\left(\vec{x}_f, t_f\right) + \int_{t_0}^{t_f} F\left(\vec{x}(t), \vec{u}(t)\right) dt \\
&\underline{\text{subject to}}: \quad \dot{\vec{x}} = f\left(\vec{x}(t), \vec{u}(t)\right) \\
&\qquad\qquad \vec{x}(t_0) = \vec{x}^0 \\
&\qquad\qquad t_0 = t^0 \\
&\qquad\qquad t_f = t^f \\
&\qquad\qquad \vec{e} = \vec{x}\left(t_f\right) \\
&\qquad\qquad \vec{h}^L \le \vec{h} \le \vec{h}^U
\end{aligned}
\tag{1.12}
$$

Solving the optimal control problem yields the trajectory of the controls over time that achieves the desired end state and minimizes the cost functional. The cost functional may be minimized if the necessary conditions of Pontryagin's principle are satisfied [2]. But before the necessary conditions can be introduced, a few more mathematical relationships need to be defined. The first is the Hamiltonian:

$$H\left(\vec{\lambda},\vec{x},\vec{u},t\right)=F\left(\vec{x},\vec{u},t\right)+\vec{\lambda}^{T}\bullet\vec{f}\left(\vec{x},\vec{u},t\right) \tag{1.13}$$

The Hamiltonian is composed of the running cost and the inner product of the costate vector, $\vec{\lambda}$, with the state space dynamics, $\vec{f}\left(\vec{x},\vec{u},t\right)$. The running cost and state space dynamics have already been introduced. The costate vector, or covector, is a vector that relates each element of the state vector to the cost, as defined in the problem. Each element of the covector has units of cost unit per state unit; the covector provides a means of measuring the state vector in a more meaningful way than is possible in the typical Euclidian method. In other words, the calculation $\left\|\vec{x}\right\|_2=\sqrt{x_1^2+x_2^2+x_3^2}$ is only meaningful if all elements of $\vec{x}$ are in the same units; if one element is a measure of distance, another a measure of acceleration and another a measure of mass, then this calculation is meaningless. The covector enables conversion of the state vector elements into common units, specifically units of cost. The costate vector is not known beforehand and only becomes defined through the process of solving the optimal control problem. In fact, the behavior of the costate vector is what admits an optimal control solution.

The next relationship to be defined is the Endpoint Lagrangian:

$$\overline{E}\left(\vec{x}_f,\vec{\upsilon},t_f\right)=E\left(\vec{x}_f,t_f\right)+\vec{\upsilon}^{T}\cdot\vec{e}\left(\vec{x}_f\right) \tag{1.14}$$

The form of the Endpoint Lagrangian parallels the Hamiltonian. It is comprised of the endpoint cost, $E\left(\vec{e}_f, t_f\right)$, and the inner product of $\vec{\upsilon}$ with the endpoint function, $\vec{e}\left(\vec{x}_f\right)$. Like the costate vector, $\vec{\upsilon}$ is a vector of multipliers related to the endpoint function and is not known beforehand.

The optimal control solution is one which satisfies the system dynamics, problem constraints and also the necessary conditions as laid out in Pontryagin's principle. The first condition is the Hamiltonian minimization condition (HMC). HMC requires that the Hamiltonian be minimized with respect to the control variable over the entire problem time horizon. Depending on the problem, it may be as simple as setting the derivative of the Hamiltonian with respect to the control equal to zero:

$$\frac{\partial H}{\partial \vec{u}} = 0 \tag{1.15}$$

But if the problem involves path constraints, as many do, HMC is only satisfied if the Lagrangian of the Hamiltonian in minimized [2]. The Lagrangian of the Hamiltonian is defined as

$$\overline{H}\left(\vec{\mu}, \vec{\lambda}, \vec{x}, \vec{u}, t\right) = H\left(\vec{\lambda}, \vec{x}, \vec{u}, t\right) + \vec{\mu}^T \bullet \vec{h}\left(\vec{x}, \vec{u}, t\right) \tag{1.16}$$

where $H\left(\vec{\lambda}, \vec{x}, \vec{u}, t\right)$ is the Hamiltonian, $\vec{\mu}$ is the path constraint covector and $\vec{h}\left(\vec{x}, \vec{u}, t\right)$ is the vector of path constraints. Now HMC becomes

$$\frac{\partial \overline{H}}{\partial \vec{u}} = 0 \quad \text{and} \quad \vec{\mu} \dagger \vec{h} \tag{1.17}$$

where the notation $\vec{\mu} \dagger \vec{h}$ is defined to mean that $\vec{\mu}$ and $\vec{h}$ satisfy the complementarity condition [2], which is defined in equation (1.18).

$$\mu_i \begin{cases} \leq 0 & if \quad h_i(\bar{u}) = h_i^L \\ = 0 & if \quad h_i^L < h_i(\bar{u}) < h_i^U \\ \geq 0 & if \quad h_i(\bar{u}) = h_i^U \\ unrestricted & if \quad h_i^L = h_i^U \end{cases} \tag{1.18}$$

The next necessary condition is the Hamiltonian value condition, which simply states

$$\mathcal{H}\left[@t_f\right] = -\frac{\partial \overline{E}}{\partial t_f} \tag{1.19}$$

where $\mathcal{H}\left[@t_f\right]$ is the value of the minimized Hamiltonian at the final time. The Hamiltonian value condition provides a value, or boundary condition, for the trajectory of the Hamiltonian throughout the problem.

The next condition that must be satisfied is the Hamiltonian evolution equation. The Hamiltonian evolution equation is

$$\frac{d\mathcal{H}}{dt} = \frac{\partial H}{\partial t} \tag{1.20}$$

The adjoint equations must be determined to find the optimal solution. The adjoint equations define the dynamics of the costates. In the presence of path constraints, the adjoint equations are defined as

$$-\dot{\bar{\lambda}} = \frac{\partial \overline{H}}{\partial \bar{x}} \tag{1.21}$$

The final condition that must be met is the transversality value condition. Like the Hamiltonian value condition, the transversality condition provides boundary conditions for the costate trajectory and is given by

$$\bar{\lambda}\left(t_f\right) = \frac{\partial \bar{E}}{\partial \bar{x}_f} \tag{1.22}$$

The process of defining and evaluating the necessary conditions forms the preliminary analysis necessary to solve an optimal control problem. This analysis does not typically provide the solution, but simply provides a new problem which, when solved, provides the optimal control solution. The necessary conditions can also be used to validate the optimality of a candidate solution to problem (1.12). The resulting problem is a Hamiltonian boundary value problem, where the additional adjoint equations double the size of the original problem! The original problem formulation may not have had enough boundary conditions specified to solve the boundary value problem, and when that is the case, the transversality conditions provide the missing information.

Unfortunately, solving differential algebraic boundary value problems can be challenging, to say the least. Some success can be had with certain numerical approaches, such as a shooting method or collocation method, but these approaches are ill suited for some problems and may require a near perfect initial guess to determine the solution.

Pseudospectral optimal control theory is an alternative and more robust approach for solving optimal control problems [3]. A numerical instantiation of the theory is found in the MATLAB tool, DIDO [2], [4]. Use of DIDO does not relieve the operator from evaluating the validity of the solution. The satisfaction of necessary conditions should be verified, and the candidate control solution should be evaluated to verify that it produces the desired end state without violating any applied constraints.

DIDO is used to solve all optimal control problems in this thesis. As is the accepted standard practice [2], each solution will be evaluated using the ODE45 propagator resident in MATLAB to verify that the candidate control trajectory results in the desired end state. Further, the satisfaction of necessary conditions will be verified for each solution.

D. THESIS OBJECTIVES AND SCOPE

The first objective of this thesis is to study a variety of closed-loop spacecraft attitude control architectures, examining the effectiveness of each with respect to optimal control implementation. Spacecraft attitude maneuvers are most commonly executed as eigenaxis maneuvers. Because these are effectively one-dimensional rotations, the initial control architecture study will examine one-dimensional double integrator systems. The second objective of this thesis will be to develop a closed-loop optimal control method that incorporates the actual system response, modifying the optimal solution in real-time for one-dimensional rotational systems. The final objective is to translate the closed-loop optimal control methods developed for one-dimensional systems to a three-dimensional concept that can be applied to spacecraft maneuvers.

E. THESIS OUTLINE

This thesis will begin with an introduction to classical control techniques, followed by an introduction to optimal control analysis techniques. It will then explore the minimum time optimal control implementations in several one-dimensional closed-loop rotational systems, including an examination of the effects of uncertainty on each optimal control implementation. Then, an closed-loop optimal control solution (i.e., real-time optimal control) will be developed for the one-dimensional problem. Finally, the one-dimensional RTOC method will be translated to three-dimensions and applied to eigenaxis maneuvers of three-dimensional rigid bodies.

II. EVALUATION OF CANDIDATE ARCHITECTURES FOR CLOSED-LOOP OPTIMAL CONTROL

This chapter explores implementation of optimal control solutions by examining several variations of two basic closed-loop control architectures. The two basic architectures are referred to as guided control and feed-forward control. In the guided control implementation, the optimal position and angular velocity trajectories are used as control inputs rather than the step input typically used in classical control analysis. In contrast, the feed-forward control architecture will apply a separate control torque command, τ_{cmd}, directly to the rotating body in addition to the contribution of the PD controller feedback arising from a step change in the commanded position; this models a direct manipulation of the actuator to achieve a specific output torque. Optimal control techniques will be applied around each control architecture to determine the minimum time solution. The architectures will be compared to each other based on typical engineering figures of merit such as the nominal settling time as well as how each architecture responds uncertainty in the value of the rotational inertia.

It should be noted that it has long been established that the minimum time solution for single degree of freedom maneuvers consists of applying the maximum torque to accelerate and then decelerate to achieve the desired maneuver [5]; this is commonly known as “bang-bang” control. While this solution is known and is expected to be manifested in the following optimal control analysis, differences in implementation of this solution in various closed-loop control architectures will be evaluated. Importantly, the traditional “bang-bang” solution is commonly implemented in an open-loop manner, but open-loop control cannot account for system uncertainties such as variations in system rotational moments of inertia. When optimizing the control of existing closed-loop systems, different implementations may be required depending on the limitations of the existing system, leading to differences in the input signals needed to obtain a “bang-bang” input to the plant.

A. STATE-GUIDED ARCHITECTURE

The first method of implementation of optimal control for the double integrator is through state guidance. The optimal control problem is setup to find the minimum maneuver time using a guided state as the control variable. Because the PD controller is based on both a position and velocity commanded states, both must be determined. The problem formulation used here requires that the commanded position and commanded velocity not be completely independent, but instead that the velocity is the time derivative of the position (as with normal kinematics). Thus, the control architecture is shown in Figure 6 and optimal control problem formulation is as follows:

> Problem Statement — State Guided Control: Perform a minimum time rotation of a rigid body with a pre-existing PD controller using commanded state guidance. The initial system will be in a position of zero radians at zero velocity, and the final state will be at a position of one radian and zero velocity.

This system model is assumed to have a rotational inertia of $1\ kg \cdot m^2$ and the torque actuator is limited to total of $60\ N \cdot m$ in both the positive or negative direction. These system attributes will apply to each control architecture and problem formulation in the sequence.

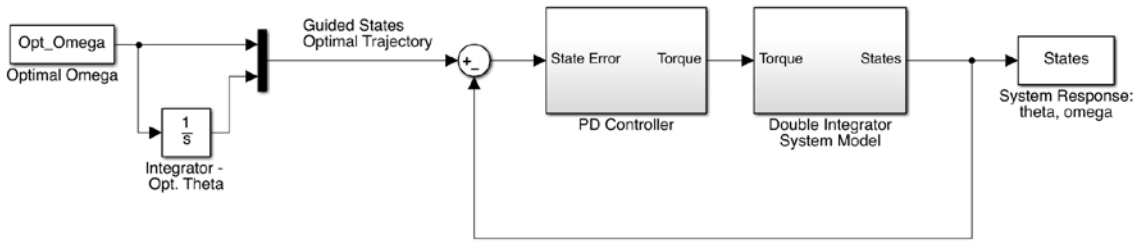

Figure 6. State-guided optimal control architecture

$$
\begin{aligned}
&\underline{\text{States}}: && \vec{x} = \begin{bmatrix} \theta \\ \omega \\ \theta_{cmd} \end{bmatrix} && \underline{\text{Controls}}: \ \vec{u} = \left[\omega_{cmd}\right] \\
&\underline{\text{minimize}}: && J\left[\vec{x}(\bullet), \vec{u}(\bullet), t_f\right] = t_f \\
&\underline{\text{subject to}}: && \dot{\theta} = \omega \\
& && \dot{\omega} = \frac{1}{J_e}\left[k_p\theta_{cmd} - k_p\theta + k_v\omega_{cmd} - k_v\omega\right] \\
& && \dot{\theta}_{cmd} = \omega_{cmd} \\
& && t_0 = 0 \\
& && t_f = t^f \\
& && \vec{x}_0^T = \left[0,0,0\right]^T \\
& && \vec{x}_f^T = \left[1,0,1\right]^T \\
& && -60 \le \left[k_p\theta_{cmd} - k_p\theta + k_v\omega_{cmd} - k_v\omega\right] \le 60
\end{aligned}
\tag{1.23}
$$

The process of solving this first optimal control problem will be presented in detail; for brevity, only highlights pertaining to the analysis of the problems thereafter will be presented. First, an explanation of the problem formulation is offered. The states in this problem include the system angular position, θ; the angular velocity, ω; and the guided or commanded position, θ_{cmd}; and there is only one control variable, the guided or commanded angular velocity, $\vec{u} \equiv \omega_{cmd}$. The fact that the commanded position is a state rather than a control may come as a surprise since it is considered a control variable from the perspective of classical PD controls. However, as previously mentioned, the trajectory of the commanded position is not independent, but is a function of the commanded velocity via kinematics; thus, the commanded position is part of the state space in this problem formulation.

The cost functional is simple. In the case of a minimum time problem, the parameter to be minimized is time. Thus, the cost functional is simply the final time, t_f, with no running cost. The state dynamics, initial and final states are self-explanatory. The last piece of the problem formulation is the definition of the

constraint on the total torque which cannot exceed $\pm 60\ N \cdot m$. Note that this value was selected arbitrarily.

The first step in solving the optimal control problem is to define the Hamiltonian:

$$H\left(\vec{\lambda},\vec{x},\vec{u},t\right) = F\left(\vec{x},\vec{u},t\right) + \vec{\lambda} \bullet \vec{f}\left(\vec{x},\vec{u},t\right)$$
$$= \begin{bmatrix} \lambda_\theta \\ \lambda_\omega \\ \lambda_{\theta_{cmd}} \end{bmatrix}^T \cdot \begin{bmatrix} \omega \\ \frac{1}{J_e}\left[k_p\theta_{cmd} - k_p\theta + k_v\omega_{cmd} - k_v\omega\right] \\ \omega_{cmd} \end{bmatrix}$$

$$H\left(\vec{\lambda},\vec{x},\vec{u},t\right) = \lambda_\theta\omega + \lambda_\omega \frac{1}{J_e}\left[k_p\theta_{cmd} - k_p\theta + k_v\omega_{cmd} - k_v\omega\right] + \lambda_{\theta_{cmd}}\omega_{cmd} \tag{1.24}$$

The next step is to evaluate the Hamiltonian Minimization Condition (HMC). Because of the presence of the path constraint on the total torque, HMC is satisfied through the minimization of the Lagrangian of the Hamiltonian, given by

$$\overline{H}\left(\vec{\mu},\vec{\lambda},\vec{x},\vec{u},t\right) = H\left(\vec{\lambda},\vec{x},\vec{u},t\right) + \vec{\mu}^T \bullet \vec{h}\left(\vec{x},\vec{u},t\right)$$
$$\overline{H}\left(\vec{\mu},\vec{\lambda},\vec{x},\vec{u},t\right) = \lambda_\theta\omega + \lambda_\omega \frac{1}{J_e}\left[k_p\theta_{cmd} - k_p\theta + k_v\omega_{cmd} - k_v\omega\right] + \lambda_{\theta_{cmd}}\omega_{cmd} + \mu_{\tau_{tot}}\tau_{tot} \tag{1.25}$$

where $\mu_{\tau_{tot}}$ is the path constraint covector for the total torque and τ_{tot} is the total torque ($\tau_{tot} = k_p\theta_{cmd} - k_p\theta + k_v\omega_{cmd} - k_v\omega$), as defined in the problem formulation, equation (1.23). Now, HMC becomes

$$\frac{\partial \overline{H}}{\partial \vec{u}} = 0 \quad \text{and} \quad \vec{\mu} \dagger \vec{h} \tag{1.26}$$

Evaluating the first portion of HMC yields:

$$\frac{\partial \overline{H}}{\partial \bar{u}} = \frac{\lambda_\omega k_v}{J_e} + \lambda_{\theta_{cmd}} + \mu_{\tau_{tot}} k_v = 0$$
$$\mu_{\tau_{tot}} = -\frac{\lambda_\omega}{J_e} - \frac{\lambda_{\theta_{cmd}}}{k_v} \tag{1.27}$$

Evaluating the second portion of HMC, the complementarity condition, reveals the following switching structure:

$$\tau_{tot} \begin{cases} = h^L & if \quad \mu_{\tau_{tot}} \le 0 \\ \in \left(h^L, h^U\right) & if \quad \mu_{\tau_{tot}} = 0 \\ = h^U & if \quad \mu_{\tau_{tot}} \ge 0 \end{cases}$$
$$\left[k_p \theta_{cmd} - k_p \theta + k_v \omega_{cmd} - k_v \omega\right] \begin{cases} = -60 & if \quad \mu_{\tau_{tot}} \le 0 \\ \in (-60, 60) & if \quad \mu_{\tau_{tot}} = 0 \\ = 60 & if \quad \mu_{\tau_{tot}} \ge 0 \end{cases} \tag{1.28}$$

The totality of the HMC, equations (1.27) and (1.28), provides a formula for determining the control variable, ω_{cmd} , in terms of the other states and covectors. The satisfaction of the conditions of equation (1.28) will be checked as part of the solution validation process.

The next step in solving the optimal control problem is to define the costate dynamics using the adjoint equation, $-\dot{\bar{\lambda}} = \frac{\partial \overline{H}}{\partial \bar{x}}$. Because of the presence of path constraints, the adjoint equations are based on the Lagrangian of the Hamiltonian:

$$\dot{\lambda}_\theta = \frac{\lambda_\omega k_p}{J_e} + \mu_{\tau_{tot}} k_p$$
$$\dot{\lambda}_\omega = \frac{\lambda_\omega k_v}{J_e} - \lambda_\theta + \mu_{\tau_{tot}} k_v \tag{1.29}$$
$$\dot{\lambda}_{\theta_{cmd}} = -\frac{\lambda_\omega k_p}{J_e} - \mu_{\tau_{tot}} k_p$$

The Hamiltonian value condition yields the following:

$$\begin{aligned} H\left[@t_f\right] &= -\frac{\partial \overline{E}}{\partial t_f} = -\frac{\partial}{\partial t_f}\left(t_f\right) \\ H\left[@t_f\right] &= -1 \end{aligned} \tag{1.30}$$

Evaluation of the Hamiltonian evolution equation gives:

$$\begin{aligned} \frac{d\mathcal{H}}{dt} &= \frac{\partial H}{\partial t} \\ \frac{d\mathcal{H}}{dt} &= 0 \end{aligned} \tag{1.31}$$

The Hamiltonian value condition combined with the Hamiltonian evolution equation indicate that the Hamiltonian of the optimal solution will be constant at a value of $H = -1$ throughout the maneuver. Because of the construct of the cost functional and the Hamiltonian, the fact that $H = -1$ is common to all minimum time problems.

The transversality condition, $\vec{\lambda}\left(t_f\right) = \frac{\partial \overline{E}}{\partial \vec{x}_f}$, is the final condition to be analyzed. Its evaluation yields the following:

$$\begin{aligned} \lambda_\theta\left(t_f\right) &= \upsilon_1 \\ \lambda_\omega\left(t_f\right) &= \upsilon_2 \\ \lambda_{\theta_{cmd}}\left(t_f\right) &= \upsilon_3 \end{aligned} \tag{1.32}$$

In this problem, transversality value condition indicates that the final value of the covectors should be equal to what is at this point another unknown quantity (i.e., the values of υ_n). This, clearly, will not be helpful in developing the solution, but will provide another means of verifying a potential solution's optimality.

The optimal control problem of equation (1.23) was solved using the DIDO software. The resulting solution was tested in a verification and validation model, which simply consisted of an ODE propagator in MATLAB. The DIDO solution results are presented in Figures 7–11.

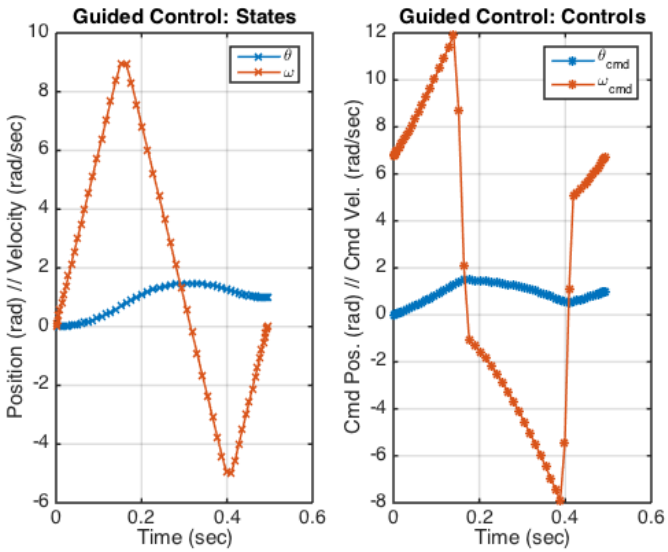

Figure 7. State and control trajectories of optimal control solution for guided optimal control architecture

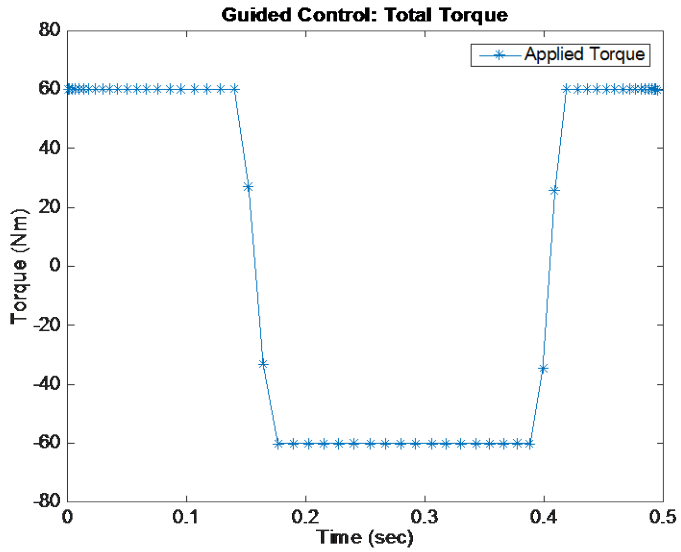

Figure 8. Trajectory of applied torque for state-guided optimal control architecture

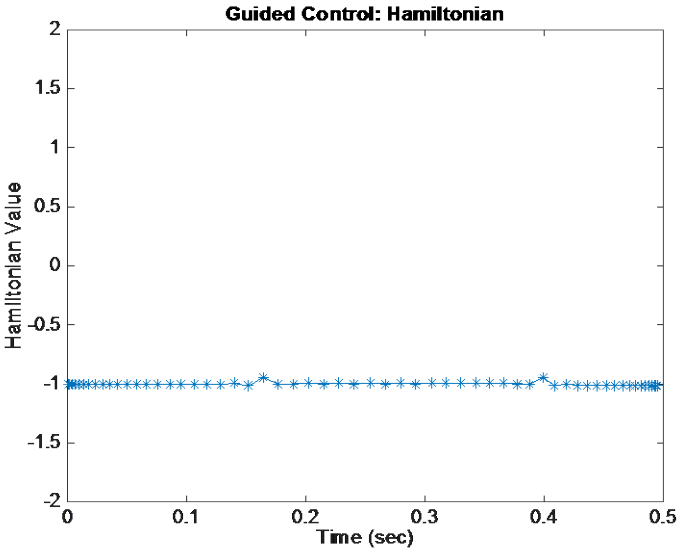

Figure 9. Hamiltonian trajectory in state-guided optimal control solution

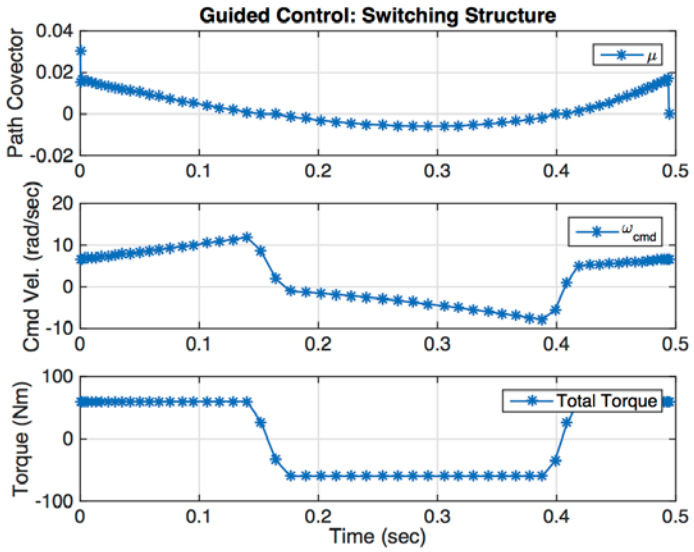

Figure 10. Switching function trajectory in state-guided optimal control solution

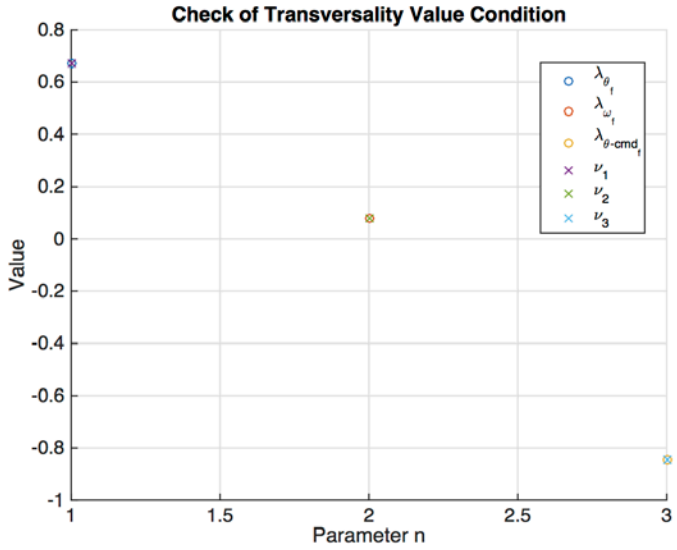

Figure 11. Transversality value condition for guided optimal control solution

Figure 7 shows the response of the system when the optimal control solution is applied in a guided control architecture; the plot on the right within Figure 7 depicts the control, ω_{cmd}, throughout the maneuver. Note that the

optimal control solution modulates the control trajectory in order to meet but not exceed the maximum torque constraint, as depicted by the plot of total applied torque in Figure 8. But note also that the applied torque is not consistent with the expected "bang-bang" optimal torque trajectory; it is instead "bang-bang-bang." This third application of maximum torque is necessary to reduce the system's velocity to zero; this is likely due to the undamped nature of the PD controller. The presence of this third "bang" may explain why a conventional open-loop "bang-bang" solution may not give the correct closed-loop response.

The satisfaction of the Hamiltonian minimization condition can be verified in Figure 10 (i.e., that the control trajectory obeys the switching function). Note that the maximum and minimum values of the control, ω_{cmd}, vary throughout the maneuver, as would be expected from the HMC in this problem due to the constraint on total torque. The trajectory of total applied torque, which is constrained at $\pm 60\ Nm$ illustrates the satisfaction of the HMC more clearly.

The trajectory of the Hamiltonian is plotted in Figure 9. It is, as shown, constant at a value of -1, illustrating the satisfaction of the Hamiltonian value condition and the Hamiltonian evolution equation. Finally, Figure 11 plots the final state covector values ($\lambda_n(t_f)$) and the endpoint covector values (υ_n), graphically depicting satisfaction of the transversality condition. These results provide additional assurance that the solution obtained from DIDO is in fact optimal.

B. FEED-FORWARD CONTROL ARCHITECTURE

The second major architecture type being evaluated consists of a feed-forward torque signal with a closed-loop PD controller. This architecture simulates the ability to manipulate the actuator directly. This system is depicted in Figure 12. Note that the PD controller is still intact, and it also still has the step input of the original control architecture. But a separate torque signal is routed around the PD controller directly to the plant; this torque input, τ, is the control variable in the optimization of this architecture. To the best of the author's

knowledge, the optimization of this particular type of architecture has not been studied before.

> Problem Statement: Perform a minimum time rotation of a rigid body with a pre-existing PD controller using feed-forward control. The initial system will be in a position of zero radians at zero velocity, and the final state will be at a position of one radian and zero velocity.

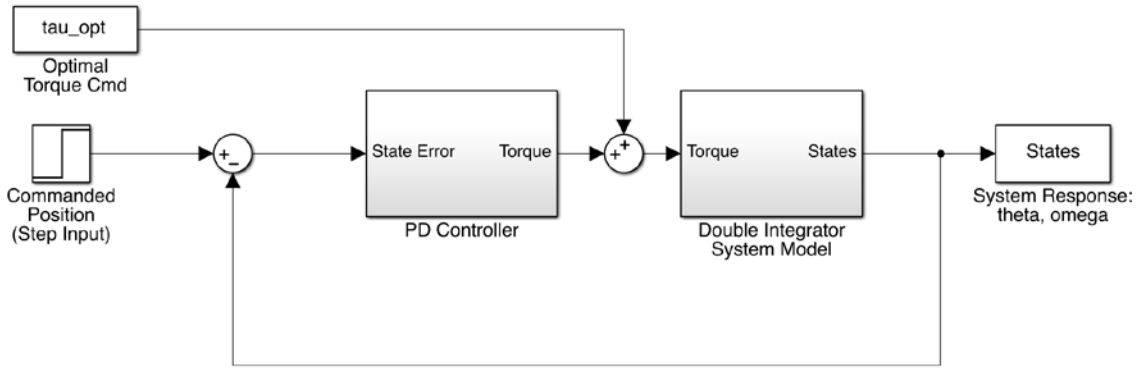

Figure 12. Feed-forward optimal control architecture

$$
\begin{aligned}
&\underline{\text{States}}: && \bar{x} = \begin{bmatrix} \theta \\ \omega \end{bmatrix} && \underline{\text{Controls}}: \ \bar{u} = [\tau] \\
&\underline{\text{minimize}}: && J\left[\bar{x}(\bullet), \bar{u}(\bullet), t_f\right] = t_f \\
&\underline{\text{subject to}}: && \dot{\theta} = \omega \\
& && \dot{\omega} = \frac{1}{J_e}\left[k_p\theta_{cmd} - k_p\theta - k_v\omega + \tau\right] \\
& && t_0 = 0 \\
& && t_f = t^f \\
& && \bar{x}_0^T = [0,0]^T \\
& && \bar{x}_f^T = [1,0]^T \\
& && \theta_{cmd} = 1 \\
& && -60 \le \left[k_p\theta_{cmd} - k_p\theta - k_v\omega + \tau\right] \le 60
\end{aligned}
\tag{1.33}
$$

In the problem formulation captured in equation (1.33), the commanded angular velocity, ω_{cmd}, is set to zero throughout the maneuver, and is therefore omitted in the system dynamics.

Evaluation of HMC yields the following necessary conditions:

$$\mu_{\tau_{tot}} = -\frac{\lambda_{\omega}}{J_e} \tag{1.34}$$

$$\left[k_p\theta_{cmd} - k_p\theta - k_v\omega + \tau\right]\begin{cases} = -60 & if \quad \mu_{\tau_{tot}} \le 0 \\ \in (-60, 60) & if \quad \mu_{\tau_{tot}} = 0 \\ = 60 & if \quad \mu_{\tau_{tot}} \ge 0 \end{cases} \tag{1.35}$$

Evaluation of the Hamiltonian value condition and the Hamiltonian evolution equation yield the typical minimum time problem conditions, specifically that the Hamiltonian should be constant at a value of -1. Similar to the guided control problem, the transversality value condition in this problem yields the following information:

$$\begin{aligned} \lambda_{\theta} &= \upsilon_1 \\ \lambda_{\omega} &= \upsilon_2 \end{aligned} \tag{1.36}$$

The results of the feed-forward optimal control architecture are presented in Figures 13–17. The plot on the left within Figure 13 illustrates the state trajectories while Figure 14 illustrates the applied torque throughout the maneuver. These results are consistent with the quintessential “bang-bang” optimal control for the minimum time double integrator problem. Figure 16 illustrates how the control architecture accomplishes this; the control variable, the feed-forward torque signal τ, is modulated in response to the PD feedback torque contribution such that the total applied torque is either the maximum positive or negative torque as necessary to create the “bang-bang” torque profile at the plant input. Note also that the control torque profile relative to the switching function

satisfies the HMC; recall that the control constraint is derived from the constraint of the total torque limits.

Finally, it is observed that the feed-forward control architecture accomplishes the maneuver in approximately half the time required for the guided control architecture (0.26 seconds vs. 0.51 seconds). This is due to the fact that in this architecture, the well-known “bang-bang” control can be recovered despite the action of the feedback PD controller.

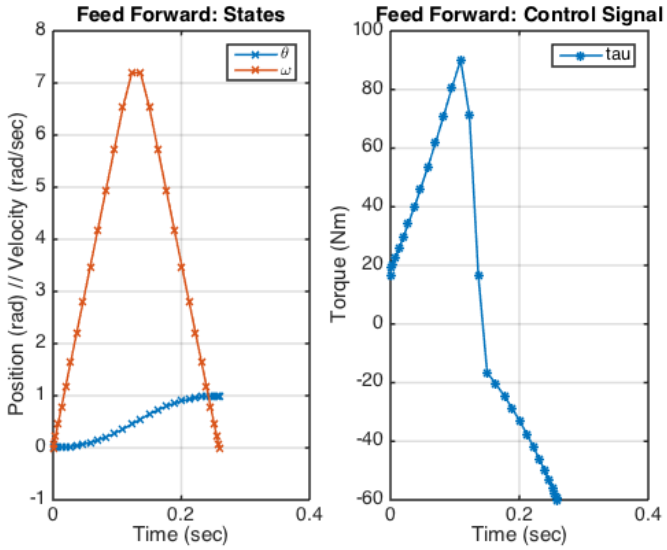

Figure 13. State and control trajectories of optimal control solution for feed-forward architecture

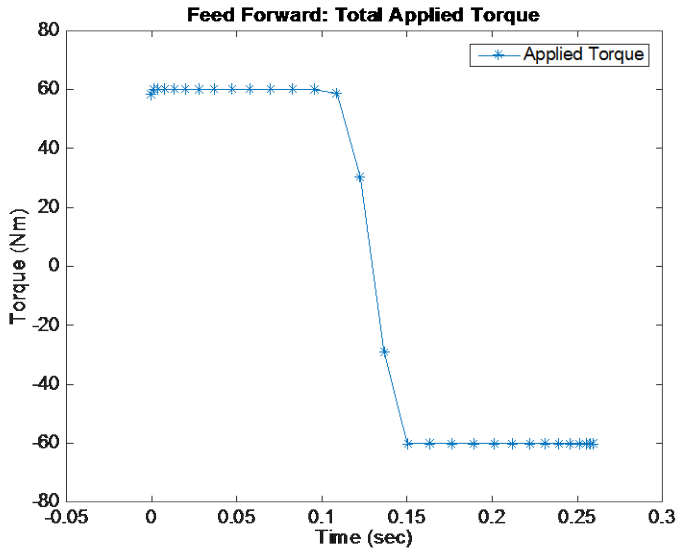

Figure 14. Trajectory of total applied torque in optimal control solution for feed-forward architecture

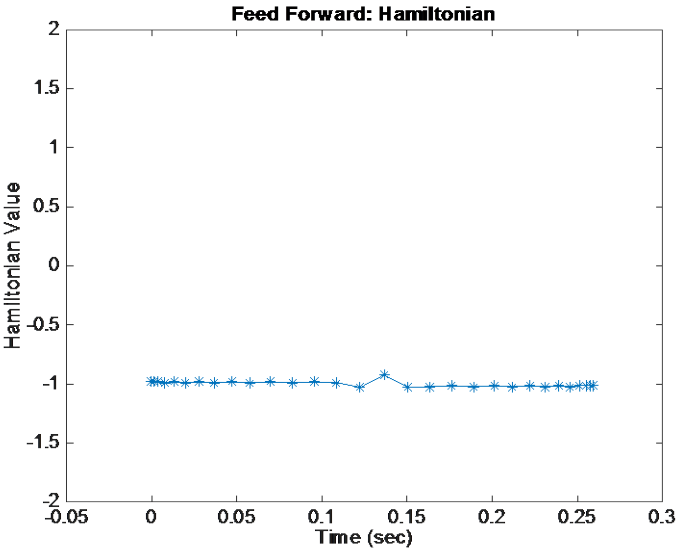

Figure 15. Hamiltonian for optimal control solution for feed-forward architecture

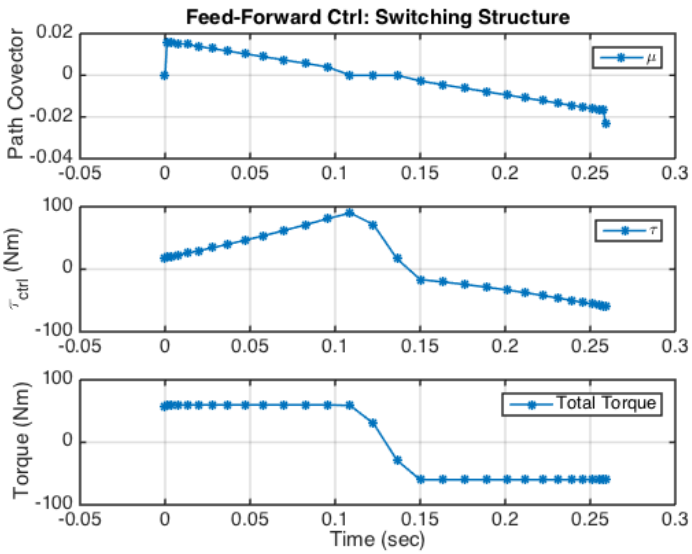

Figure 16. Switching function in optimal control solution for feed-forward architecture

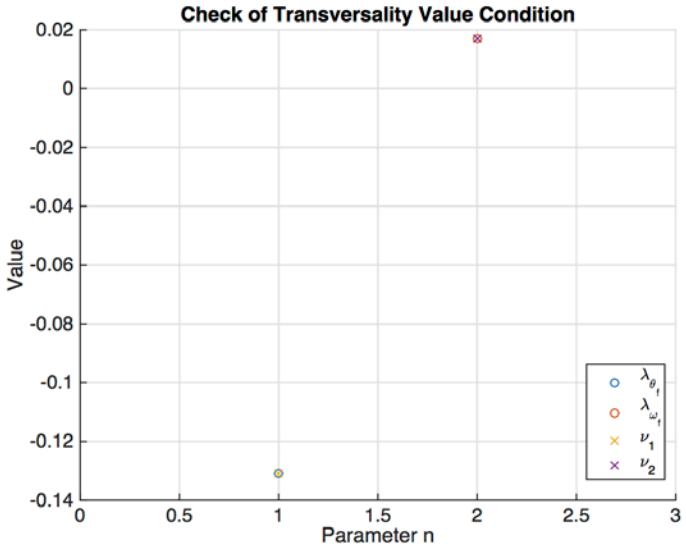

Figure 17. Transversality condition in optimal control solution for feed-forward architecture

C. ACCELERATION-GUIDED CONTROL ARCHITECTURE

The first variation of the basic guided control architecture is to use rotational acceleration as the control variable. The position and rate trajectories

are determined based on the acceleration trajectory and are then used as the state guidance (as in section A). This control architecture and the optimal control problem are depicted in Figure 18 and equation (1.37). As the preceding results indicate, optimal control solutions can sometimes recommend control trajectories with discontinuities, which may be undesirable in some circumstances. For example, discontinuities can excite flexible modes in a system, producing undesirable motion. Adding an integrator and a new control variable will remove the discontinuities and smooth out the guidance trajectories.

> Problem Statement: Perform a minimum time rotation of a rigid body with a pre-existing PD controller using rotational acceleration as the control. Rotational acceleration will be integrated to form position and velocity guidance for the PD controller. The initial system state will be in a position of zero radians at zero velocity, and the final state will be at a position of one radian and zero velocity.

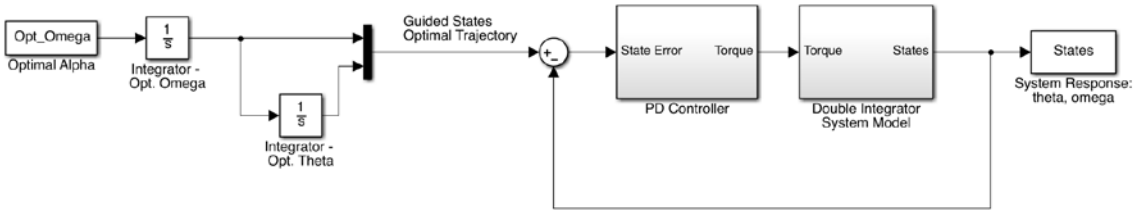

Figure 18. Acceleration-guided optimal control architecture

$$
\begin{aligned}
&\underline{\text{States:}} \quad \vec{x} = \begin{bmatrix} \theta \\ \omega \\ \theta_{cmd} \\ \omega_{cmd} \end{bmatrix} \qquad \underline{\text{Controls:}} \quad \vec{u} = [\alpha] \\
&\underline{\text{minimize:}} \quad J\left[\vec{x}(\bullet), \vec{u}(\bullet), t_f\right] = t_f \\
&\underline{\text{subject to:}} \quad \dot{\theta} = \omega \\
&\qquad \dot{\omega} = \frac{1}{J_e}\left[k_p\theta_{cmd} - k_p\theta + k_v\omega_{cmd} - k_v\omega\right] \\
&\qquad \dot{\theta}_{cmd} = \omega_{cmd} \\
&\qquad \dot{\omega}_{cmd} = \alpha \\
&\qquad t_0 = 0 \\
&\qquad t_f = t^f \\
&\qquad \vec{x}_0^T = [0,0,0,0]^T \\
&\qquad \vec{x}_f^T = [1,0,1,0]^T \\
&\qquad -60 \le \left[k_p\theta_{cmd} - k_p\theta + k_v\omega_{cmd} - k_v\omega\right] \le 60 \\
&\qquad -80 \le \alpha \le 80
\end{aligned}
\tag{1.37}
$$

In problem (1.37), an angular acceleration is an appropriately limited control variable, so the position and velocity guidance (i.e. θ_{cmd} and ω_{cmd}) are now state variables.

Analysis of the HMC in this problem yields the same conditions identified in (1.28) and the following additional conditions:

$$
\mu_\alpha = -\lambda_{\omega_{cmd}} \tag{1.38}
$$

$$
\alpha \begin{cases} = -80 & if \quad \mu_\alpha \le 0 \\ \in (-80, 80) & if \quad \mu_\alpha = 0 \\ = 80 & if \quad \mu_\alpha \ge 0 \end{cases} \tag{1.39}
$$

The Hamiltonian value condition, Hamiltonian evolution equation and transversality value conditions are all similar to those found in the previous

problems. The results of the acceleration-guided optimal control solution are presented in the Figures 19–24.

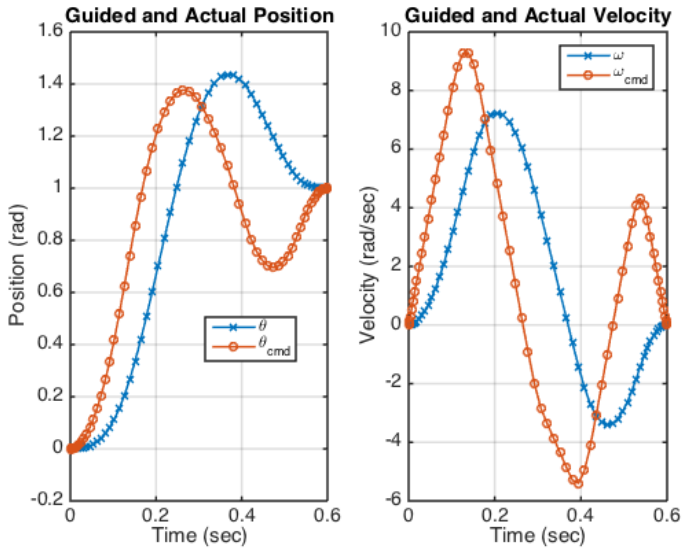

Figure 19. Commanded and actual state trajectories in acceleration-guided optimal control solution

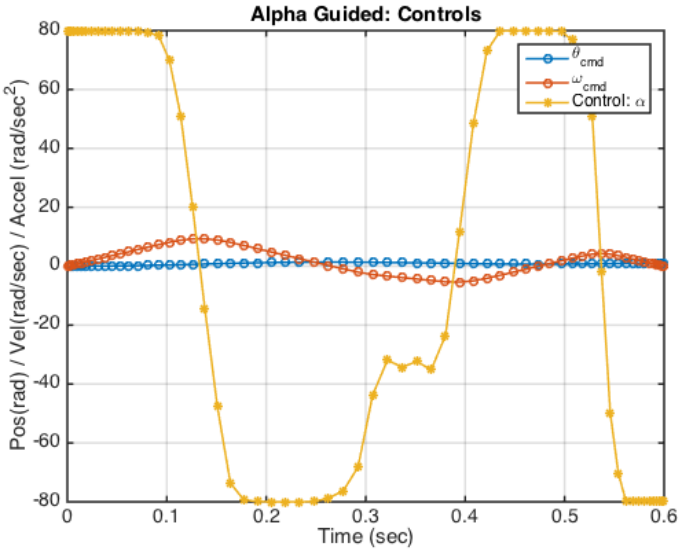

Figure 20. Control and guidance trajectories in acceleration-guided optimal control solution

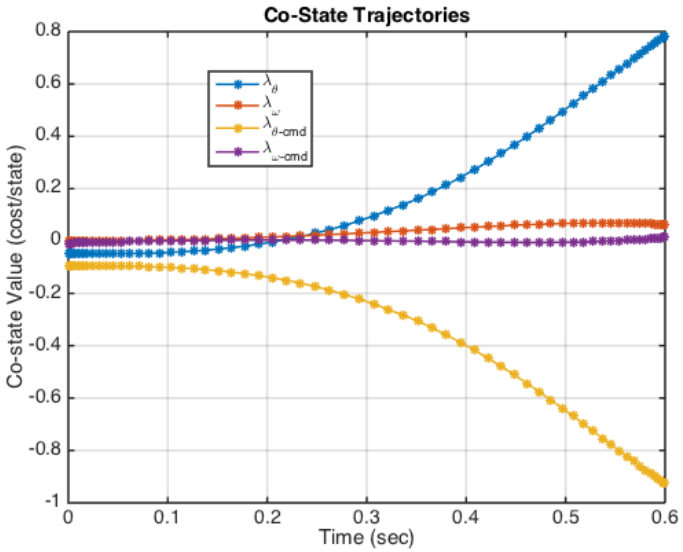

Figure 21. Costate trajectories in acceleration-guided optimal control solution

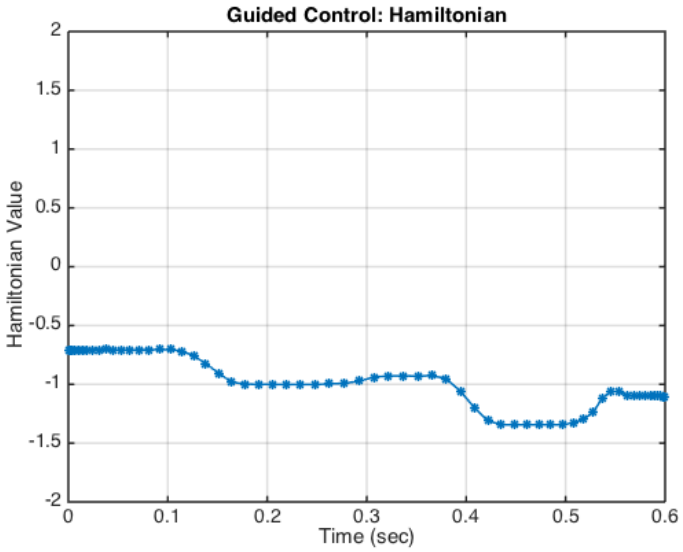

Figure 22. Hamiltonian in acceleration-guided optimal control solution

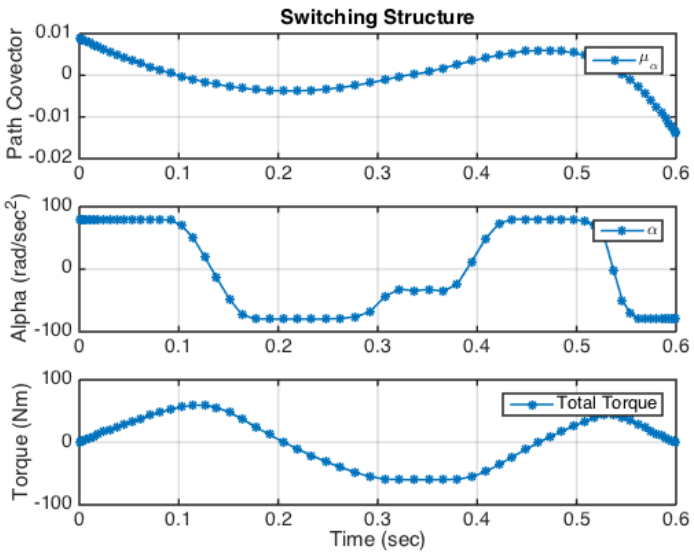

Figure 23. Switching function in acceleration-guided optimal control solution

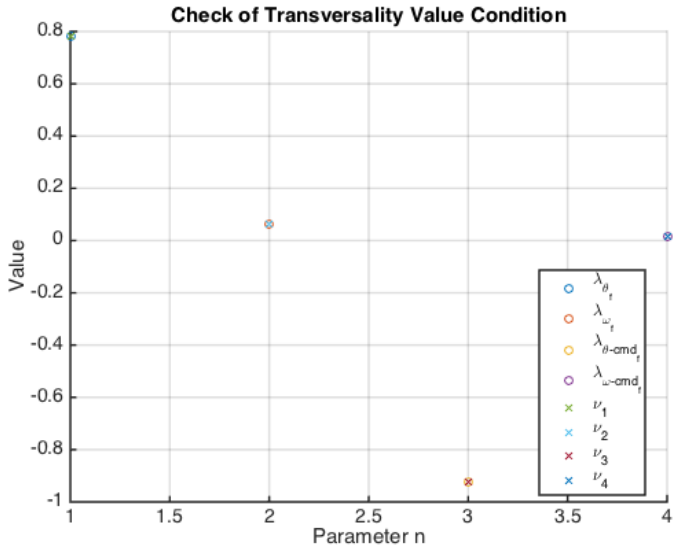

Figure 24. Transversality condition in acceleration-guided optimal control solution

The results indicate that an acceleration-guided architecture is even slower than the state guidance architecture, requiring more time to complete the same maneuver. Note that while the control signal and switching function are

consistent with the HMC, the applied torque does not remain at its maximums for very long. This result is predicted by classical control theory. The position and rate controls in this architecture are based on the integrated acceleration signal; in classical control terms, this adds another pole to the overall transfer function, thus making the system less responsive.

It must also be noted, however, that this solution is not quite optimal. The Hamiltonian value is close to, but not exactly -1 throughout the maneuver, and it is not constant. Additionally, the control trajectory seems to move from minimum to maximum a little slowly. This is particularly noticeable around 0.35 seconds into the maneuver. Note that at that time, the switching function is hovering close to zero, the switching boundary line. Examining the range of the switching function and the costates indicates that these results are suffering from a scaling issue. DIDO is most effective at determining an optimal solution when the controls, states and costates are the same order of magnitude, but in this case, $\lambda_{\omega_{cmd}}$ is several orders of magnitude smaller than the states or control. However, these results do approximate the expected results, namely that using acceleration as the control variable slows the response. Addressing the apparent scaling issue will be saved for future work.

D. ACCELERATION FEED-FORWARD CONTROL ARCHITECTURE

The next control architecture is a variation on the acceleration-based control architecture. Like concept described in section C, this architecture uses rotational acceleration as the control variable. In the feed-forward architecture the rotational acceleration supplies both a position and velocity guidance input as well as a computed torque feed-forward input. The feed-forward torque is based on the acceleration guidance and the nominal, or estimated, system inertia. It is important to distinguish this nominal inertia from the actual system inertia; the difference is the uncertainty in the system that will be evaluated in later sections. The acceleration feed-forward architecture and the associated optimal control problem are presented Figure 25 and equation (1.40).

Problem Statement: Perform a minimum time rotation of a rigid body with a pre-existing PD controller using rotational acceleration as the control. Acceleration will be integrated to form position and velocity guidance for the PD controller and also scaled by the nominal system inertia to produce a feed-forward torque input. The initial system state will be in a position of zero radians at zero velocity, and the final state will be at a position of one radian and zero velocity.

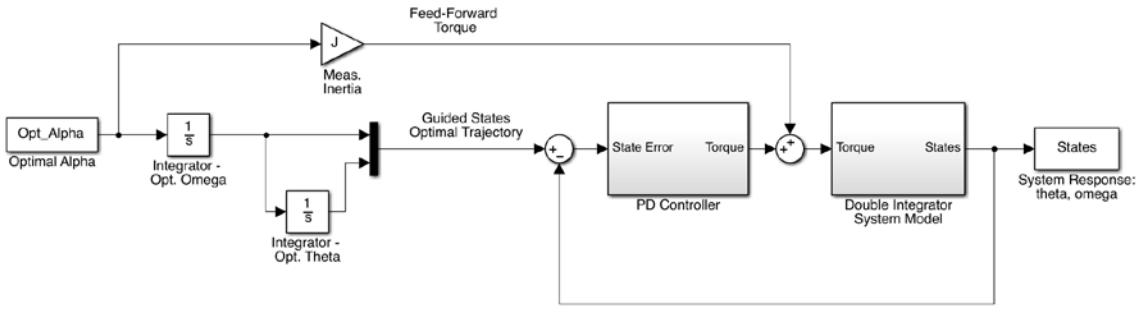

Figure 25. Acceleration feed-forward control architecture

$$\underline{\text{States}}: \quad \vec{x} = \begin{bmatrix} \theta \\ \omega \\ \theta_{cmd} \\ \omega_{cmd} \end{bmatrix} \qquad \underline{\text{Controls}}: \ \vec{u} = [\alpha]$$

$$\underline{\text{minimize}}: \quad J\left[\vec{x}(\bullet), \vec{u}(\bullet), t_f\right] = t_f$$

$$\underline{\text{subject to}}: \quad \dot{\theta} = \omega$$

$$\dot{\omega} = \frac{\alpha J_{nom}}{J_{act}} + \frac{1}{J_{act}}\left[k_p\theta_{cmd} - k_p\theta + k_v\omega_{cmd} - k_v\omega\right]$$

$$\dot{\theta}_{cmd} = \omega_{cmd}$$

$$\dot{\omega}_{cmd} = \alpha \qquad (1.40)$$

$$t_0 = 0$$

$$t_f = t^f$$

$$\vec{x}_0^T = [0,0,0,0]^T$$

$$\vec{x}_f^T = [1,0,1,0]^T$$

$$-60 \le \left[\alpha J_{nom} + k_p\theta_{cmd} - k_p\theta + k_v\omega_{cmd} - k_v\omega\right] \le 60$$

Note that in this problem formulation, the nominal rotational inertia, J_{nom}, is distinguished from the actual rotational inertia, J_{act}. This is a more significant distinction for the purposes of analyzing the effects of inertia uncertainty on the system performance; from the perspective of the optimal control solution, these values are assumed to be equal.

Evaluation of HMC in this problem yields (1.28) in addition to the following switching structure:

$$\mu_{\tau_{tot}} = -\frac{\lambda_{\omega}}{J_{act}} - \frac{\lambda_{\omega_{cmd}}}{J_{nom}}$$

and (1.41)

$$\alpha \begin{cases} = -60 & if \quad \mu_{\alpha} \leq 0 \\ \in (-60, 60) & if \quad \mu_{\alpha} = 0 \\ = 60 & if \quad \mu_{\alpha} \geq 0 \end{cases}$$

Evaluation of the Hamiltonian value condition, Hamiltonian evolution equation and transversality condition all yield similar results as the previous problems. The results of the acceleration feed-forward control architecture are presented Figures 26–29.

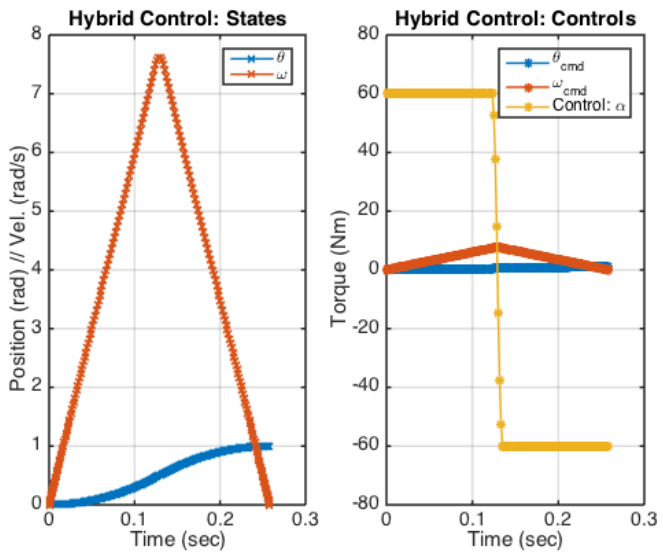

Figure 26. State and control trajectories in acceleration feed-forward optimal control solution

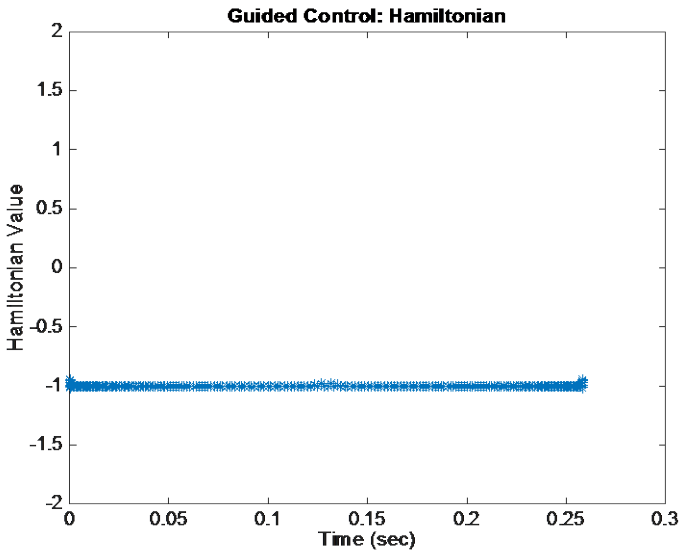

Figure 27. Hamiltonian in acceleration feed-forward optimal control solution

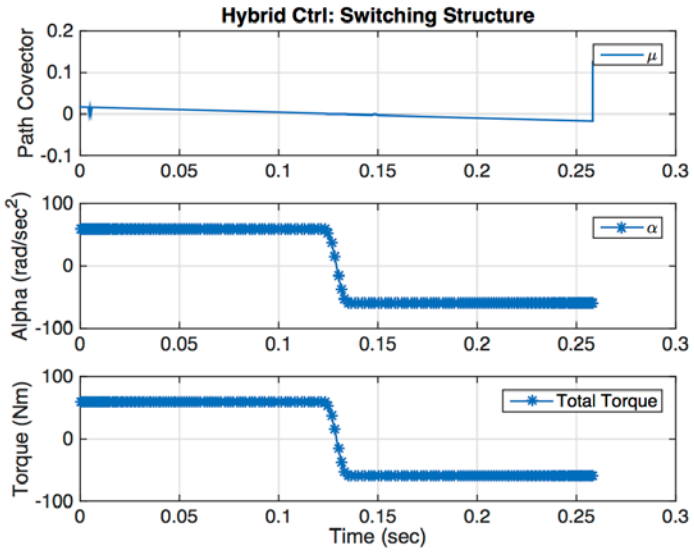

Figure 28. Switching function in acceleration feed-forward optimal control solution

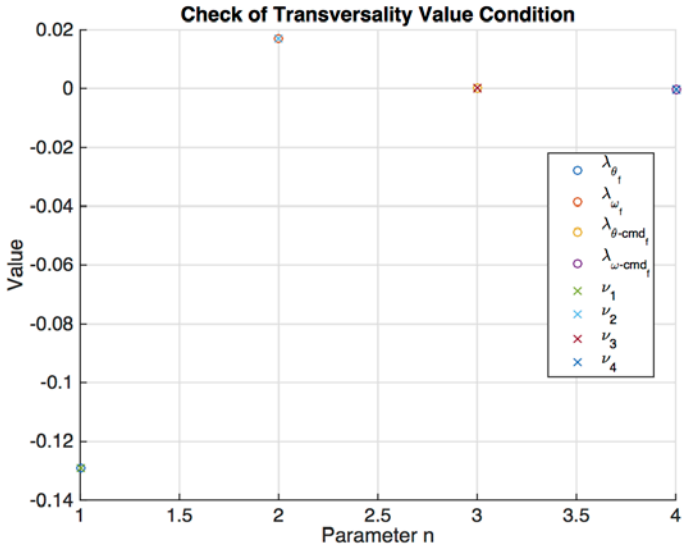

Figure 29. Transversality condition in acceleration feed-forward optimal control solution

The response using the acceleration feed-forward control architecture is very similar to the previous feed-forward control architecture where the feed-forward torque was solved directly. This similarity extends even to the behavior of

the switching function. An examination the underlying similarities to evaluate the mathematical equivalency of the two architectures should be pursued in future work.

E. SUMMARY OF INITIAL CONTROL ARCHITECTURE STUDY

This chapter presented and evaluated the optimal control solutions to several closed-loop control architectures. The results indicate that a feed-forward optimal control implementation is most effective for minimum time maneuvers, completing a maneuver in nearly half the time compared to state-guided control architectures. This result was true for both a torque feed-forward as well as the acceleration feed-forward control architectures.

III. CONTROL ARCHITECTURE VARIATIONS

The results so far indicate that the feed-forward architecture of Chapter II outperforms the guided control architecture variations in terms of both the minimum maneuver time and minimum effort. (See Appendix A for minimum effort solutions.) While the optimization of the guided control architectures should be credited with reducing the maneuver time (recall that the baseline PD controller had a settling time of 0.9 sec), the optimized feed-forward architectures are faster still. It is noteworthy that some degree of overshoot is present in the system responses in all variations of guided control that is absent in all variations of the feed-forward control. The following variations on the guided control architecture will examine the effects of changes on the PD controller gains on the optimal solution.

A. ARCHITECTURE VARIATIONS: OPTIMAL K_V

The first variation will evaluate the velocity gain, k_v, as a parameter to be optimized, to determine if the performance of the guided control architectures can be improved by increasing the damping of the PD controller, which would in turn reduce the overshoot in a standard PD controller.

The control architecture in this variation, shown in Figure 30, is essentially the same as the original guided control architecture but includes the gain k_v as a variable parameter. To be clear, k_v can be varied to determine the optimal value, but remains constant for the duration of any maneuver. This simulates finding the optimal setting for k_v which will remain fixed thereafter.

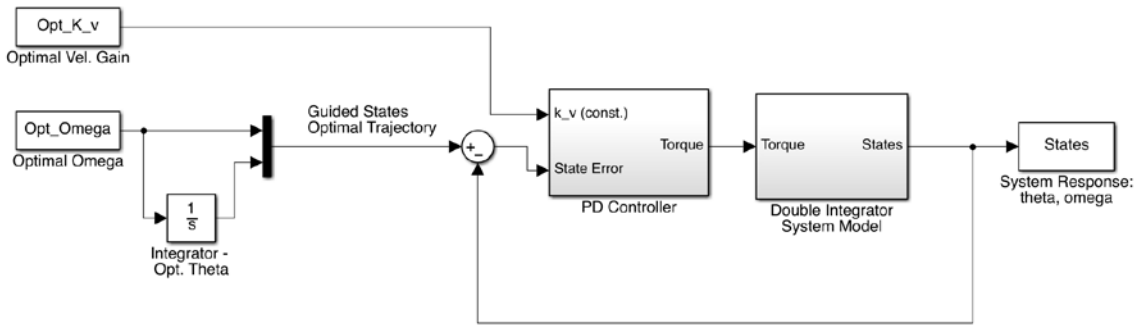

Figure 30. Guided control architecture with selectable velocity gain, k_v.

Problem Statement—Guided Control Variation: Optimal k_v: Perform a minimum time rotation of a rigid body with a pre-existing PD controller using commanded state guidance; velocity gain, k_v, can be varied but will remain constant for the duration of the maneuver. The initial system will be in a position of zero radians at zero velocity, and the final state will be at a position of one radian and zero velocity.

$$\underline{\text{States}}: \quad \vec{x} = \begin{bmatrix} \theta \\ \omega \\ \theta_{cmd} \\ k_v \end{bmatrix} \qquad \underline{\text{Controls}}: \ \vec{u} = \left[\omega_{cmd} \right]$$

$$\underline{\text{minimize}}: \quad J\left[\vec{x}(\bullet), \vec{u}(\bullet), t_f \right] = t_f$$

$$\underline{\text{subject to}}: \quad \dot{\theta} = \omega$$

$$\dot{\omega} = \frac{1}{J_e}\left[k_p \theta_{cmd} - k_p \theta + k_v \omega_{cmd} - k_v \omega \right]$$

$$\dot{\theta}_{cmd} = \omega_{cmd}$$

$$\dot{k}_v = 0 \qquad (1.42)$$

$$t_0 = 0$$

$$t_f = t^f$$

$$\vec{x}_0^T = \left[0,0,0,k_v \right]^T$$

$$\vec{x}_f^T = \left[1,0,1,k_v \right]^T$$

$$-60 \le \left[k_p \theta_{cmd} - k_p \theta + k_v \omega_{cmd} - k_v \omega \right] \le 60$$

Analysis of this problem formulation returns to the same pattern as the other minimum time problems. The HMC yields a switching structure, the Hamiltonian trajectory should be constant at -1 and the final costate values should equal the endpoint covector. The switching structure is presented in equation (1.43) and plots of the solution results are shown in Figures 31–35.

$$\mu_{\tau_{tot}} = -\frac{\lambda_{\omega}}{J_e} - \frac{\lambda_{\theta_{cmd}}}{k_v}$$

and (1.43)

$$\left[k_p\theta_{cmd} - k_p\theta + k_v\omega_{cmd} - k_v\omega\right]\begin{cases} = -60 & if \quad \mu_{\tau_{tot}} \le 0 \\ \in(-60, 60) & if \quad \mu_{\tau_{tot}} = 0 \\ = 60 & if \quad \mu_{\tau_{tot}} \ge 0 \end{cases}$$

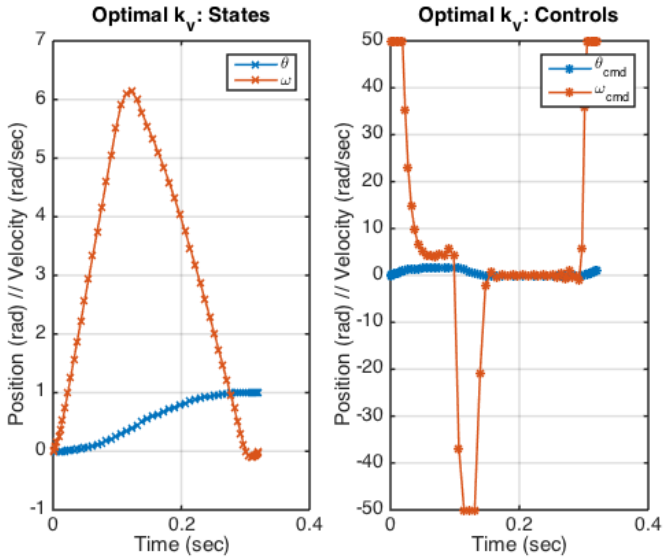

Figure 31. States and control trajectories for gain optimization solution

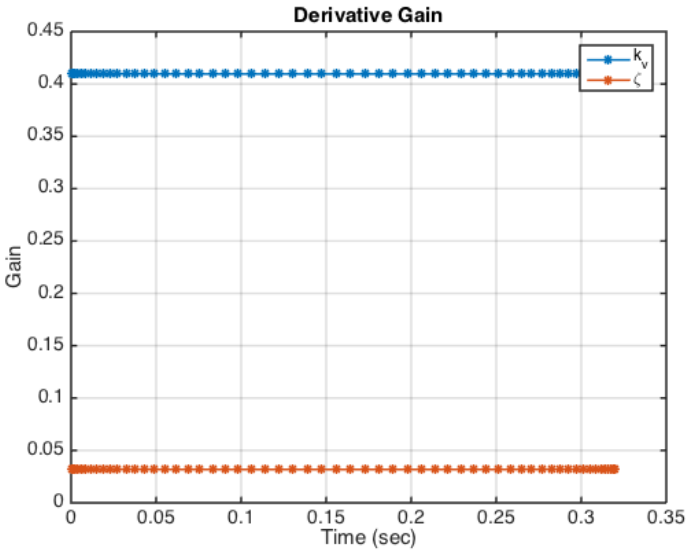

Figure 32. Optimal k_v and damping ratio

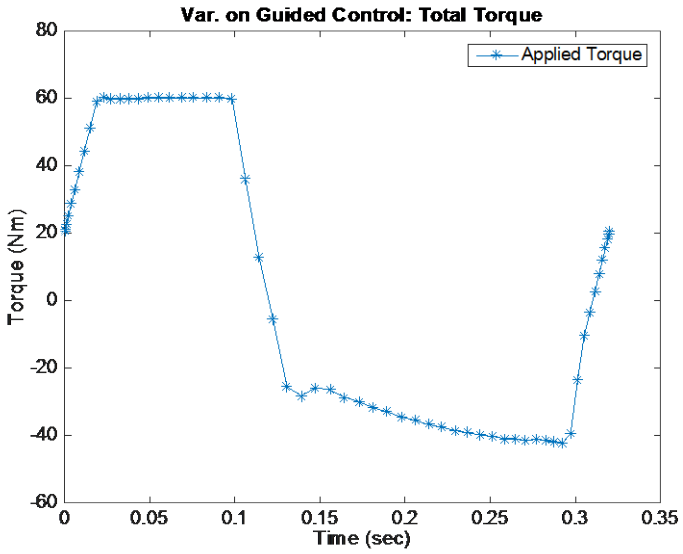

Figure 33. Trajectory of total torque in optimal k_v solution

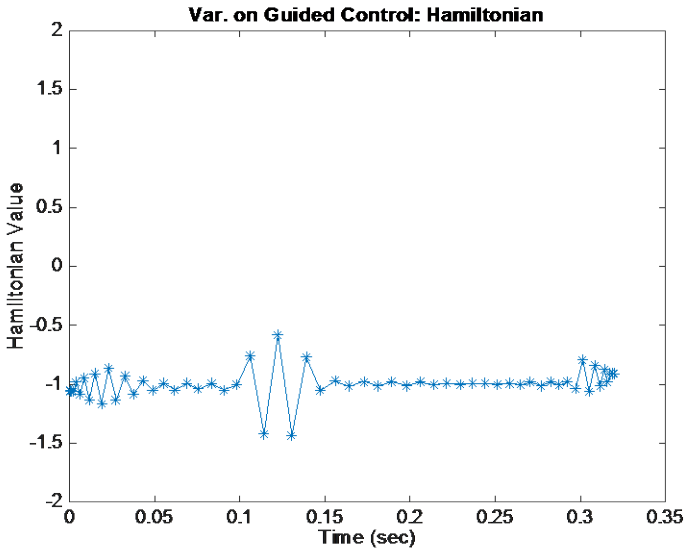

Figure 34. Hamiltonian trajectory of optimal k_v solution

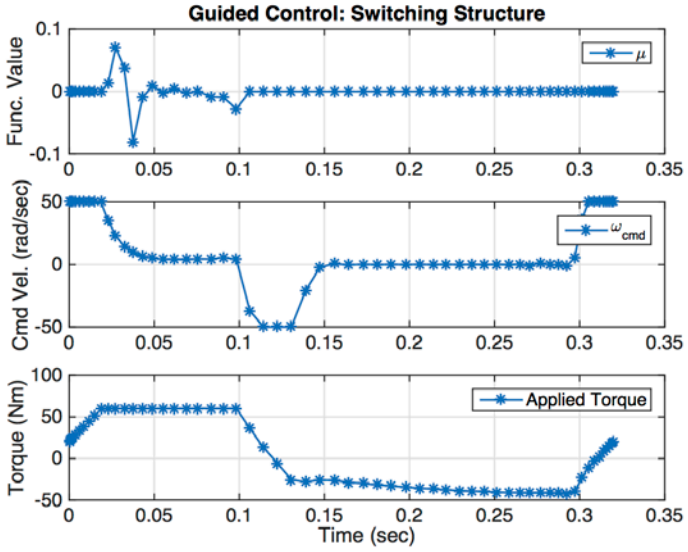

Figure 35. Switching function, control and total torque trajectories of optimal k_v solution

The results plotted in Figure 31 show that the maneuver time can be reduced by changing the velocity gain, but it still does not reach the performance of the feed-forward architecture results. While difficult to discern in Figure 31, some overshoot remains; this is evident in the velocity trajectory, which has a

negative excursion toward the end to compensate for the overshoot. Nevertheless, the change in velocity gain (and consequently the damping ratio) did succeed in reducing the overshoot and improving the performance.

Interestingly, the reduction in overshoot of the optimal solution was achieved by *reducing* the velocity gain and damping ratio, making the system more underdamped than it was before. In classical control methods, this would result in greater overshoot, more oscillations about the final position and longer total maneuver time. This is a very counterintuitive result that could be further investigated in future work.

It should be noted that some of the necessary conditions are not entirely met. The Hamiltonian is not as smooth as the Hamiltonian evolution equation would require, and because the path covector, μ, is very close to zero for much of the trajectory, the HMC is difficult to verify. Like the acceleration guided optimal control architecture solution, this solution quality could be improved by proper scaling.

B. ARCHITECTURE VARIATIONS: HIGH-BANDWIDTH CONTROL

Another aspect of the system that bears further investigation is the effect the control system gains on the optimal control solution. Recall that the proportional and derivative gains in the baseline system were designed to produce a settling time of 0.9 sec under classical control law, but these gains can be modified to achieve a much faster response with a shorter settling time. Such a modification would most benefit the optimal control architectures that are based on state guidance because with faster response times, the high-bandwidth system would follow the state guidance much more closely.

The maneuver time for the state guidance optimal control architecture was approximately 0.5 sec. Given the objective of having a system response that more closely follows the state guidance, the gains will be recalculated based on a settling time of 0.05 seconds (i.e., 10 times faster). This will achieve a quicker “settling” on the moving target embedded in the guided control trajectories due to

the higher control bandwidth. Using the equations and procedures detailed when describing the baseline system, the new proportional and derivative gains are:

$$k_p = 13,456$$
$$k_v = 160.1 \tag{1.44}$$

The utility of increasing the gains will be evaluated for both the guided control and feed-forward control architectures.

1. High-bandwidth Guided Optimal Control

The problem statement, formulations and descriptive equations and conditions for the high-bandwidth guided optimal control are all the same as the original (low bandwidth) state-guided architecture, so they will not be repeated here. The system response with the increased gains is presented in Figures 36 and 37.

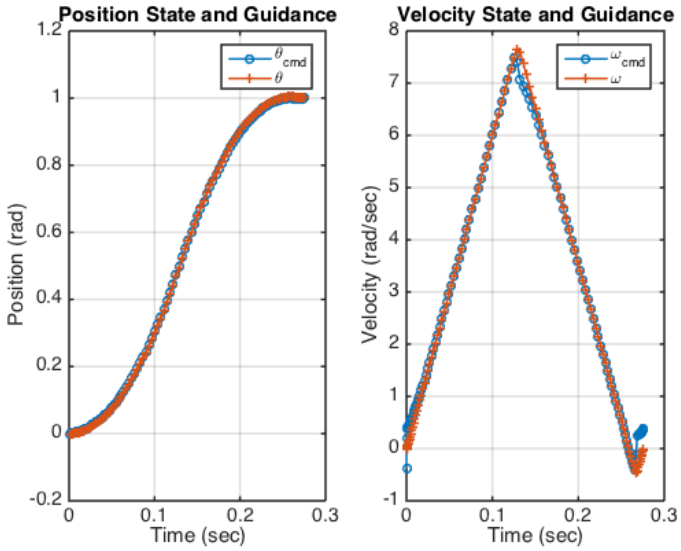

Figure 36. States and commanded states in optimal control solution for high-bandwidth guided control

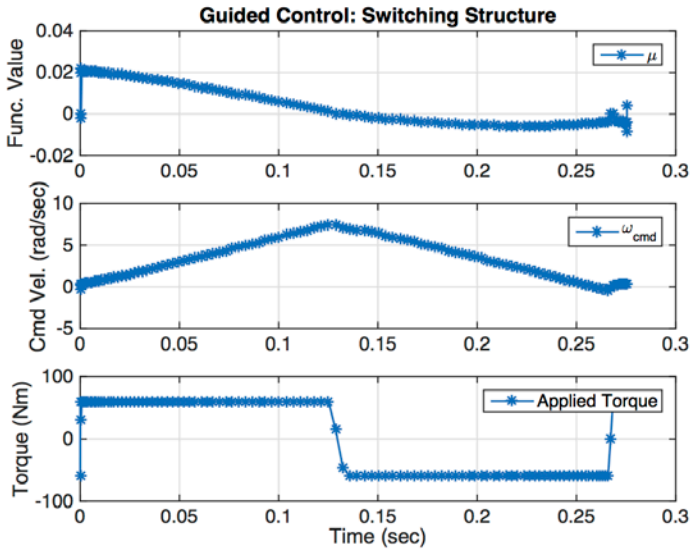

Figure 37. Switching function in optimal control solution for high-bandwidth guided control

The response for the high-bandwidth control system is remarkable in that the performance of the feed-forward architecture with the low gains is nearly matched simply by increasing the gains of the PD controller; the guided control with increased gains completes the maneuver in 0.27 seconds, whereas the feed-forward architecture with the lower gains completes the maneuver in 0.26 seconds. Recall that the guided control architecture with the original, lower gains completed the maneuver in 0.5 seconds. A small amount of overshoot in the response remains, although it is nearly imperceptible in Figure 36; this may be reason that the response does not quite match the response of the feed-forward system. Note also that the third “bang” of torque is still present, albeit for a much smaller duration. Although increasing the gains has allowed the high-bandwidth system to better track the guided inputs, the control loop is much more susceptible to noise effects than the lower bandwidth feedback.

2. High-bandwidth Feed-Forward Optimal Control

The response of the guided control architecture was dramatically improved when the gains were increased. Because the feed-forward architecture

essentially bypasses the controller feedback to produce the maximum torque in a bang-bang trajectory, the responsiveness of the controller which is determined by the gains should not be a factor in the overall system response. To verify this hypothesis, the high-bandwidth optimal control problem is solved. This problem formulation and analysis, matches the original feed-forward problem so they will not be represented here. The results are illustrated in Figures 38 and 39.

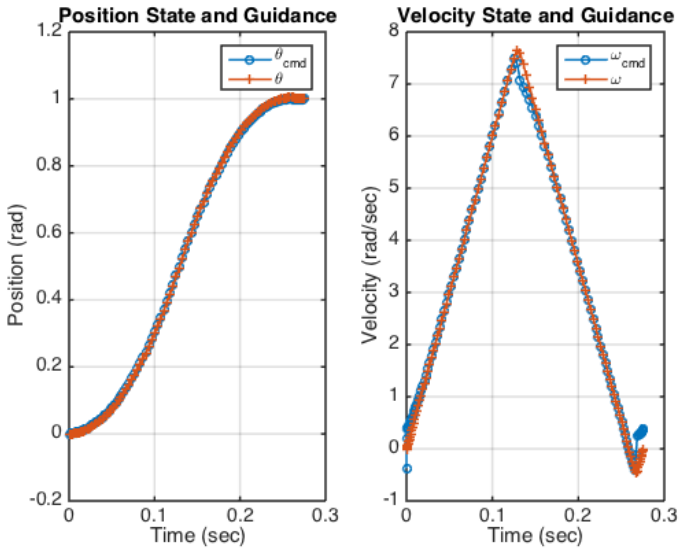

Figure 38. State and control trajectory of high-bandwidth feed-forward optimal control

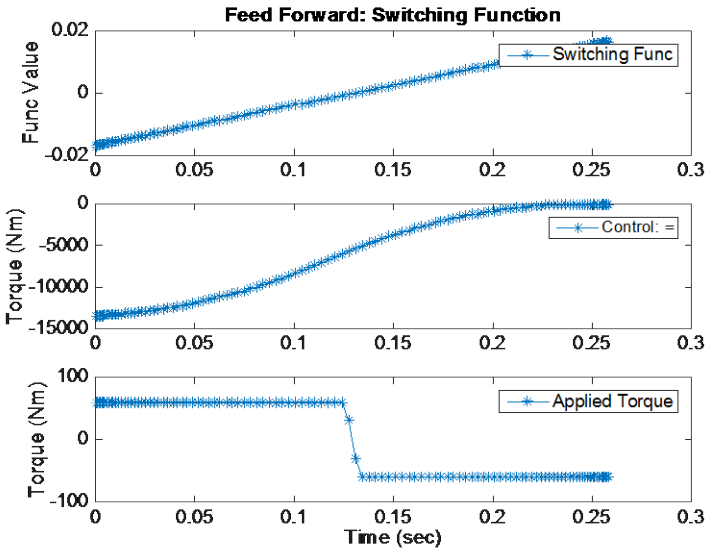

Figure 39. Switching function of high-bandwidth feed-forward optimal control

The feed-forward solution completes the maneuver in 0.26 seconds; this is the same maneuver time as the first feed-forward solution with the lower gains. Note also that the control torque is modulated to affect the same “bang-bang” torque profile as in the first feed-forward solution, and that Figure 39 illustrates that the necessary condition is satisfied.

The extreme values of the control torque produced in this solution are an artificiality of the model and warrants some explanation. Recall that the feed-forward architecture retains the step input as a commanded position guidance. With the increased gains, the torque signal produced by the PD controller alone would be very high, on the order of 10^5 Nm. Because the total applied torque constraint of ± 60 Nm is still in effect, the optimal control solution modulates the control torque such that the when combined with the feedback torque from the PD controller, the total torque does not exceed this constraint. This was also true of the first feed-forward architecture, but the effect was much smaller due to the smaller feedback gains.

3. High-bandwidth Acceleration Feed-Forward Control

The next step to explore the performance of the architecture with the increased gains is to apply the same increased gains to the acceleration feed-forward control architecture. Recall that in this architecture, rotational acceleration is the control variable. Based on the rotation acceleration guidance, the position and velocity state guidance is provided to the PD controller; also, a feed-forward torque signal is produced based on the product of the rotational acceleration and the nominal rotational inertia. Recall that in the hybrid architecture with the original lower gains, the performance matched the feed-forward architecture, with a maneuver time of 0.26 seconds. The performance in this architecture with the increased gains is expected to be similar. The model, problem formulation and necessary conditions are the same for this architecture as they were for the original hybrid architecture, so they will not be recapitulated here. The results of this problem are presented in Figures 40 and 41.

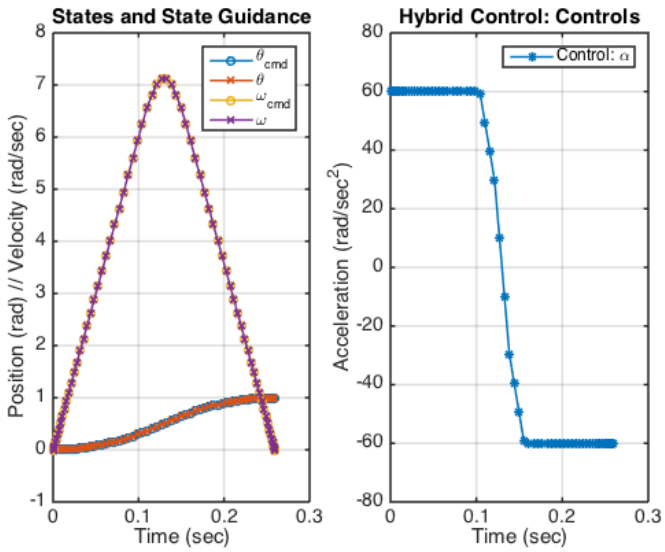

Figure 40. State and control trajectories in optimal control solution for high-bandwidth acceleration feed-forward architecture

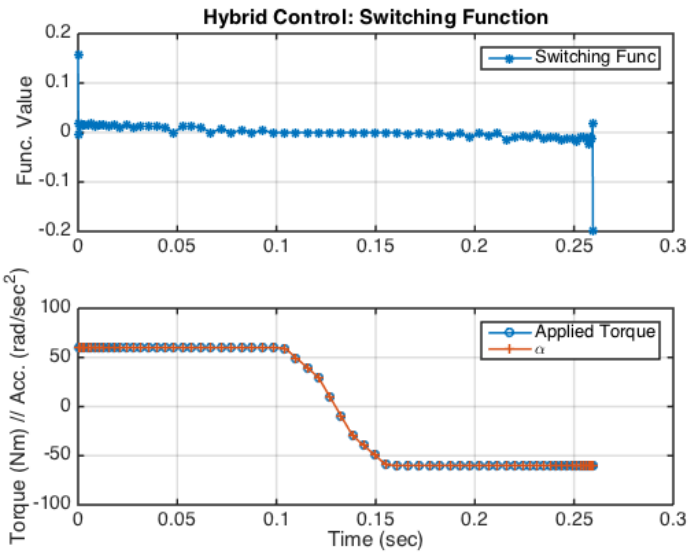

Figure 41. Switching function in optimal control solution for high-bandwidth acceleration feed-forward architecture

The state trajectories match the command states exactly; they are plotted over each other in Figure 40 to highlight this fact. Note also that the maneuver time in this case, like the feed-forward architecture previously discussed, completes the maneuver in 0.26 seconds and is not improved with the increased gains.

C. SUMMARY

This chapter explored the implication of manipulating the PD controller gains in achieving an optimal minimum time maneuver for several control architectures. The results indicate that the control bandwidth of an architecture with a feed-forward control input does not affect its performance. Conversely, if the optimal control implementation is limited to state guidance, increasing the control bandwidth of the feedback loop enables the system to more closely follow the optimal state trajectory, and reduces maneuver time. This, however, comes at the cost of increased susceptibility to noise in the feedback loops.

IV. IMPACTS OF UNCERTAINTY ON ONE-DIMENSIONAL CLOSED-LOOP OPTIMAL CONTROL

The primary purpose of implementing optimal control with feedback is to correct for the uncertainties that will invariably occur in real world systems. The uncertainty evaluated in this study consists of uniformly distributed ±10% uncertainty in the rotational inertia; this degree of uncertainty is typical in real astronautical systems. Variations in the actual rotational inertia of the system will result in variations of the settling time for a given maneuver. The settling time is defined as the time required for the system to reach and stay within 2% of the commanded or final position. (Note that this definition of settling time, a typical figure of merit in control design, differs from the maneuver time predicted by the optimal control solution which corresponds to reaching the exact desired end state.)

The data presented in this chapter result from the verification and validation (V&V) of the optimal control solutions developed and discussed in the previous chapters of this thesis. For each control architecture, the V&V is executed with a simple ODE45 propagator based on the control variable trajectory from the optimal control solution and the system dynamics. For illustrative purposes, selected results of V&V analyses for both the guided optimal control and feed-forward optimal control architectures are presented in Figures 42 and 43. As predicted in the optimal control solution, the feed-forward position trajectory has minimal overshoot; the overshoot that does exist in these plots is due to the variation of the actual inertia. Note also the comparatively large overshoot of the trajectories in the guided optimal control systems; this is nearly 50% overshoot, much greater than even the baseline system response, which had only a 5% overshoot. In spite of the large overshoot, the nominal settling time of guided optimal control solution is half of that of the baseline system. It must be noted that in a real world application, a 50% overshoot may

not be acceptable due to other constraints or considerations, regardless of the settling time.

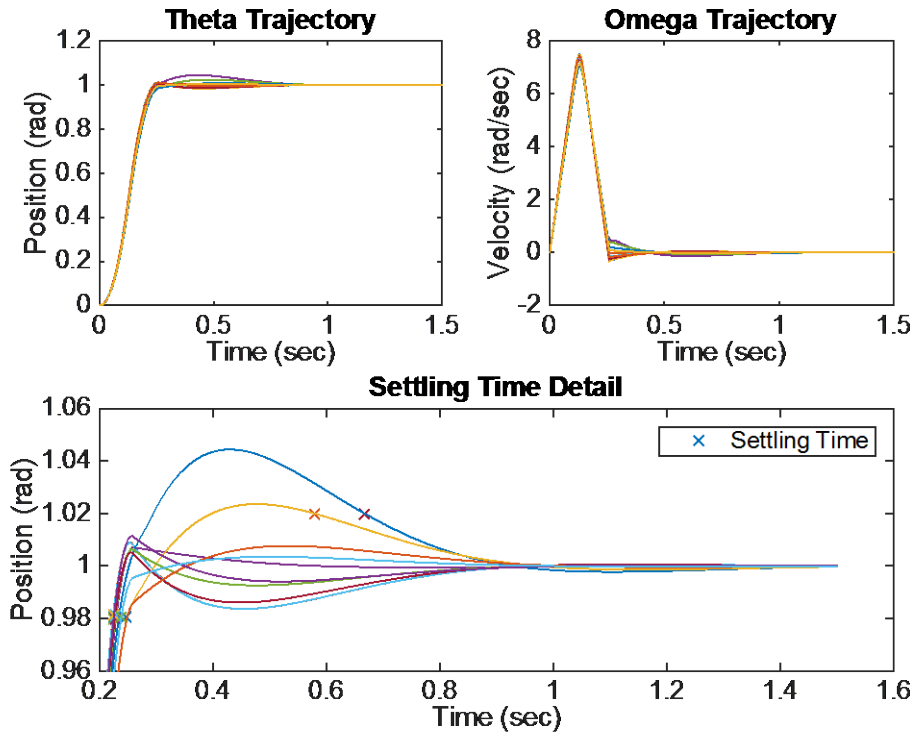

Figure 42. Feed-forward optimal control with inertia uncertainty

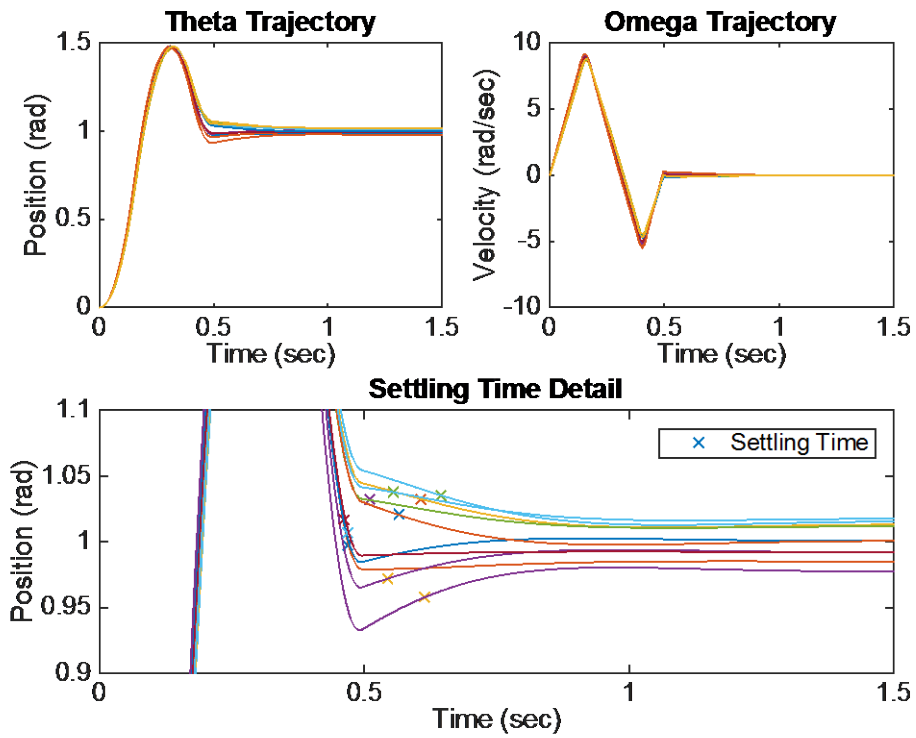

Figure 43. State-guided optimal control with inertia uncertainty

The overall impact of the inertia uncertainty is evaluated using a Monte Carlo analysis. Monte Carlo analysis is particularly useful in analyzing the behavior of systems with multiple sources of variation, such as noisy signals or design uncertainties. In a Monte Carlo analysis, a simulation is repeated numerous times allowing each source of noise or uncertainty to vary individually according to its own probability function to determine the impact of all sources of uncertainty on the overall performance of the system. Strictly speaking, because there is only one source of uncertainty, a Monte Carlo analysis is not necessary in this case, but this analytical approach can be applied as more sources of variation and uncertainty are incorporated in future work.

A. ANALYSIS OF UNCERTAINTY RESULTS

The results of a Monte Carlo analysis of the impact of a uniformly distributed variation of rotational inertia in each optimal control architecture are

presented in Appendix B. These plots are combined scatter plot and histograms; the scatter plot contains a data point on the inertia and settling time axes for each simulation and the histograms illustrate the probability distribution of the data. In addition to better illustrating the results, this structure also facilitates confirmation that the selected inertia values were drawn from a uniform distribution.

The results of the simulations with inertia variation show the impacts that uncertainty can have on the system response. Note that the feed-forward architecture and acceleration feed-forward architecture both have similar distributions of settling time, and are both, generally, better performing than the guided control architecture. Interestingly, while the mean, mode, and median settling time of the feed-forward and acceleration feed-forward architecture responses were all better than those of the guided control architectures—nearly half of the time of the guided control architecture settling time—there were also some outlier settling times that were actually worse than the worst response of the guided control architecture. Unlike the distribution of settling times in the guided control architecture, the distribution of the outliers in the feed-forward and hybrid results is fairly uniform and does not appear to be part of a larger trend. This may simply be an artifact of the numerical approximations used in the ODE45 propagator and should be investigated further.

Another interesting observation from the simulations is that when the gains of the PD controller are increased, the performance of the guided control architecture improves dramatically. Indeed, in terms of setting times, the performance of all three architectures is nearly the same, with only hundredths of seconds separating them (less than 1%). Further, with the increased gains, the inertia uncertainty has virtually no impact on settling time for any of the architectures. (A few “outliers” exist in the guided control architecture response, but again these results differ from the mean by only hundredths of seconds.)

The variation of control effort with inertia across the architectures is also interesting. (Control effort is defined using the traditional quadratic cost metric; see Appendix A for further discussion of control effort.) In each case, the control

effort required varies linearly with inertia. While this result is intuitive at some level in that it requires more work to displace a larger object than a smaller object, it is also intuitive to expect that the incorporation of the optimal control methods with feedback designed for a particular inertia would result in the need for additional feedback torque (i.e., control effort) when applied to off-nominal inertias. As an example, in the feed-forward architecture, in the nominal system response should precisely achieve the desired end state based on the feed-forward torque signal alone; any off-nominal cases would have that same torque application but would also require feedback torque to compensate for the actual (off-nominal) state after the application of the feed-forward torque. It seems intuitive that this would have resulted in a parabolic or v-shaped distribution of control effort, with the minimum at an inertia of $1.0\ kg \cdot m^2$. That this effect does not appear in the data bears further investigation. An example distribution is extracted from Appendix B and presented in Figure 44.

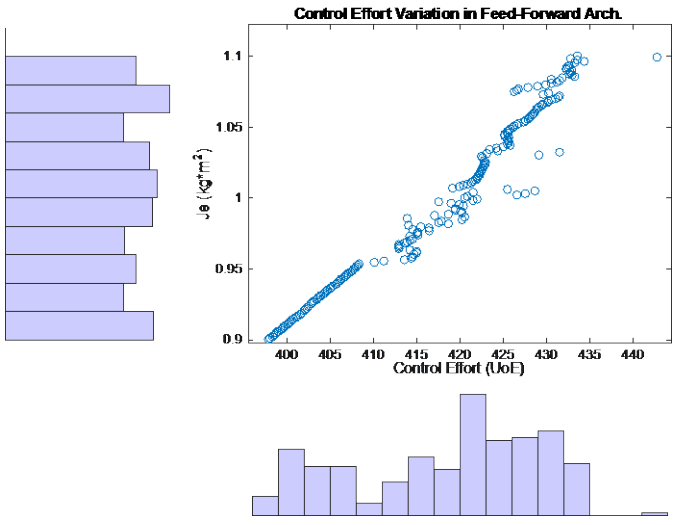

Figure 44. Impact of uncertainty on optimal acceleration feed-forward architecture

Another interesting observation is that that the acceleration feed-forward architecture does not have better performance in terms of settling time compared

to the feed-forward architecture, which was not expected. Because the acceleration feed-forward architecture uses both feed-forward and guided state control, a sort of “belt and suspenders” approach, this was expected to provide better feedback compensation for the off-nominal trajectories resulting from off-nominal inertias. The optimal state trajectories contained in the state guidance is for the nominal inertia; a different inertia would have a different optimal trajectory. In retrospect, attempting to guide the system to follow a sub-optimal trajectory should not be expected to achieve optimal results. However, note that while this is the case for internal variations and uncertainties, acceleration feed-forward control would likely improve performance in the presence of external disturbances. In that case, the inclusion of state guidance would allow deviation from the optimal trajectory to be more quickly detected and corrected and would likely result in improved overall system performance.

B. CONCLUSION OF CLOSED-LOOP OPTIMAL CONTROL ARCHITECTURE STUDY

So far, this study has evaluated several closed-loop implementations of optimal control architectures, highlighting some advantages and disadvantages amongst the variants. Closing the control loop is an approach that enables compensating for system uncertainties; such effects were simulated using variation of inertia as the source of uncertainty. The well known “bang-bang” control was manifest in some of the architectures that incorporated a feed forward torque, but the architectures that were based entirely on state guidance required a “bang-bang-bang” control profile.

The performance differences across the architectures were interesting. With the initial, lower PD gains, the feed forward architectures completed the maneuver in half of the time as the state guidance architectures. But, if the system’s PD gains can be manipulated, the performance of the feed forward architecture can be matched with state guidance control architectures. The increased PD gains provide the additional advantage of dramatically reducing

performance variance due to inertia uncertainty, a feature of high-bandwidth control.

The results and insights gained in this study will spawn several avenues of future work. One aspect that bears further study is the underlying relationship between the feed forward optimal control architecture and the acceleration feed-forward optimal control architecture. That the performance could be replicated in two different architectures indicates that there may be some fundamental control relationship that could be further exploited. Additionally, and more broadly, the concepts developed for the one-dimensional double integrator system can now be applied to three-dimensional rotating bodies.

THIS PAGE INTENTIONALLY LEFT BLANK

V. A REAL-TIME OPTIMAL CONTROLLER FOR ONE-DIMENSIONAL ROTATIONAL MANEUVERS

The previous exploration of closed-loop optimal control architectures demonstrated that the feed-forward architecture and its variants achieve the best performance in terms of executing minimum time maneuvers. In light of this finding, the feed-forward architecture and optimal control solution will be further developed. If an analytical solution to the feed-forward control torque can be found, this solution could easily be transitioned to a real-time implementation in which the feed-forward torque is continuously modified and updated in response to current feedback measurements to achieve the minimum time maneuver in the presence of system uncertainties, external disturbances and other non-idealities.

A. ANALYSIS OF THE FEED-FORWARD CONTROL TORQUE

In this section, an expression for the feed-forward control torque is developed. Recall that the PD controller produces a feedback torque based on the difference between the commanded states and the actual states (i.e., the state error).

In the feed-forward architecture, the total torque applied to the plant is the sum of the feed-forward control torque, $\tau_{ctrl}(t)$, and the PD controller feedback torque. The total torque is described by the following equation:

$$\tau_{tot}(t) = \tau_{ctrl}(t) + k_p\left(\theta_{cmd}(t) - \theta(t)\right) - k_v\omega(t) \tag{1.45}$$

The commanded position, $\theta_{cmd}(t)$, is a step function:

$$\theta_{cmd}(t) = \theta_D u(t), \tag{1.46}$$

where

$$u(t)=\begin{cases} 0, & for \quad t<0 \\ 1, & for \quad t\geq 0 \end{cases}$$

and the scalar θ_D is the magnitude of the commanded position. Note also that the angular rate is the time derivative of position.

$$\omega(t)=\frac{d\theta}{dt} \tag{1.47}$$

With the preceding substitutions, total torque is given by the following equation:

$$\tau_{tot}(t)=\tau_{ctrl}(t)+k_p\left(\theta_D u(t)-\theta(t)\right)-k_v\frac{d\theta}{dt} \tag{1.48}$$

The classical analysis technique of Laplace Transforms, as described in Chen [1] will be helpful in further analyzing this problem. Taking the Laplace Transform of the total torque equation, (1.48), yields the following:

$$\mathcal{L}\left\{\tau_{tot}(t)\right\}=\mathcal{L}\left\{\tau_{ctrl}(t)+k_p\left(\theta_D u(t)-\theta(t)\right)-k_v\frac{d\theta}{dt}\right\}$$

$$\tau_{tot}(s)=\tau_{ctrl}(s)+\frac{\theta_D k_p}{s}-k_p\Theta(s)-k_v\left(s\cdot\Theta(s)-\theta_0\right)$$

$$\tau_{tot}(s)=\tau_{ctrl}(s)+\frac{\theta_D k_p}{s}-\left(k_p+k_v s\right)\Theta(s)+k_v\theta_0 \tag{1.49}$$

To solve for the feed-forward control torque, $\tau_{ctrl}(s)$, the system's position response in the frequency domain, $\Theta(s)$, may be substituted into (1.49). A complete expression of the system response consists of both the response due to control inputs as well as the response due to the system initial conditions, known as the zero-state response and the zero-input response, respectively [1].

An advantage of working in the Laplace domain is that the total system response is simply the sum of the various responses:

$$\Theta(s) = \Theta_{ZS}(s) + \Theta_{ZI}(s) \tag{1.50}$$

To facilitate the development of the zero state response, $\Theta_{ZS}(s)$, a more detailed block diagram of the closed-loop feed-forward architecture is presented in Figure 45.

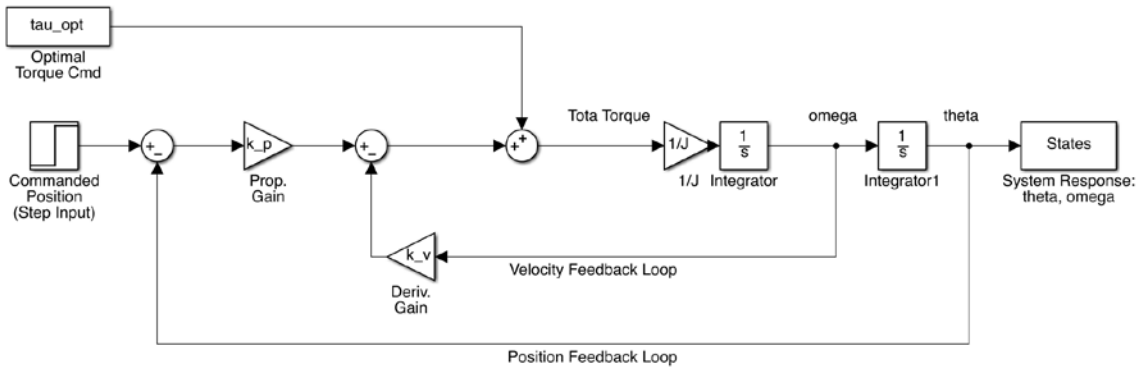

Figure 45. Detailed block diagram of closed-loop feed-forward optimal control architecture

This control architecture has two control inputs, the control torque, $\tau_{ctrl}(s)$, and commanded position, $\Theta_{cmd}(s)$. In a fashion similar to the expression of the overall system response, the expression of the zero state response is the sum of the response to each of the control inputs individually. This expression is determined by finding the transfer function due to each input while setting the other input to zero. Using this idea and the typical block diagram manipulation techniques yields the following equation for the zero state response:

$$\Theta_{ZS}(s)=\frac{\Theta(s)}{\Theta_{cmd}(s)}\cdot\Theta_{cmd}(s)+\frac{\Theta(s)}{\tau_{ctrl}(s)}\cdot\tau_{ctrl}(s)$$

$$\Theta_{ZS}(s)=\left(\frac{k_p}{Js^2+k_vs+k_p}\right)\cdot\Theta_{cmd}(s)+\left(\frac{1}{Js^2+k_vs+k_p}\right)\cdot\tau_{ctrl}(s) \tag{1.51}$$

An analysis of the total torque equation will enable developing the zero input response.

$$\begin{aligned} J\ddot{\theta}(t)&=\tau_{tot}(t)\\ J\ddot{\theta}(t)&=\tau_{ctrl}(t)+k_p\left(\theta_{cmd}(t)-\theta(t)\right)-k_v\omega(t)\end{aligned} \tag{1.52}$$

Setting both inputs to zero and taking the Laplace transform yields the following:

$$\mathcal{L}\left\{J\ddot{\theta}_{ZI}(t)\right\}=\mathcal{L}\left\{-k_p\theta(t)-k_v\frac{d\theta}{dt}\right\}$$

$$s^2\cdot\Theta_{ZI}(s)-s\cdot\theta_0-\dot{\theta}_0=\frac{1}{J}\left[-k_p\Theta_{ZI}(s)-k_vs\cdot\Theta_{ZI}(s)+k_v\theta_0\right]$$

$$\left[s^2+\frac{k_v}{J}s+\frac{k_p}{J}\right]\cdot\Theta_{ZI}(s)=\dot{\theta}_0+s\cdot\theta_0+\frac{k_v}{J}\theta_0$$

$$\Theta_{ZI}(s)=\frac{\omega_0}{s^2+\frac{k_v}{J}s+\frac{k_p}{J}}+\frac{\left(s+\frac{k_v}{J}\right)\theta_0}{s^2+\frac{k_v}{J}s+\frac{k_p}{J}} \tag{1.53}$$

Thus, the total system response can be described by the following equation:

$$\Theta(s)=\Theta_{ZS}(s)+\Theta_{ZI}(s)$$

$$\Theta(s)=\left(\frac{k_p}{Js^2+k_vs+k_p}\right)\cdot\Theta_{cmd}(s)+\left(\frac{1}{Js^2+k_vs+k_p}\right)\cdot\tau_{ctrl}(s)+\frac{\omega_0}{s^2+\frac{k_v}{J}s+\frac{k_p}{J}}+\frac{\left(s+\frac{k_v}{J}\right)\theta_0}{s^2+\frac{k_v}{J}s+\frac{k_p}{J}} \tag{1.54}$$

Substituting the system response, $\Theta(s)$, into the equation for the total torque, $\tau_{tot}(s)$, and conducting a significant number of partial fraction reductions yields the following expression for the control torque:

$$\tau_{tot}(s) = \tau_{ctrl}(s) \cdot \left(\frac{Js^2}{Js^2 + k_v s + k_p} \right) + k_p \theta_D \cdot \left(\frac{Js^2}{Js^3 + k_v s^2 + k_p s} \right) - \frac{\left(\omega_0 k_v + \theta_0 k_p \right) \cdot s + \omega_0 k_p}{s^2 + \frac{k_v}{J} s + \frac{k_p}{J}}$$

$$\tau_{ctrl}(s) = \tau_{tot}(s) \cdot \left(\frac{Js^2 + k_v s + k_p}{Js^2} \right) - \frac{k_p \theta_D}{s} + \frac{k_v \omega_0 + k_p \theta_0}{s} + \frac{k_p \omega_0}{s^2} \tag{1.55}$$

Equation (1.55) for the feed-forward control torque is given in terms of the total torque. Fortunately, the previous optimal control analysis provides some insight into what the total torque function should be for an optimal maneuver. In the optimal maneuver, the total torque profile (in the time domain) is the “bang-bang” profile, as depicted in the Figure 46. More specifically, the initial torque application is at the maximum torque limit for some amount of time; after the proper interval, torque is applied at the maximum negative torque limit until the maneuver is complete at which point the torque is reduced to zero.

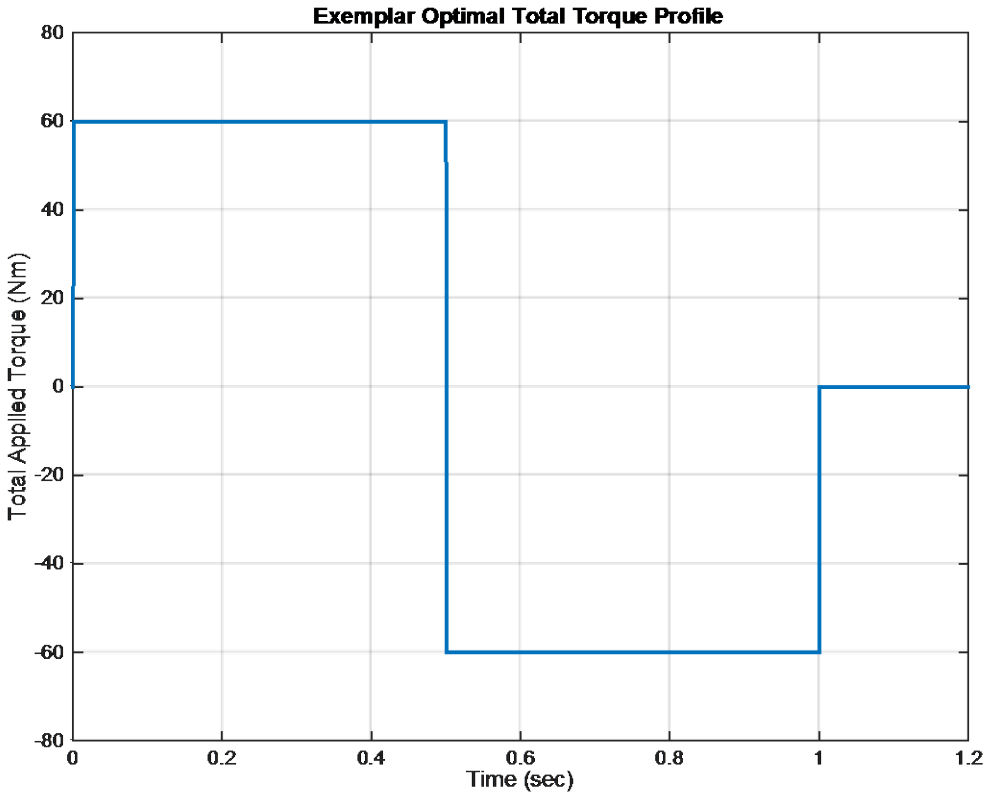

Figure 46. Example of optimal total torque trajectory

In the example shown in Figure 45, the maximum torque limits are ±60Nm, the switch time, t_{sw}, is 0.5 seconds and the maneuver is completion time, t_f, is 1.0 sec. Note that in this example, the switch time is exactly halfway through the maneuver. While this would be expected for a maneuver that starts from rest (i.e. $\omega_0 = 0$), if the initial conditions were different, the duration of each torque interval would be modified accordingly. Examples of such a situation will be given in a future section when the kinematics of the bang-bang maneuver are described.

A general form of the optimal total torque, τ_{tot}^*, profile is defined mathematically in the following equation:

$$\tau_{tot}^{*}(t) = \tau_{\max} \cdot u(t) - 2\tau_{\max} \cdot u\left(t - t_{sw}\right) + \tau_{\max} \cdot u\left(t - t_f\right) \tag{1.56}$$

Taking the Laplace transform of (1.56) yields the following:

$$\begin{aligned} \mathcal{L}\left\{\tau_{tot}^{*}(t)\right\} &= \mathcal{L}\left\{\tau_{\max} \cdot u(t) - 2\tau_{\max} \cdot u\left(t - t_{sw}\right) + \tau_{\max} \cdot u\left(t - t_f\right)\right\} \\ \tau_{tot}^{*}(s) &= \tau_{\max}\left[\frac{1}{s} - \frac{2}{s} \cdot e^{-t_{sw} \cdot s} + \frac{1}{s} \cdot e^{-t_f \cdot s}\right] \end{aligned} \tag{1.57}$$

Substituting (1.57) into (1.55) yields the following:

$$\tau_{ctrl}(s) = \tau_{\max}\left[\frac{1}{s} - \frac{2}{s} \cdot e^{-t_{sw} \cdot s} + \frac{1}{s} \cdot e^{-t_f \cdot s}\right] \cdot \left(\frac{Js^2 + k_v s + k_p}{Js^2}\right) - \frac{k_p \theta_D}{s} + \frac{k_v \omega_0 + k_p \theta_0}{s} + \frac{k_p \omega_0}{s^2}$$

$$\begin{aligned} \tau_{ctrl}(s) = {} & \frac{k_p \omega_0}{s^2} + \frac{k_v \omega_0 + k_p\left(\theta_0 - \theta_D\right)}{s} \ldots \\ & + \tau_{\max}\left(\frac{Js^2 + k_v s + k_p}{Js^3}\right) - 2\tau_{\max}\left(\frac{Js^2 + k_v s + k_p}{Js^2}\right) \cdot e^{-t_{sw} s} + \tau_{\max}\left(\frac{Js^2 + k_v s + k_p}{Js^2}\right) \cdot e^{-t_f s} \end{aligned} \tag{1.58}$$

Taking the inverse Laplace transform of (1.58) yields:

$$\begin{aligned} \tau_{ctrl}(t) = {} & \omega_0 k_p t + \omega_0 k_v + k_p\left(\theta_0 - \theta_D\right) \ldots \\ & + \tau_{\max}\left[\tfrac{k_p}{2J} t^2 + \tfrac{k_v}{J} t + 1\right] \ldots \\ & - 2\tau_{\max} \cdot u\left(t - t_{sw}\right) \cdot \left[\tfrac{k_p}{2J}\left(t - t_{sw}\right)^2 + \tfrac{k_v}{J}\left(t - t_{sw}\right) + 1\right] \ldots \\ & + \tau_{\max} \cdot u\left(t - t_f\right) \cdot \left[\tfrac{k_p}{2J}\left(t - t_f\right)^2 + \tfrac{k_v}{J}\left(t - t_f\right) + 1\right] \end{aligned} \tag{1.59}$$

Equation (1.59) describes the control torque trajectory for the optimal minimum time maneuver for use with closed-loop feed-forward architecture. The only unknowns remaining in this equation are the switch time and the final maneuver time. But the bang-bang nature of the maneuver simplifies calculation of these remaining unknown variables. By dividing the maneuver into two separate constant acceleration phases, the kinematic equations of constant

acceleration motion can be used to calculate the switch and final times. Figure 47 illustrates this concept.

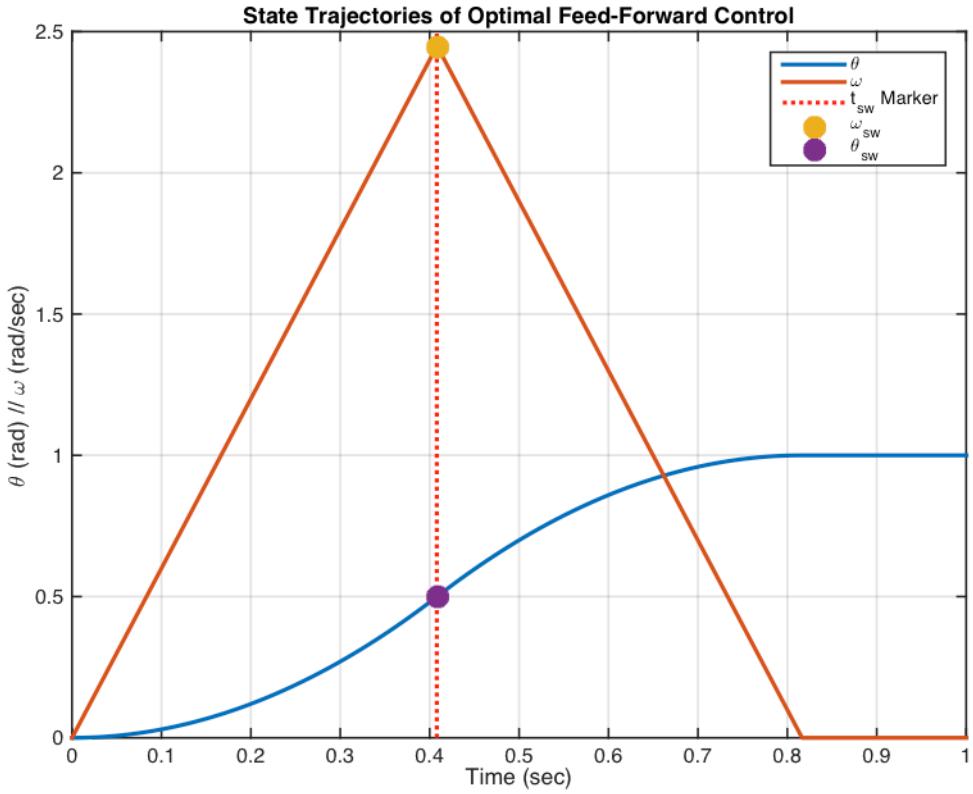

Figure 47. Example of state trajectories in minimum time maneuver

The calculation of the points of interest for the bang-bang maneuver, namely the switch time and final time, is accomplished with the following basic kinematic equations. Note that this process is predicated on the assumption that the initial and final conditions are known and that the acceleration is constant at the maximum value (in each phase).

$$\alpha = \frac{\tau_{\max}}{J} \tag{1.60}$$

$$\theta - \theta_0 = \omega_0 t + \tfrac{1}{2}\alpha t^2 \tag{1.61}$$

$$\omega^2 = \omega_0^2 + 2\alpha\left(\theta - \theta_0\right) \tag{1.62}$$

$$\omega_f = \omega_0 + \alpha \cdot t \tag{1.63}$$

The position that coincides with the switch time, θ_{sw}, can be solved by examining both phases of the maneuver (refer to Figure 46 for an illustration):

Phase 1: $\omega_{sw}^2 = \omega_0^2 + 2\alpha\left(\theta_{sw} - \theta_0\right)$ (1.64)

Phase 2: $\omega_f^2 = \omega_{sw}^2 + 2\left(-\alpha\right)\left(\theta_f - \theta_{sw}\right)$ (1.65)

Rearranging both (1.64) and (1.65) to solve for ω_{sw}^2 and setting them equal to each other leads to the following equation for θ_{sw}:

$$\omega_0^2 + 2\alpha\left(\theta_{sw} - \theta_0\right) = \omega_f^2 - 2\left(-\alpha\right)\left(\theta_f - \theta_{sw}\right)$$
$$4\alpha\theta_{sw} = \omega_f^2 - \omega_0^2 + 2\alpha\theta_f + 2\alpha\theta_0$$

$$\theta_{sw} = \frac{\omega_f^2 - \omega_0^2}{4\alpha} + \frac{\theta_f + \theta_0}{2} \tag{1.66}$$

Having solved for θ_{sw}, the rest of the calculations fall out as follows:

$$\omega_{sw} = \sqrt{\omega_f^2 - 2\left(-\alpha\right)\left(\theta_f - \theta_{sw}\right)} \tag{1.67}$$

$$t_{sw} = \frac{\omega_{sw} - \omega_0}{\alpha} + t_0 \tag{1.68}$$

$$t_f = \frac{\omega_f - \omega_{sw}}{-\alpha} + t_{sw} \tag{1.69}$$

B. ANALYTICAL SOLUTION TO MINIMUM TIME FEED-FORWARD MANEUVER

The preceding section developed an analytical solution for the optimal feed-forward control torque to achieve a minimum time maneuver. This solution will now be compared to the control torque trajectory determined numerically, as discussed and presented in the previous chapter.

Recall that the rotational inertia is taken to be 1 kgm^2, the maximum torque is 60 Nm. The initial conditions are $\theta_0 = 0,\ \omega_0 = 0$; and the final conditions are $\theta_f = 1,\ \omega_f = 0$. Figure 48 illustrates the comparison.

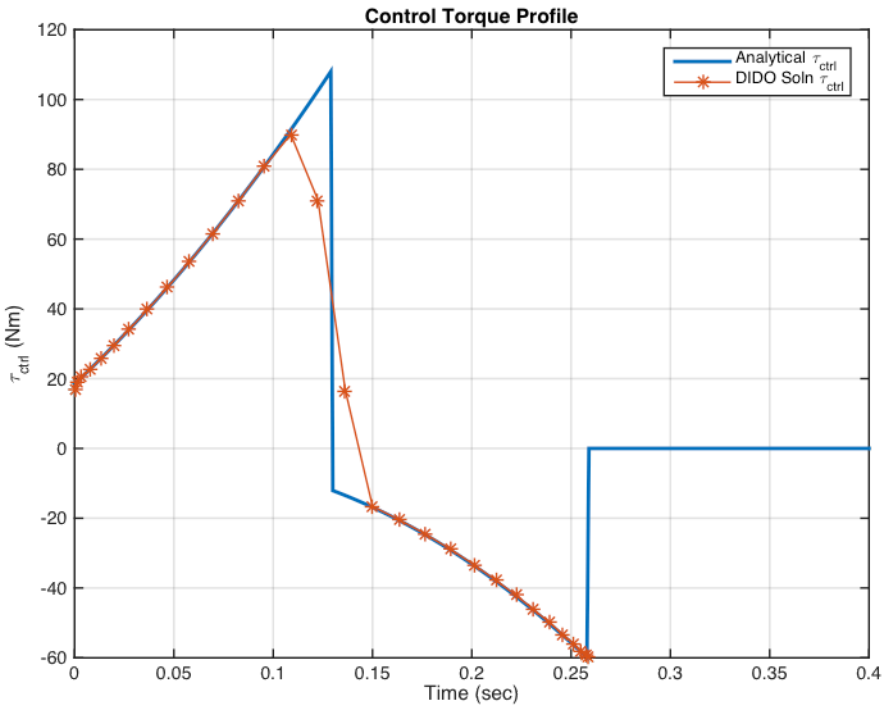

Figure 48. Comparison of analytical and numerical solution for control torque trajectory

Figure 48 clearly shows that the analytical solution developed in section B is correct. The added benefit of the analytical solution over the numerical solution

is that the control torque trajectory is precisely defined at any arbitrary time, *t*, throughout the maneuver. Consequently, the total torque profile is a more crisp bang-bang. This results in the ability to execute a more precise maneuver.

C. TRANSITIONING TO REAL-TIME OPTIMAL CONTROL

Transitioning the analytical solution developed in section A to a real time optimal control solution will require several adaptations. These adjustments include accommodating all maneuvers types (e.g., forward motion, reverse motion, and non-rest-to-rest maneuvers) and modifying the control torque equation for a shifting time reference.

1. Variations on the Bang-Bang Profile

The minimum time problem discussed to this point has consisted of a particular set of boundary conditions leading to a particular bang-bang maneuver solution. The problem assumed forward motion (from $\theta_0 = 0$ to $\theta_f = 1$) from an initial rest condition to a final rest condition (i.e., $\omega_0 = 0,\ \omega_f = 0$). For such a problem, the minimum time maneuver consists of the application of maximum positive torque for some duration of time followed by an application of maximum negative torque for some other duration of time. As previously mentioned, starting from a non-rest condition would simply modify the durations of the positive and negative torque applications, without affecting the general torque profile of positive followed by negative maximum torque applications.

It is conceivable that the initial conditions are such that only a single torque application is necessary (a single-bang maneuver). More interestingly, it is conceivable that the initial velocity is so great that, even with application of maximum negative torque, the system would overshoot the commanded final position. In such an over-speed situation, the optimal total torque application is still a bang-bang profile, however the signs are reversed and the optimal bang-bang trajectory would consist of maximum negative torque application followed by maximum positive torque. Such a sequence is illustrated in Figure 49. In a

similar way, the combination of initial conditions will dictate the total torque profile for maneuvers in the reverse direction.

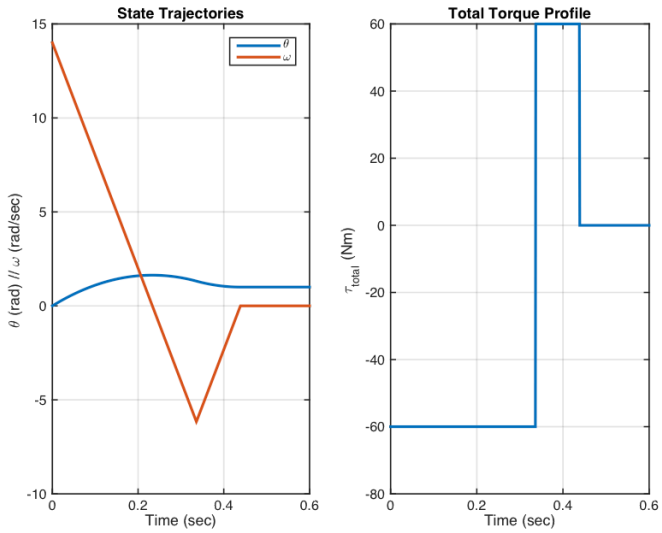

Figure 49. Example of an over-speed maneuver in the positive direction

As Athans and Falb demonstrated [5], the variety of conditions (e.g., forward, reverse, forward over-speed and reverse over-speed) is best illustrated in the normalized state plane (normalized in that the final conditions are at the origin of the state plane).[1] Examine Figure 50; this is a plot of trajectories of optimal maneuvers from various initial conditions. System states in quadrants III and IV are forward maneuvers; system states in quadrants I and II are reverse maneuvers. The dotted red lines are state trajectories resulting from the application of maximum negative torque and the dotted blue lines are state trajectories resulting from the application of maximum positive torque. Assuming that the desired final conditions are at the origin, the solid red line is the collection of states from which the system can be driven to the final conditions with a single

[1] The use of the state plane to illustrate this point is inspired by the work of Athans and Falb's real-time optimal control method [5]. The inclusion of an underlying PD controller distinguishes the results of this thesis from their work, but because the optimal total torque trajectories at the plant input are the same, the kinematic effects are also the same.

application of maximum negative torque; and the solid blue line is the collection of states from which the system can be driven to the final conditions with a single application of maximum positive torque [5]. If the system states, initial or otherwise, of a forward maneuver are above the solid red line, it is in an over-speed condition and will overshoot the final position; if the system states of a reverse maneuver are below the solid blue line, then it is also in an over-speed condition, but in the other direction.

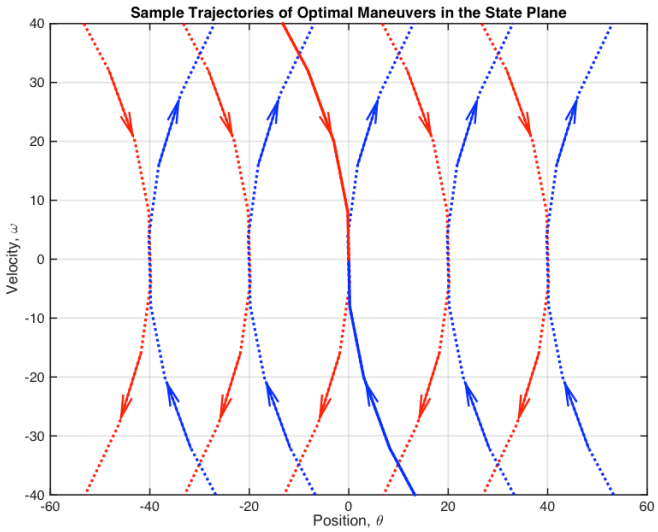

Figure 50. Sample trajectories of optimal maneuvers in the state plane, based on Athans and Falb [3]

As Figure 50 illustrates, ω_{sw} can be used to determine whether or not an over-speed condition exists. When stepping through the kinematic calculations for a forward maneuver, if the value of ω_{sw} is less than the current value of ω, then the system is rotating too fast for maximum deceleration to stop at the commanded final position. When such a condition exists, a new set of switch and final times should be calculated based on the over-speed bang-bang maneuver. The new equations are developed in the same fashion as (1.66) through (1.69); they are presented in (1.70) through (1.73) without derivation.

$$\theta_{sw} = \frac{\omega_0^2 - \omega_f^2}{4\alpha} + \frac{\theta_0 + \theta_f}{2} \tag{1.70}$$

$$\omega_{sw} = \sqrt{\omega_0^2 + 2(-\alpha)(\theta_{sw} - \theta_0)} \tag{1.71}$$

$$t_{sw} = \frac{\omega_{sw} - \omega_0}{(-\alpha)} + t_0 \tag{1.72}$$

$$t_f = \frac{\omega_f - \omega_{sw}}{\alpha} + t_{sw} \tag{1.73}$$

A similar test can be applied to reverse maneuvers, except that in this case the over-speed condition is indicated if the value of ω_{sw} is greater than the value of ω.

Strictly speaking, a second category of optimal maneuver does exist. It is certainly conceivable that the system's initial states are such that only a single "bang" of torque is necessary to drive the system to the commanded final conditions. This is the case if the states are on the solid red or blue lines in Figure 50. However, the developed kinematic calculations already address this situation. If the system states reside in this locus of points that need only a single application of torque, then the kinematic equations will indicate a switch time that is immediate or in the past and direct the system to implement the second and final phase of a "bang-bang" maneuver (i.e., only a single application of either positive or negative maximum torque). Therefore, the treatment of this scenario separately is not necessary for implementation.

2. Adjusting to the Times

Implementation of the analytical feed-forward control torque formula as a real-time optimal control will entail the recalculation of the optimal maneuver parameters on regular intervals. But, because the maneuver is already underway, the evaluation of the equations presented thus far will have to be

adjusted for the current clock time. In other words, the control torque equations discussed to this point assume that time starts at zero, but that will not be the case once the maneuver is initiated. The adjustment for clock time is made through the substitution of real-time variables:

$$\begin{aligned} t^* &= t - t_{update} \\ t_{sw}^* &= t_{sw} - t_{update} \\ t_f^* &= t_f - t_{update} \\ \theta_{update} &= \theta\left(t_{update}\right) \\ \omega_{update} &= \omega\left(t_{update}\right) \end{aligned} \tag{1.74}$$

Substituting the real-time variables into the control torque equation yields the following:

$$\begin{aligned} \tau_{ctrl}(t) = {} & \omega_{update} k_p t^* + \omega_{update} k_v + k_p(\theta_{update} - \theta_D)... \\ & + \tau_{\max}\left[\tfrac{k_p}{2J}\left(t^*\right)^2 + \tfrac{k_v}{J} t^* + 1\right]... \\ & - 2\tau_{\max} \cdot u\left(t^* - t_{sw}^*\right) \cdot \left[\tfrac{k_p}{2J}\left(t^* - t_{sw}^*\right)^2 + \tfrac{k_v}{J}\left(t^* - t_{sw}^*\right) + 1\right]... \\ & + \tau_{\max} \cdot u\left(t^* - t_f^*\right) \cdot \left[\tfrac{k_p}{2J}\left(t^* - t_f^*\right)^2 + \tfrac{k_v}{J}\left(t^* - t_f^*\right) + 1\right] \end{aligned} \tag{1.75}$$

3. Incorporating Dead-Zone

Real systems cannot apply infinitesimally small amounts of torque nor can they apply any amount of torque for an infinitesimally short duration of time. A dead-band is implemented in real systems to accommodate these limitations and prevent chattering of actuators when the system is sufficiently close to the desired end states. Even in mathematical models, dead-bands are useful, not only to incorporate another element of realism, but also to prevent numerical excursions near the end state. In the case of the RTOC system developed here, a dead-band is implemented to prevent recalculation of maneuver parameters that would execute an excessively short bang-bang maneuver. But, since the

dead-band only applies to the feed-forward control torque, it does not prevent the continued operation of the PD controller.

This last point illustrates a significant advantage of this RTOC method over others. A real-world implementation of similar RTOC systems, such as that described by Athans and Falb [5], must include a dead-band for the reasons already described. When combined with the dead-band, most maneuvers will not end by reaching the commanded end state, due to the uncertainties in the system inertia. Instead, the system will come very close to the final position with some very small, but non-zero, velocity and will slowly coast past the commanded end position; then, when the limits of the dead-band are exceeded, a short application of maximum torque will send the system slowly drifting past the commanded position in the other direction. This appears in the state plane as a limit cycle in which the system circles the commanded end-state. In contrast, when the PD controller-based RTOC system developed here is within the RTOC dead-band and no longer executing bang-bang maneuvers, the PD controller will continue to regulate the state error to zero.

A dead-band is implemented in this RTOC system to prevent recalculation of the maneuver parameters once the system states are sufficiently close to the commanded states. The results presented in this thesis are based on a dead band of $\left|\theta - \theta_D\right| \leq 0.05$ and $\left|\omega - \omega_D\right| \leq 0.1$. The choice of these parameters is up to the designer. Although not implemented in the controller developed in this thesis, the designer should also consider applying a dead-band, or tolerance, to the over-shoot decision variable, ω_{sw}. Some scenarios resulting in minor overshoot as indicated by the value of ω_{sw} may achieve sufficient end-state precision more quickly than if an over-shoot maneuver sequence were initiated.

The RTOC algorithm with PD inner loop is summarized as follows:

1. Check Update Time Interval (this is the frequency that the maneuver parameters and τ_{ctrl} are recalculated, specified by the designer)

2. Check Dead-Band

3. Initiate calculation of maneuver parameters:

   a. Determine maneuver direction (forward or reverse)
   b. Calculate switch and final times
   c. Check for over-speed condition; if over-speed, recalculate switch and final times

4. Update τ_{ctrl}; account for direction of maneuver and over-speed condition

D. A NOTE ON MODELING THE RTOC CONTROLLER

The RTOC system described in this thesis is modeled in MATLAB using a fixed step ODE4 solver. Fixed step solvers are typically less accurate and take longer to execute than variable step solvers, and are not normally preferred for developing numerical solutions. However, variable step solvers achieve their faster run times by attempting relatively large step sizes, comparing errors and re-calculating as necessary to reduce their error; consequently, they tend to "jump around" in time in the course of their computation. Because this RTOC algorithm involves computing and implementing the optimal control torque based on progressing system states, it is imperative that the calculations occur sequentially; thus, a fixed step solver is preferred for implementing this system. Indeed, attempting to model this RTOC controller with a variable step solver simply failed to produce accurate results.

E. RESULTS AND ANALYSIS OF THE RTOC CONTROLLER

The first simulation of the RTOC controller, presented in Figures 51–56, is for the nominal case (i.e., actual rotational inertia is equal to the nominal inertia). Again, this is a forward maneuver (from $\theta_0 = 0$ to $\theta_f = 1$) from an initial rest condition to a final rest condition (i.e. $\omega_0 = 0,\ \omega_f = 0$). These results were obtained using a 0.0001 sec step size with MATLAB's ODE4 solver.

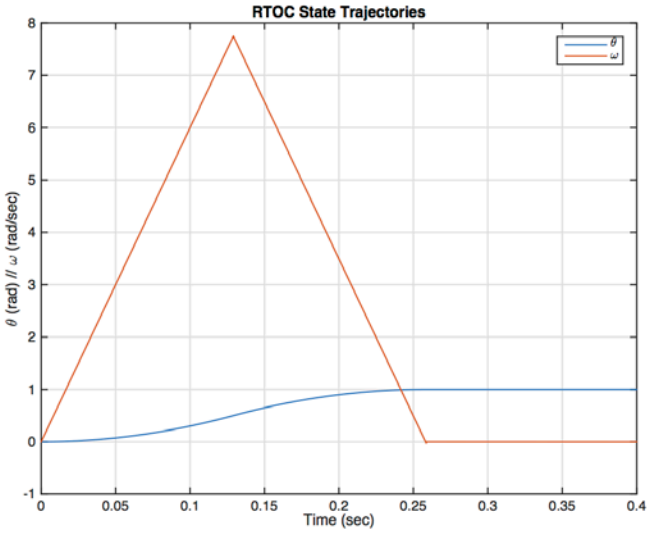

Figure 51. Time response of the nominal system (i.e., no inertia uncertainty) using RTOC controller

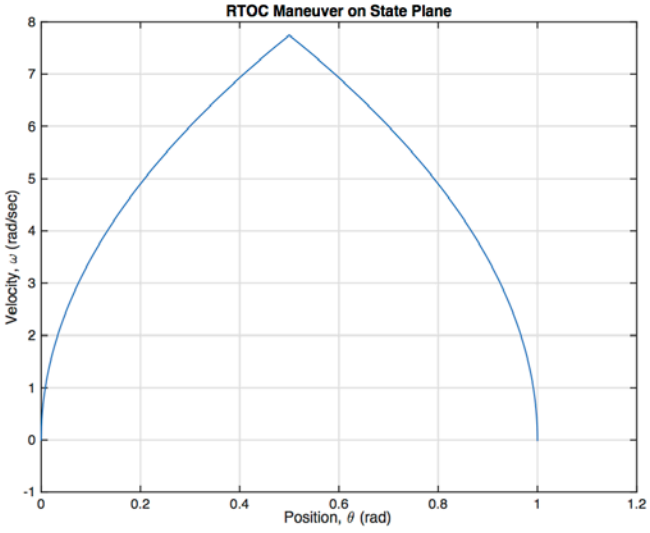

Figure 52. Response of nominal system (i.e., no inertia uncertainty) in the state plane

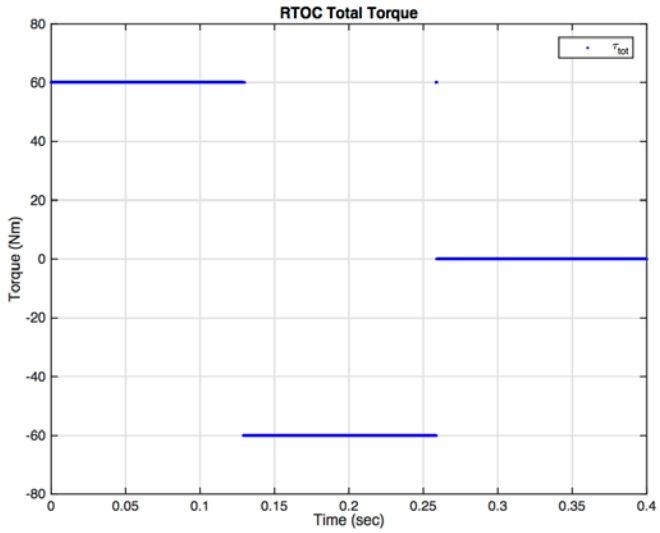

Figure 53. Total torque trajectory of nominal system with RTOC control

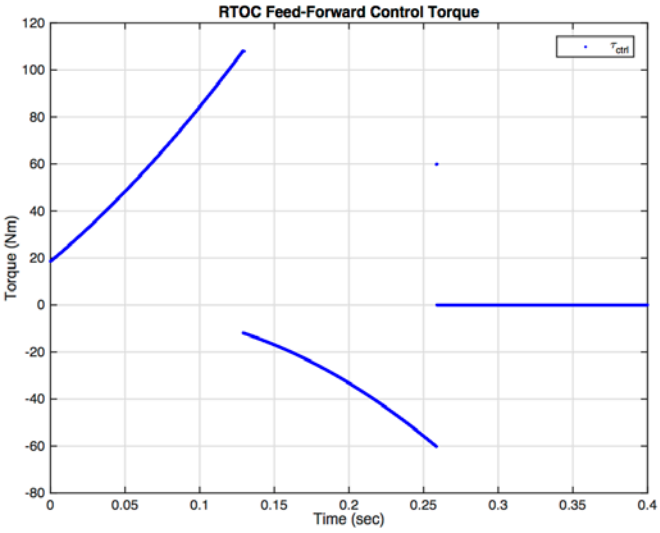

Figure 54. Feed-forward control torque trajectory of nominal system under RTOC control

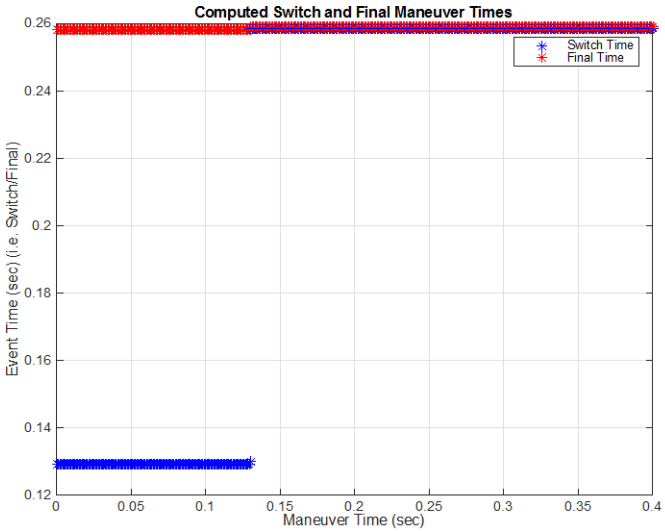

Figure 55. Switch and final time throughout maneuver of nominal system under RTOC control

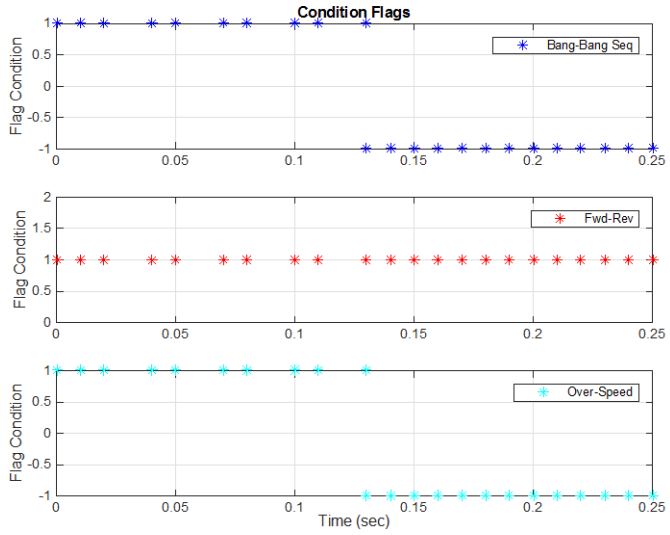

Figure 56. RTOC algorithm condition flags during maneuver of nominal system

Figure 53 contains a brief application of a positive maximum torque at the end of the maneuver. This is a result of the numerical error of the ODE4 fixed step solver. Due to the numerical error, the RTOC algorithm determined that the

system was in a slight over-speed condition; consequently, it implemented the forward maneuver over-speed controls, which would entail maximum negative torque followed by an application of maximum positive torque. The over-speed condition is imperceptible in the state trajectories. This phenomenon is also captured in the other plots.

In Figure 55, the Switch and Final times are constant through most of the maneuver; but at 0.13 sec the RTOC algorithm detected a slight over-speed condition due to numerical error of the ODE4 solver. When the over-speed condition is detected, new switch and final times are computed for an over-speed maneuver. The time span between the switch and final time during the over-speed maneuver indicate the degree of the over-speed condition (i.e., very small).

Figure 56 plots a series of algorithm flags to illustrate the internal workings of the algorithm throughout the maneuver; they are only plotted when the system is outside of the RTOC dead-band. This indicates that the over-speed condition was determined at time 0.13 sec. The flag values have the following meanings: Fwd-Rev: +1 for Forward Maneuver, -1 for Reverse Maneuver; Over-Speed: +1 for Nominal, -1 for Over-Speed; Bang-Bang Sequence: +1 if positive max torque followed by negative max torque; -1 for negative max torque followed by positive max torque.

F. RTOC CONTROLLER PERFORMANCE IN THE PRESENCE OF INERTIA UNCERTAINTY

The numerical error and resulting over-speed condition notwithstanding, the behavior of the nominal system with the RTOC controller matches the behavior of the nominal system with open-loop optimal control torque. But it is much more interesting to see how the RTOC controller deals with uncertainties. Figures 57–62 present the results of the system with an actual inertia that is 150% greater than nominal; this is an excessive amount of uncertainty but is an excellent illustration of the power of this RTOC controller.

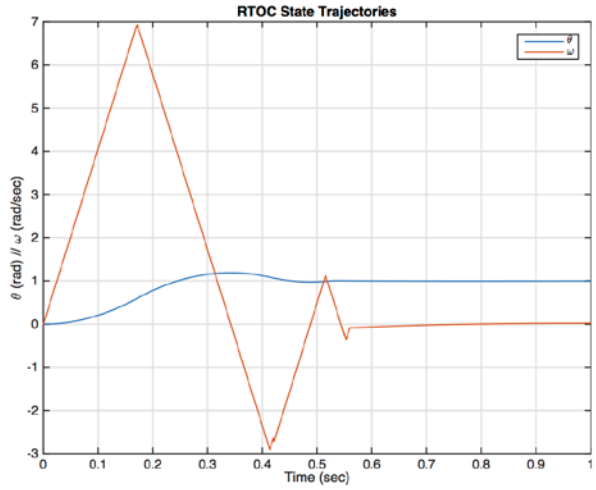

Figure 57. State trajectories of system with 50% inertia uncertainty using RTOC controller

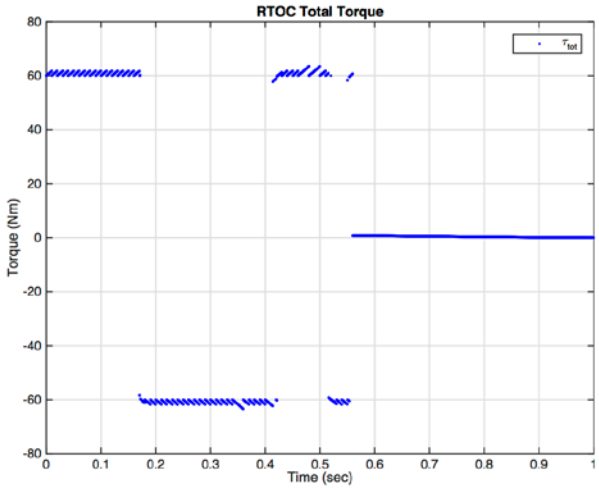

Figure 58. Total torque trajectory of system with 50% inertia uncertainty using RTOC controller

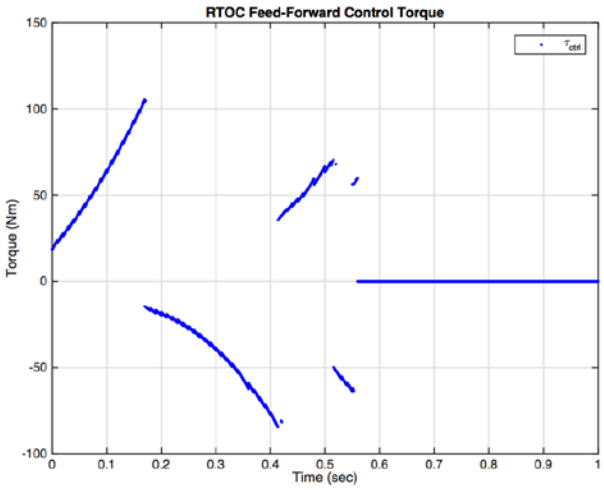

Figure 59. Control torque trajectory of system with 50% inertia uncertainty using RTOC controller

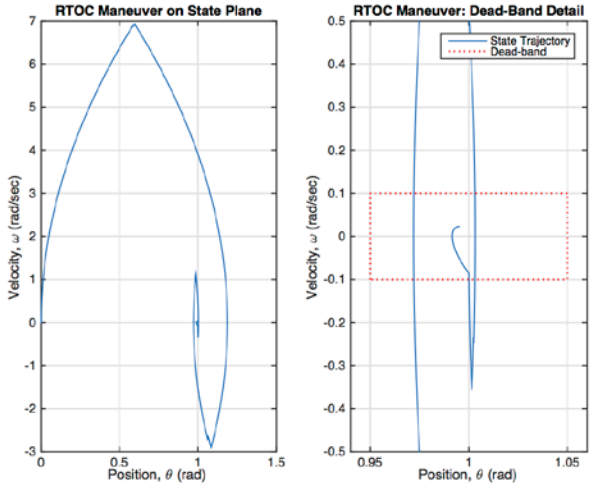

Figure 60. Maneuver of system with 50% inertia uncertainty using RTOC controller in the state plane

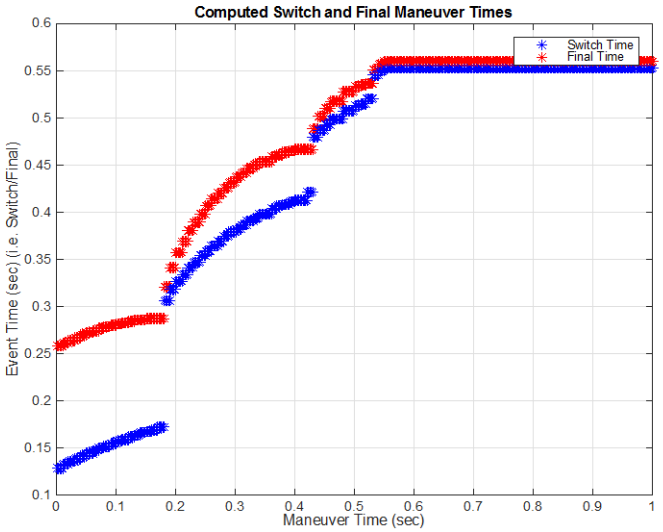

Figure 61. Switch and final time computations for system with 50% inertia uncertainty using RTOC controller

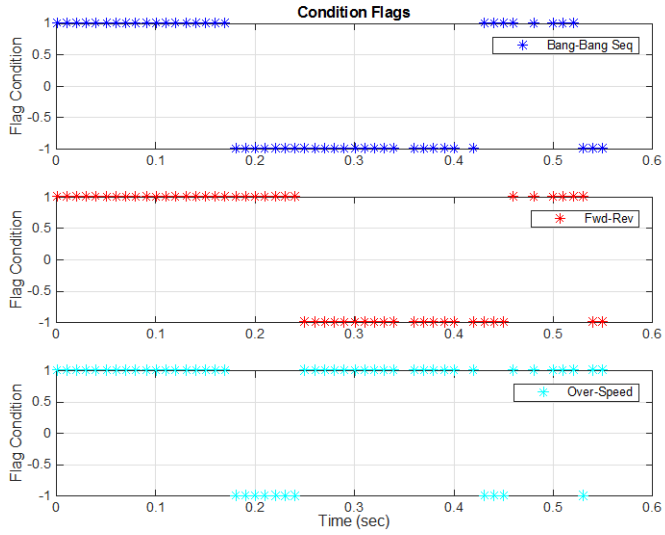

Figure 62. Condition flags throughout maneuver of system with 50% inertia uncertainty using RTOC controller

In the simulation, the actual inertia is 150% of the nominal inertia. With this degree of uncertainty, the system experiences an over-speed condition twice, most evident in velocity state excursions below 0 rad/sec in Figure 57. Even with

these uncertainties, the system settles within 1% of the final position in 0.445 sec.

Because the nominal inertia is a factor in calculating the control torque, the total torque plotted in Figure 58 slightly exceeds the limit of +/- 60 Nm. However, since the RTOC algorithm regularly samples the current states and recalculates the control torque trajectory, the total torque only reaches the extreme values of +63.51 and -63.46 Nm.

The state trajectory plotted in Figure 60 illustrates the over-speed conditions that the system experiences. The detail shown in the sub-plot on the right illustrates the behavior of the system within the dead-band. Observe that although the RTOC algorithm will not execute a new bang-bang maneuver to continue to drive the system to the commanded final states, the PD controller does continue to drive the system to the final states.

The dramatic shifts in switch times plotted in Figure 61 at approximately 0.18, 0.42 and 0.55 seconds all correlate to changes in the bang-bang sequence, either due to a change in the direction of the maneuver (i.e., overshooting the commanded final position) or to shifting to an over-speed condition.

G. COMPARISON TO OPEN-LOOP OPTIMAL CONTROL SOLUTION

For the purpose of comparison, the results of a system with an actual inertia of 150% of nominal but using a static optimal control solution will now be presented. In this scenario, the feed-forward control torque trajectory is computed at the beginning of the maneuver based on the initial conditions and nominal inertia, and remains unchanged throughout the maneuver (i.e., is not updated with any state or system feedback). The results of open-loop feed-forward optimal control simulation are presented in Figures 63–66.

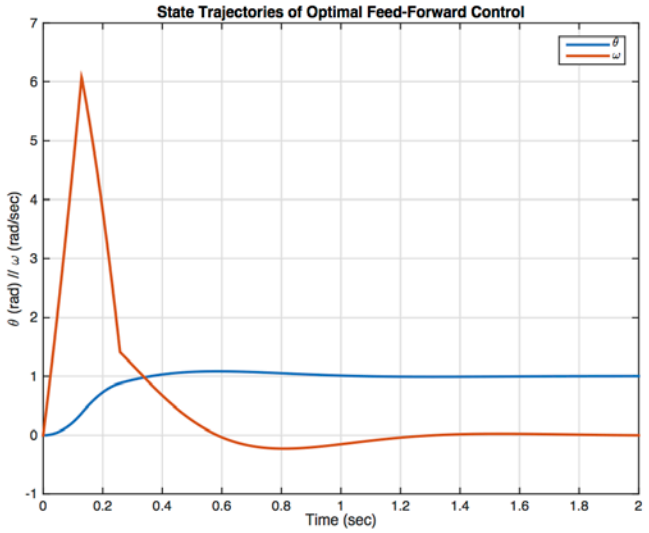

Figure 63. State trajectories of system with 50% inertia uncertainty using static feed-forward optimal control

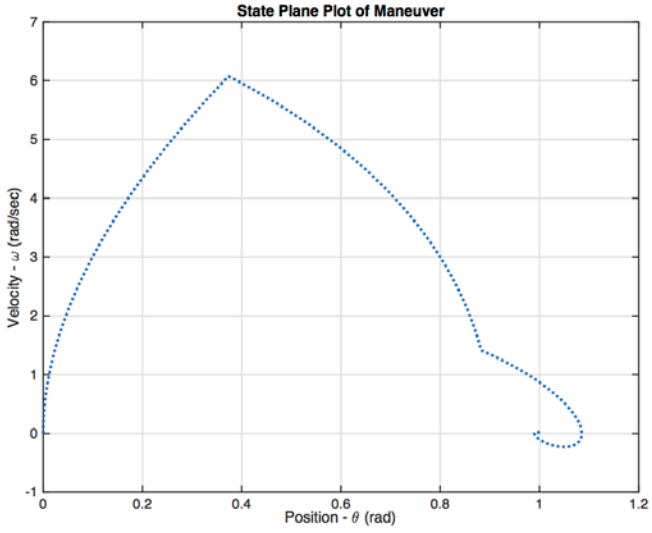

Figure 64. Maneuver of system with 50% inertia uncertainty using static feed-forward optimal control

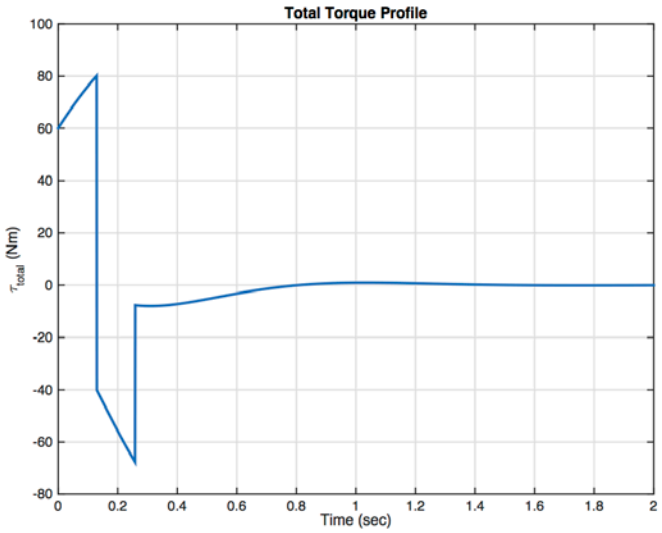

Figure 65. Total torque trajectory of system with 50% inertia uncertainty using static feed-forward optimal control

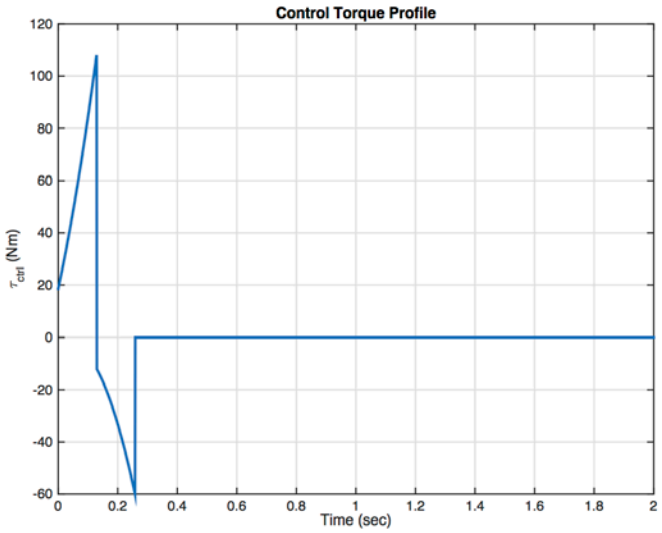

Figure 66. Control torque trajectory of system with 50% inertia uncertainty using static feed-forward optimal control

This system reaches and remains within 1% of the final position after 1.002 seconds. While the system is well short of the final commanded states when the feed-forward control torque expires, the PD controller continues to drive

the system to the commanded final states. The long settle time following completion of the control torque input is due to the low bandwidth of the PD controller.

The total torque profile plotted in Figure 65 is clearly not the optimal bang-bang profile. The maximum torque limit of 60 Nm is well exceeded, reaching a maximum value greater than 80 Nm. The control torque profile plotted in Figure 66 is exactly correct—for a different system. Unfortunately, because this system's actual inertia is 50% greater than the nominal inertia which factors into the computation of this torque profile, this torque trajectory is completely incorrect, resulting in a comparatively long maneuver time.

H. FURTHER ANALYSIS OF THE RTOC CONTROLLER

The comparison of the performance differences between the RTOC system and the open-loop optimal control system for a plant with 50% inertia uncertainty is stark. The RTOC system completes the maneuver, using a 1% settling metric, in 0.445 seconds, while the open-loop system required 1.002 seconds to settle at the same position. Another important advantage of the RTOC system is that the total torque excursion beyond the nominal limit is much smaller at a max of 63.51 Nm compared to the static feed-forward method which exceed 80 Nm. This would allow a designer to reduce the saturation margin and employ more of the system's torque capability without risking saturation. Alternatively, employment of a saturation mechanism preventing the torque application from actually exceeding 60 Nm may produce even longer settling times in the static feed-forward controller whereas such a limit would have minimal impact on the performance of the RTOC controller.

I. SUMMARY

The closed-loop real-time optimal control system with an integrated PD controller developed in this thesis has a variety of advantages, chiefly improved maneuver time performance. While the static optimal control solution integrated

with the closed-loop PD controller also reaches the final end state, the presence of inertia error may have significant impacts on the performance of this system. In contrast, the RTOC controller senses the off-nominal state trajectory and actively adjusts to achieve a more time optimal maneuver. To be sure, the inertia error is built into the RTOC controller logic (i.e., the nominal inertia is a factor in the optimal control torque formula), and it is not able to achieve an optimal maneuver for the off-nominal system, but the performance is dramatically better than the alternative static optimal control trajectory.

An unexpected advantage is that the RTOC controller remains closer to the torque limit, minimizing the torque envelope violations. This aspect allows the designer to reduce the control margins that would have otherwise been imposed, enabling the RTOC controller to more efficiently utilize actual system capability.

The techniques applied in the development of this one-dimensional RTOC controller can be employed in a broad range of control applications for space systems. As such, the concepts developed here will be expanded for multi-dimensional systems in the next chapter.

THIS PAGE INTENTIONALLY LEFT BLANK

VI. DEVELOPMENT OF REAL-TIME OPTIMAL CONTROL METHODS FOR EIGENAXIS MANEUVERS

A. INTRODUCTION

The previous chapter illustrated the benefit of a real-time optimal controller (RTOC) in a single degree of freedom system (SDOF). This chapter will describe the translation of the developed concept to a system with three degrees of rotational freedom (3DOF), such as a spacecraft. The maneuver performed by the SDOF system is analogous to an eigenaxis maneuver for a 3DOF system, in which the system rotates about a fixed axis during the transition from one orientation to another. The RTOC controller will be extended to accommodate these types of maneuvers.

An eigenaxis maneuver is a maneuver in which the rigid body rotates about a single axis, specifically the eigenaxis, to reach a new attitude. An eigenaxis rotation in three dimensional rotational space may intuitively seem to be analogous to a straight line displacement in three dimensional Euclidean space, but three dimensional rotational space is not simply connected; consequently, not only is an eigenaxis rotation not necessarily the shortest displacement from one orientation to another, the eigenaxis maneuver has been demonstrated to not be the fastest maneuver from one orientation to another [6]. But the fact that rotational space is not simply connected means that the optimal reorientation trajectory is not readily apparent or formulaically computed. Instead, the optimal trajectory must be determined using optimal control methods and algorithms for each individual maneuver. Because the optimal maneuver often follows a trajectory that is not easily anticipated, the prospect of off-eigenaxis maneuvers leaves operators and engineers anxious about potential attitude constraint violations (such as pointing an optical sensor at the sun, etc.). While these constraints can easily be incorporated into the maneuver optimization and modern processing power is more than capable of running embedded

optimization software, the fact remains that eigenaxis maneuvers are preferred and are nearly ubiquitous in the current space industry.

B. OVERVIEW OF ROTATIONAL MOTION IN THREE DIMENSIONS

Rotational motion in three dimensions is governed by the conservation of angular momentum. The change of angular momentum, $\vec{H}$, of a rigid body in the inertial reference frame is equal to the externally applied torques. Conservation of momentum applies regardless of what reference frame used to describe the orientation of the system, but when using the body-fixed reference frame, a cross product term emerges, in accordance with the transport theorem [7]. The dynamics of a rigid body's attitude are described in (1.76), where $\vec{H}_B$ is the angular momentum in the body reference frame and $\vec{\omega}$ is the angular velocity of the body frame with respect to the inertial reference frame.

$$\dot{\vec{H}}_B + \vec{\omega} \times \vec{H}_B = \vec{T}_{ext} \tag{1.76}$$

Noting that the angular momentum of the rigid body is equal to the product of system's inertia, J, and angular rate, $\boldsymbol{\omega}$, and incorporating an additional control torque, $\vec{u}$, equation (1.76), becomes

$$J\dot{\vec{\omega}} + \left(\vec{\omega} \times J\vec{\omega}\right) = \vec{T}_{ext} + \vec{u} \tag{1.77}$$

1. Momentum Exchange Devices

Spacecraft attitude slewing commonly employs a momentum exchange device to produce control torque, $\vec{u}$. Common momentum exchange devices include reaction wheels and control moment gyros. These are systems that possess some sort of angular momentum within themselves. Thus, the total system angular momentum is equal to the sum of the spacecraft's momentum, $\vec{H}_{s/c}$, and the momentum stored in the momentum exchange device, $\vec{h}$. Because the conservation of momentum must be maintained, the rotation rate of the

spacecraft can be modified through angular momentum exchange between the spacecraft and the aptly named momentum exchange device. As articulated by Wie [7], the attitude dynamic equation results from substituting the total angular momentum into equation (1.76) and incorporating the same substitutions applied to equation (1.77) ; the result is shown in equation (1.78).

$$J\dot{\vec{\omega}} + \dot{\vec{h}} + \vec{\omega} \times \left(J\vec{\omega} + \vec{h} \right) = \vec{T}_{ext} \tag{1.78}$$

The control torque, $\vec{u}$, referenced in equation (1.77) can thus be set equal to the sum $\dot{\vec{h}} + \left(\vec{\omega} \times \vec{h} \right)$; hence, control torques are produced by commanding changes in the momentum exchange device's angular momentum vector.

2. Zero-Net Bias Control

The vector cross product that arises in the dynamics equation is known as the gyroscopic torque. The direction of this torque is orthogonal to the axis of rotation. A common control technique is to incorporate a counter-gyroscopic torque to cancel out this motion. In that case, the control torque can be viewed to have two components: a torque component to effect the desired acceleration and a counter-gyroscopic torque component whose purpose is to ensure the system does not accelerate in the $\vec{\omega} \times J\vec{\omega}$ direction. This method has the obvious drawback of expending energy and torque capacity solely to maintain alignment with the eigenaxis; counter-gyroscopic torque does not produce motion but instead prevents off-eigenaxis motion.

Many satellites in low earth orbit are operated as zero-net bias systems. Momentum exchange devices are actually systems of multiple rotating components, such as reaction wheels or control moment gyros. As such, the angular momentum of the whole system is equal to the sum of the angular momentum of each individual rotating component. A zero-biased system is one in which the rotating elements are arranged and balanced in such a way that the sum of their angular momentum vectors is equal to zero in the quiescent state.

Therefore, when the spacecraft is not rotating, the total angular momentum is also zero.

$$\begin{aligned}\vec{H}_{tot} &= J\vec{\omega} + \vec{h} = \vec{0} \\ &= J \cdot \begin{bmatrix} 0 \\ 0 \\ 0 \end{bmatrix} + \begin{bmatrix} 0 \\ 0 \\ 0 \end{bmatrix} = \vec{0}\end{aligned} \tag{1.79}$$

The advantage of a zero-net bias control system is that during maneuvers, the angular momentum of the momentum exchange device and the angular momentum of the spacecraft are swapped for one another. Conservation of angular momentum means that the angular momentum of the spacecraft is equal and opposite the angular momentum of the momentum exchange device.

$$\vec{H}_{tot} = J \cdot \begin{bmatrix} \omega_1 \\ \omega_2 \\ \omega_3 \end{bmatrix} + \begin{bmatrix} h_1 \\ h_2 \\ h_3 \end{bmatrix} = \vec{0} \tag{1.80}$$

Naturally, when equation (1.80) is substituted into the dynamics equation, the gyroscopic term goes to zero ($\vec{\omega} \times \vec{0} = \vec{0}$).

The ability to achieve zero bias is predicated on having four or more actuators, which is the case in most momentum control arrays. It also requires nearly constant momentum management, ensuring that momentum does not accumulate in any one direction in response to external disturbance torques (such as atmospheric drag, gravity gradient, etc.).

3. Attitude Kinematics

The attitude or orientation of a rotational system can be mathematically described in various ways, but the most commonly used is the quaternion [7]. The quaternion is a four-element vector defined in (1.81). According the Euler's rotation theorem, any rotation or sequence of rotations of a rigid body can be

described by a single rotation by an angle θ about a specific axis, $\hat{e}$; these are known as the eigen angle and eigenaxis. A quaternion is defined in these terms to describe a system's attitude with respect to some reference attitude [7].

$$\bar{q} = \begin{bmatrix} e_1 \sin\left(\frac{\theta}{2}\right) \\ e_2 \sin\left(\frac{\theta}{2}\right) \\ e_3 \sin\left(\frac{\theta}{2}\right) \\ \cos\left(\frac{\theta}{2}\right) \end{bmatrix} \tag{1.81}$$

The quaternion kinematic equations are given as [7]:

$$\begin{aligned} \dot{\bar{q}} &= \tfrac{1}{2}\vec{\omega}^{\times} q \\ &= \frac{1}{2}\begin{bmatrix} 0 & \omega_3 & -\omega_2 & \omega_1 \\ -\omega_3 & 0 & \omega_1 & \omega_2 \\ \omega_2 & -\omega_1 & 0 & \omega_3 \\ -\omega_1 & -\omega_2 & -\omega_3 & 0 \end{bmatrix}\begin{bmatrix} q_1 \\ q_2 \\ q_3 \\ q_4 \end{bmatrix} \end{aligned} \tag{1.82}$$

Together, equations (1.77) and (1.82) describe the complete rotational dynamics of a rigid body in response to applied torques.

C. OPTIMAL EIGENAXIS CONTROL ARCHITECTURE

Similar to the SDOF RTOC controller, the control architecture for the 3DOF system will consist of a closed-loop that produces feedback torques proportional to the attitude and velocity error and a feed-forward torque signal to produce the nominally optimal total torque trajectory necessary to complete the maneuver in the minimum time. The analog to the PD controller used in SDOF systems is the quaternion error feedback controller for 3DOF systems, as described by Wie [7]. Like the PD controller, the quaternion error feedback

controller produces a torque signal that is proportional to the error between the commanded and actual attitude, as determined by the quaternion error, and the error between the commanded and actual rotational rate. The control architecture for this system is shown in Figure 67.

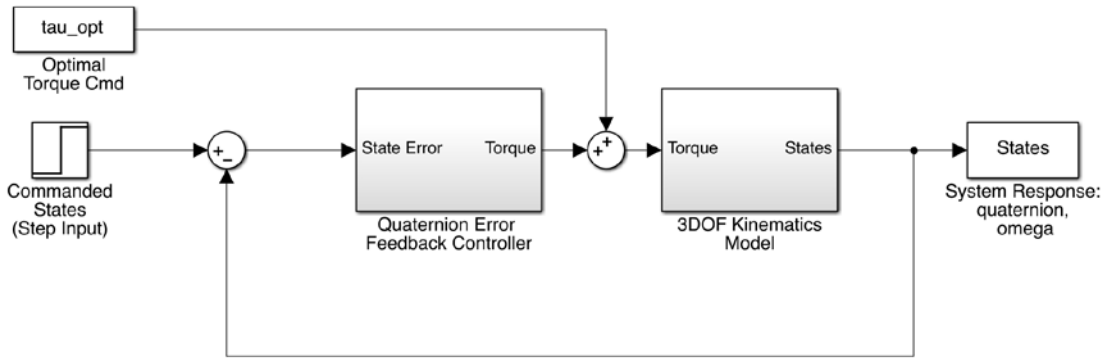

Figure 67. Feed-forward optimal control architecture with quaternion error feedback

Similar to the SDOF system, the total torque applied to the body of this 3DOF system is the sum of the feed-forward torque and the quaternion error feedback torque. External disturbance torques, $\vec{T}_{ext}$, considered to be zero. The total torque is described by (1.83).

$$\bar{\tau}_{tot} = -K \cdot \bar{q}_{error} - C\bar{\omega}_{error} + \bar{\tau}_{FF} \tag{1.83}$$

1. Quaternion Error Feedback Controllers

Similar to the PD controller, the quaternion error feedback controller applies gains, K and C, to the quaternion and angular rate errors. The quaternion error is not simply the difference between the commanded and actual quaternion, but is instead computed according to equation (1.84), where q_c is the commanded quaternion and q is the measured quaternion.

$$q_e = \begin{bmatrix} [q_{error}] \\ q_{e,4} \end{bmatrix} = \begin{bmatrix} q_{4,c} & q_{3,c} & -q_{2,c} & -q_{1,c} \\ -q_{3,c} & q_{4,c} & q_{1,c} & -q_{2,c} \\ q_{2,c} & -q_{1,c} & q_{4,c} & -q_{3,c} \\ q_{1,c} & q_{2,c} & q_{3,c} & q_{4,c} \end{bmatrix} \cdot \begin{bmatrix} q_1 \\ q_2 \\ q_3 \\ q_4 \end{bmatrix} \tag{1.84}$$

Considering the definition of a quaternion from equation (1.81), the full error quaternion, $\bar{q}_e$, can be written as follows:

$$\bar{q}_e = \begin{bmatrix} e_1 \sin\left(\frac{\theta_e}{2}\right) \\ e_2 \sin\left(\frac{\theta_e}{2}\right) \\ e_3 \sin\left(\frac{\theta_e}{2}\right) \\ \cos\left(\frac{\theta_e}{2}\right) \end{bmatrix} \tag{1.85}$$

where θ_e is the eigen angle and $e_1, e_2,$ and e_3 are the components of the eigenaxis describing the rotation from the current attitude to the commanded attitude. Note that the quaternion error vector, $\bar{q}_{error}$, used for feedback torque calculation in equation (1.83) is only the first three terms of the full error quaternion, $\bar{q}_e$, from (1.84) and (1.85).

The control methodology developed in this paper is momentum exchange device agnostic, and the detailed interaction of the device with the spacecraft will be largely ignored. Instead, a black box approach will be taken in which the control torques are simply produced without explanation as to their source.

2. Relative Alignment of Torque Vector and Eigenaxis

With the exception of rotation about one of the principle axes, rotating an asymmetrical rigid body about a particular axis, $\hat{e}$, typically requires application of torque on a different axis, $\hat{v}$. This fact is illustrated by Karpenko, King and Ross [8] with the following derivation. In the inertial reference frame (or in the body referenced frame for zero-net bias control systems), the gyroscopic terms

(i.e., the cross products) in equations (1.76) and (1.77) are not applicable, so (1.77) becomes:

$$J\dot{\vec{\omega}} = \vec{T}_{tot} \tag{1.86}$$

Rewriting equation (1.86) in terms of magnitudes and unit vectors yields:

$$\alpha J\hat{e} = \tau\hat{v} \tag{1.87}$$

where α and τ are the magnitudes of the acceleration and torque, respectively; and $\hat{e}$ and $\hat{v}$ are the unit vectors of the acceleration and torque directions, respectively. Noting that J is the inertia tensor modifying or operating on $\hat{e}$, equation (1.87) highlights the fact that $\hat{e}$ and $\hat{v}$ are not necessarily equal. The equation for $\hat{v}$ is given in equation (1.88).

$$\bar{v} = \frac{J\hat{e}}{\left\|J\hat{e}\right\|_2} \tag{1.88}$$

The relative alignment of the eigenaxis vector and the torque vector will be an important concept in the development of the subject RTOC controllers, but it is also an important concept in the selection of gains in the quaternion error feedback controller. Wie [7] developed the theorem that quaternion error feedback controller is globally asymptotically stable so long as the matrix $K^{-1}C$ is positive definite and points out that because physical inertia tensors are always positive definite, a convenient selection of gains is $K = kJ$ and $C = cJ$, where k and c are scalars properly chosen for the desired control performance. Finally, Wie suggests, without explanation, that a quaternion error control torque composed of the suggested gains and an additional counter-gyroscopic torque term will produce motion about the eigenaxis, as measured from the initial attitude (i.e., at $t = t_0$), for a rest to rest maneuver; Wie's suggested form of quaternion error feedback torque is shown in equation (1.89). In Wie's formulation, commanded velocity is always zero [7].

$$\vec{u} = -kJ\vec{q}_{error} - cJ\vec{\omega} + \vec{\omega} \times J\vec{\omega} \tag{1.89}$$

3. Quaternion Error Feedback Gain Selection

A closer examination of Wie's quaternion error feedback torque, with the help of substituting definitions and concepts already introduced, will be instructive in developing the RTOC controllers. Equation (1.89) is rewritten in a modified but equivalent form for rest-to-rest maneuver (i.e., $\vec{\omega}(t=0) = \vec{0}$ and $\vec{\omega}_{cmd} = \vec{0}$) in equation (1.90).

$$\vec{u}(t) = -k \cdot J \cdot \hat{e} \cdot \sin\left(\frac{\theta_e(t)}{2}\right) - c \cdot J \cdot \left\|\vec{\omega}(t)\right\|_2 \cdot \hat{e} + \vec{\omega} \times J\vec{\omega} \tag{1.90}$$

This formulation of the quaternion error feedback torque illustrates why the gain choices recommended by Wie are not only satisfactory, but necessary to accomplish an eigenaxis maneuver. The initial torque, before any motion has begun, is due only to the quaternion error feedback term; when written in the form shown in (1.90), the direction of that torque is explicit: it is in the $\hat{v}$ direction, due to the presence of the $J \cdot \hat{e}$ quantity [as described in (1.87)]. As the maneuver progresses, the rotation of the body, and therefore the angular velocity, is in the $\hat{e}$ direction. Because the velocity error component of the feedback torque also contains the $J \cdot \hat{e}$ quantity, this feedback torque is also produced in the $\hat{v}$ direction.

Finally, note that the counter-gyroscopic torque ($\vec{\omega} \times J\vec{\omega}$) is orthogonal to both $\hat{e}$ and $\hat{v}$. When the quaternion error feedback torque formula suggested by Wie is substituted in the rigid body kinematics equation [equation (1.77)] as the control torque, $\vec{u}$, the gyroscopic terms cancel out. Thus, for a system with using the Wie's suggested quaternion error feedback control [equation (1.89)], the net torque is indeed in the $\hat{v}$ direction as required (assuming zero external torques). It must be noted, however, that in order to cancel out the gyroscopic torque, some portion of the actuator capability must be reserved, thereby reducing the overall effectiveness of the actuator system.

4. Quaternion Error Feedback System Parameters

The gains used in this thesis are based on the work of Fields, Kocis, Williams and Karpenko and their development of a hardware-in-the-loop control moment gyro (CMG) simulator [9]. The control system in their work was a traditional quaternion error feedback controller, as described in equation (1.89). Use of these parameters, both for the system inertia as well as the controller gains, allows a straightforward performance comparison and also ensures that this study incorporates realistic system characteristics.

The system inertia tensor used in this study is

$$J = \begin{bmatrix} 3.7 & 0 & 0 \\ 0 & 4.0 & 0 \\ 0 & 0 & 7.0 \end{bmatrix} \mathrm{kg} \cdot \mathrm{m}^2 \tag{1.91}$$

This inertia tensor is actually a rotated version of the inertia used in [9]; their model contained non-zero products of inertia, indicating that the system's principle inertia axes were not exactly aligned with the body frame. This misalignment is not unusual in real systems, but most calculations and analyses are simpler if the inertia tensor is diagonal.

The controller employed in [9] was a quaternion error feedback controller with the following gains:

$$\begin{aligned} K &= 2 \cdot J \\ C &= 12.5 \cdot J \end{aligned} \tag{1.92}$$

That hardware-in-the-loop model was based on a system with four CMG's in a tetrahedral configuration each with a maximum torque limit of $\pm 1.55\ \mathrm{Nm}$. For the purposes of this study, the system is assumed to have a cube-shaped torque envelope with limits at $\pm 1.55\ \mathrm{Nm}$ in the x, y, and z directions. This is a simplifying assumption that does not represent the torque envelope available in [9], but as previously discussed, the details of the momentum exchange device are not the

main focus of this study. Note, however, that the methodology described here is not limited to cube-shaped torque envelopes.

D. TRANSLATING ONE-DIMENSIONAL RTOC METHOD TO THREE DIMENSIONAL ROTATIONS

As previously stated, the eigenaxis maneuver in three dimensions is analogous to the rotation of a body with a single degree of rotational freedom. To that end, correlating the parameters between the two control methods will facilitate development of a path toward RTOC methods in three dimensions. Two of the most important parameters in the SDOF system are the system states, θ and ω, describing the position and velocity of the body. In three-dimensional rotational space, the equivalent states are the quaternion, $\vec{q}$, and the angular rate or velocity, $\vec{\omega}$. Mapping the quaternion directly to θ is certainly possible, but not as straight forward as one would like. However, there is a direct mapping between the quaternion error and the one-dimensional position error, θ_{error}; indeed, $\theta_{error}$is a component of quaternion error [see equation (1.85)].

Mapping the three-dimensional angular rate, $\vec{\omega}$, to the one-dimensional velocity, ω, is more straightforward. However, it is important to bear in mind the dual purposes served by knowledge of the body's velocity. In the one-dimensional RTOC controller, the velocity was used not only to achieve the commanded velocity, but also to calculate the switch and final time of the bang-bang control. If the body's velocity is perfectly aligned with the eigenaxis, the relevant quantity is simply the magnitude of the angular rate vector; this quantity can be used to calculate the switch and final times of a bang-bang maneuver in exactly the same way as in the one-dimensional case. However, there may be cases where the velocity may not be perfectly aligned with eigenaxis, for example if there is some residual off-axis velocity at the beginning of a maneuver. In that case the quantity that would be used to determine the switch and final times would be the portion of the velocity that is aligned with the eigenaxis; the remainder of the angular rate would be treated as a disturbance to

be zeroed out by the feedback. The significance of this distinction will be more apparent in the development of the final version of the 3DOF RTOC controller. For now it is sufficient to point out that the angular velocity vector, as with any vector, can be written as the sum of two components: a component along the eigenaxis, and the off-axis component. This is defined mathematically with the vector dot product, as shown in equation (1.93).

$$\vec{\omega} = (\vec{\omega} \bullet \hat{e})\hat{e} + (\vec{\omega} - (\vec{\omega} \bullet \hat{e})\hat{e}) \tag{1.93}$$

There are several important quantities in the one-dimensional RTOC controller that still need to be mapped to the three-dimensional control problem. These are the maximum torque and the rotational inertia, which will be used to define the acceleration about the eigenaxis. The question of maximum torque is much more interesting in the three-dimensional problem. In one-dimension, the maximum torque is simply the stated (or allocated) limit of the motor or actuator. However, in the three-dimensional problem, the magnitude of torque that can be applied in a given direction is the two-norm of the torque vector and may vary based with the direction of the eigenaxis. For example, in this problem, the torque limit is defined by a cube-shaped envelope. This means that the maximum torque that could be applied about the x-axis (or any one of the principle axes) is $\left\| [\pm 1.55, \quad 0, \quad 0] \right\|_2 = 1.55\text{Nm}$, whereas the magnitude of torque that could be applied at one of the diagonals would be much larger, $\left\| [\pm 1.55, \quad \pm 1.55, \quad \pm 1.55] \right\|_2 = 2.68\text{Nm}$. Clearly, fully employing the capacity of a system is a fundamental principle in optimal control, so this must be incorporated into the RTOC algorithm.

For any given maneuver, the maximum torque would be that which corresponds to the largest vector aligned with $\hat{\boldsymbol{\nu}}$ [see equation (1.87)] without exceeding the torque envelope. For a cube, this torque vector can be computed with a simple algorithm. First, determine the largest component of $\hat{\boldsymbol{\nu}}$, regardless of sign; then determine the scaling factor that would make that component equal

to the torque limit, $\tau_{\max} = 1.55 \text{ Nm}$; finally, multiply the full $\hat{v}$ vector by that scaling factor. This algorithm is presented in equation (1.94).

$$\begin{aligned} a &= \max\left(\left|\hat{v}\right|\right) \\ b &= \frac{\tau_{\max}}{a} \\ \vec{\tau}_{RTOC-\max} &= b \cdot \hat{v} \end{aligned} \tag{1.94}$$

Note that the simplicity of this algorithm is due to the simplicity of the assumed torque envelope. A more complex torque envelope would necessitate a different algorithm, although the principles would be the same.

Computing the equivalent rotational inertia in the three-dimensional problem is fairly straightforward, and is in fact revealed in equation (1.87). The effective inertia about eigenaxis is $J_{eff} = \left\| J \cdot \hat{e} \right\|_2$. However, recall that in the one-dimensional RTOC controller, the inertia was used to compute the angular acceleration. In the three dimensional problem, the magnitude of the acceleration about the eigenaxis can be computed directly without the intermediate step of compute the effective inertia by rearranging equation (1.87); this is shown in equation (1.95).

$$\alpha = \left\| J^{-1} \cdot \vec{\tau}_{RTOC-\max} \right\|_2 \tag{1.95}$$

All of the major factors in the one-dimensional RTOC controller have now been mapped to the three-dimensional problem. The remaining steps are to confirm that the optimal feed-forward control compliments the quaternion error feedback torque to produce a bang-bang control about the eigenaxis and then to develop an analytical solution for the feed-forward torque, as was done with the development of the one-dimensional RTOC controller.

E. MINIMUM TIME EIGENAXIS MANEUVERS

As with the RTOC solution developed for the single degree of freedom system, the first step is to determine what the optimal control signal should be for a general eigenaxis maneuver, assuming open-loop implementation. This initial step will illustrate what the torque trajectories would be for an open-loop rotational system, informing the expectations for the optimal solution for a closed-loop system. The optimal control problem formulation is shown in equation (1.96). Note, in particular, that the control torque must contain the torque necessary to execute the maneuver as well as the torque necessary to counter any gyroscopic motion.

$$
\begin{aligned}
&\underline{\text{States}}: \quad \vec{x} = \begin{bmatrix} \vec{q} \\ \vec{\omega} \end{bmatrix} \qquad \underline{\text{Controls}}: \ \vec{u} = \begin{bmatrix} \tau_1 \\ \tau_2 \\ \tau_3 \end{bmatrix} \\
&\underline{\text{minimize}}: \quad J\left[\vec{x}(\cdot), \vec{u}(\cdot), t_f\right] = t_f \\
&\underline{\text{subject to}}: \qquad \dot{\vec{q}} = \frac{1}{2}\vec{\omega}^{\times}\vec{q} \\
&\qquad\qquad\qquad\qquad \dot{\vec{\omega}} = J^{-1}\left(\vec{u} - \left(\vec{\omega} \times J\vec{\omega}\right)\right) \\
&\qquad\qquad\qquad\qquad \vec{x}_0{}^T = \left[0,\ 0,\ 0,\ 1,\ 0,\ 0,\ 0\right]^T \\
&\qquad\qquad\qquad\qquad \begin{bmatrix} \left(q_{1_f} - 0.5\right) \\ \left(q_{2_f} - 0.5\right) \\ \left(q_{3_f} - 0.5\right) \\ \left(q_{4_f} - 0.5\right) \\ \omega_{1_f} \\ \omega_{2_f} \\ \omega_{3_f} \\ \ \end{bmatrix} = \left[0,\ 0,\ 0,\ 0,\ 0,\ 0,\ 0\right]^T \\
&\qquad\qquad\qquad\qquad t_0 = 0 \\
&\qquad\qquad\qquad\qquad t_f = t^f \\
&\qquad\qquad\qquad\qquad \begin{bmatrix} -1.55 \\ -1.55 \\ -1.55 \end{bmatrix} \le \vec{u} \le \begin{bmatrix} 1.55 \\ 1.55 \\ 1.55 \end{bmatrix} \\
&\qquad\qquad\qquad\qquad \vec{\omega} \times \vec{q}_e = \vec{0}
\end{aligned}
\tag{1.96}
$$

The dynamics of the model in (1.96) are simply the dynamics of a three dimensional rotational system, as described in equations (1.77) and (1.82). The external torque is zero, and has been dropped from the dynamics all together. Two constraints are placed on this optimization problem; specifically, the control torque is limited to the cubic envelope previously described and the maneuver must be about the given eigenaxis. The final equation in the problem formulation mathematically defines the eigenaxis maneuver constraint, ensuring that the

motion of the body is aligned with the error quaternion, which is defined in part by the eigenaxis. The resulting optimal control analysis is presented in the following sections.

1. The Hamiltonian

$$\begin{aligned} H\left(\vec{\lambda},\vec{x},\vec{u},t\right) &= F\left(\vec{x},\vec{u},t\right)+\vec{\lambda}^{T}\bullet\vec{f}\left(\vec{x},\vec{u},t\right) \\ &= \tfrac{1}{2}\lambda_{q_1}\left(\omega_3 q_2-\omega_2 q_3+\omega_1 q_4\right)\ldots \\ &+\tfrac{1}{2}\lambda_{q_2}\left(-\omega_3 q_1+\omega_1 q_3+\omega_2 q_4\right)\ldots \\ &+\tfrac{1}{2}\lambda_{q_3}\left(\omega_2 q_1-\omega_1 q_2+\omega_3 q_4\right)\ldots \\ &+\tfrac{1}{2}\lambda_{q_4}\left(-\omega_1 q_1-\omega_2 q_2-\omega_3 q_3\right)\ldots \\ &+\lambda_{\omega_1}\left(\frac{J_2-J_3}{J_1}\omega_2\omega_3+\frac{\tau_1}{J_1}\right)\ldots \\ &+\lambda_{\omega_2}\left(\frac{J_3-J_1}{J_2}\omega_1\omega_3+\frac{\tau_2}{J_2}\right)\ldots \\ &+\lambda_{\omega_3}\left(\frac{J_1-J_2}{J_3}\omega_1\omega_2+\frac{\tau_3}{J_3}\right) \end{aligned} \tag{1.97}$$

2. Evaluation of the Hamiltonian Minimization Condition

Because there are path constraints in this problem, the Hamiltonian minimization condition is only satisfied if the Lagrangian of the Hamiltonian is minimized. The Lagrangian of the Hamiltonian is defined as

$$\overline{H}\left(\vec{\mu},\vec{\lambda},\vec{x},\vec{u},t\right)=H\left(\vec{\lambda},\vec{x},\vec{u},t\right)+\vec{\mu}^{T}\bullet\vec{h}\left(\vec{x},\vec{u},t\right) \tag{1.98}$$

where $H\left(\vec{\lambda},\vec{x},\vec{u},t\right)$ is the Hamiltonian [equation (1.97)], $\vec{\mu}$ is the path constraint covector and $\vec{h}\left(\vec{x},\vec{u},t\right)$ is the vector of path constraints. In this problem, if the eigenaxis constraint is broken out into three constraints along each of the body frame axes, there are a total of six path constraints. To facilitate the development of the Lagrangian of the Hamiltonian, the path constraints are written more explicitly in equation (1.99).

$$
\begin{aligned}
h_1^L &\le \tau_1 \le h_1^U \\
h_2^L &\le \tau_2 \le h_2^U \\
h_3^L &\le \tau_3 \le h_3^U \\
h_4 = 0 &= \left[\omega_2\left(q_{2c}q_1 - q_{1c}q_2 + q_{4c}q_3 - q_{3c}q_4\right) - \omega_3\left(-q_{3c}q_1 + q_{4c}q_2 + q_{1c}q_3 - q_{2c}q_4\right)\right] \\
h_5 = 0 &= \left[-\omega_1\left(q_{2c}q_1 - q_{1c}q_2 + q_{4c}q_3 - q_{3c}q_4\right) + \omega_3\left(q_{4c}q_1 + q_{3c}q_2 - q_{2c}q_3 - q_{1c}q_4\right)\right] \\
h_6 = 0 &= \left[\omega_1\left(-q_{3c}q_1 + q_{4c}q_2 + q_{1c}q_3 - q_{2c}q_4\right) - \omega_2\left(q_{4c}q_1 + q_{3c}q_2 - q_{2c}q_3 - q_{1c}q_4\right)\right]
\end{aligned}
\tag{1.99}
$$

where $h_n^L = -1.55\text{Nm}$ and $h_n^U = 1.55\text{Nm}$ are the torque limits along each of the axes. Finally, the Lagrangian of the Hamiltonian, $\overline{H}$, for this problem is given in equation (1.100).

$$
\begin{aligned}
\overline{H} = {} & \tfrac{1}{2}\lambda_{q_1}\left(\omega_3 q_2 - \omega_2 q_3 + \omega_1 q_4\right)... \\
& + \tfrac{1}{2}\lambda_{q_2}\left(-\omega_3 q_1 + \omega_1 q_3 + \omega_2 q_4\right)... \\
& + \tfrac{1}{2}\lambda_{q_3}\left(\omega_2 q_1 - \omega_1 q_2 + \omega_3 q_4\right)... \\
& + \tfrac{1}{2}\lambda_{q_4}\left(-\omega_1 q_1 - \omega_2 q_2 - \omega_3 q_3\right)... \\
& + \lambda_{\omega_1}\left(\frac{J_2 - J_3}{J_1}\omega_2\omega_3 + \frac{\tau_1}{J_1}\right)... \\
& + \lambda_{\omega_2}\left(\frac{J_3 - J_1}{J_2}\omega_1\omega_3 + \frac{\tau_2}{J_2}\right)... \\
& + \lambda_{\omega_3}\left(\frac{J_1 - J_2}{J_3}\omega_1\omega_2 + \frac{\tau_3}{J_3}\right)... \\
& + \mu_1\tau_1 + \mu_2\tau_2 + \mu_3\tau_3 + \mu_4 h_4 + \mu_5 h_5 + \mu_6 h_6
\end{aligned}
\tag{1.100}
$$

The next step is to minimize the Lagrangian of the Hamiltonian with respect to the control. Specifically, the Hamiltonian minimization condition (HMC) can be written as

$$
\frac{\partial \overline{H}}{\partial \bar{u}} = 0 \quad \text{and} \quad \bar{\mu} \dagger \bar{h} \tag{1.101}
$$

where the notation $\bar{\mu} \dagger \bar{h}$ is defined to mean that $\bar{\mu}$ and $\bar{h}$ satisfy the complementarity condition, which is defined in equation (1.102).

$$\mu_i \begin{cases} \leq 0 & if \quad h_i(\bar{u}) = h_i^L \\ = 0 & if \quad h_i^L < h_i(\bar{u}) < h_i^U \\ \geq 0 & if \quad h_i(\bar{u}) = h_i^U \\ unrestricted & if \quad h_i^L = h_i^U \end{cases} \tag{1.102}$$

Solving the HMC problem with respect to each of the control variables reveals a switching structure that is similar to that seen in the SDOF optimization problems.

$$\mu_1 = -\frac{\lambda_{\omega_1}}{J_1} \quad \text{and} \quad \tau_1 \begin{cases} = h_1^L & if \quad \mu_1 \leq 0 \\ \in \left[h_1^L, h_1^U \right] & if \quad \mu_1 = 0 \\ = h_1^U & if \quad \mu_1 \geq 0 \end{cases} \tag{1.103}$$

$$\mu_2 = -\frac{\lambda_{\omega_2}}{J_2} \quad \text{and} \quad \tau_2 \begin{cases} = h_2^L & if \quad \mu_2 \leq 0 \\ \in \left[h_2^L, h_2^U \right] & if \quad \mu_2 = 0 \\ = h_2^U & if \quad \mu_2 \geq 0 \end{cases} \tag{1.104}$$

$$\mu_3 = -\frac{\lambda_{\omega_3}}{J_3} \quad \text{and} \quad \tau_3 \begin{cases} = h_3^L & if \quad \mu_3 \leq 0 \\ \in \left[h_3^L, h_3^U \right] & if \quad \mu_3 = 0 \\ = h_3^U & if \quad \mu_3 \geq 0 \end{cases} \tag{1.105}$$

Observe that (1.103) to (1.105) suggest that the solution may be a three-dimensional bang-bang control.

3. Adjoint Equations

The adjoint equations define the dynamics of the state covector, $\vec{\lambda}$. Again, because of the path constraints, the adjoint equations are slightly modified and take the form shown in equation (1.106).

$$-\dot{\vec{\lambda}} = \frac{\partial \overline{H}}{\partial \vec{x}} \quad \left(\text{and } \vec{\mu} \dagger \vec{h}\right) \tag{1.106}$$

The adjoint equations for this problem are shown in (1.107).

$$\begin{aligned}
-\dot{\lambda}_{q_1} &= \tfrac{1}{2}\left[-\lambda_{q_2}\omega_3 + \lambda_{q_3}\omega_2 - \lambda_{q_4}\omega_1\right] + \mu_4\left(\omega_2 q_{2c} + \omega_3 q_{3c}\right)\ldots \\
&\quad + \mu_5\left(\omega_3 q_{4c} - \omega_1 q_{2c}\right) + \mu_6\left(-\omega_1 q_{3c} - \omega_2 q_{4c}\right) \\
-\dot{\lambda}_{q_2} &= \tfrac{1}{2}\left[\lambda_{q_1}\omega_3 - \lambda_{q_3}\omega_1 - \lambda_{q_4}\omega_2\right] + \mu_4\left(-\omega_2 q_{1c} - \omega_3 q_{4c}\right)\ldots \\
&\quad + \mu_5\left(\omega_1 q_{1c} + \omega_3 q_{3c}\right) + \mu_6\left(\omega_1 q_{4c} - \omega_2 q_{3c}\right) \\
-\dot{\lambda}_{q_3} &= \tfrac{1}{2}\left[-\lambda_{q_1}\omega_2 + \lambda_{q_2}\omega_1 - \lambda_{q_4}\omega_3\right] + \mu_4\left(\omega_2 q_{4c} - \omega_3 q_{1c}\right)\ldots \\
&\quad + \mu_5\left(-\omega_1 q_{4c} - \omega_3 q_{2c}\right) + \mu_6\left(\omega_1 q_{1c} + \omega_2 q_{2c}\right) \\
-\dot{\lambda}_{q_4} &= \tfrac{1}{2}\left[\lambda_{q_1}\omega_1 + \lambda_{q_2}\omega_2 + \lambda_{q_3}\omega_3\right] + \mu_4\left(-\omega_2 q_{3c} + \omega_3 q_{2c}\right)\ldots \\
&\quad + \mu_5\left(\omega_1 q_{3c} - \omega_3 q_{1c}\right) + \mu_6\left(-\omega_1 q_{2c} + \omega_2 q_{1c}\right) \\
-\dot{\lambda}_{\omega_1} &= \tfrac{1}{2}\left[\lambda_{q_1} q_4 + \lambda_{q_2} q_3 - \lambda_{q_3} q_2 - \lambda_{q_4} q_1\right] + \lambda_{\omega_2}\omega_3\frac{J_3 - J_1}{J_2} + \lambda_{\omega_3}\omega_2\frac{J_1 - J_2}{J_3}\ldots \\
&\quad - \mu_5\left(q_{2c} q_1 - q_{1c} q_2 + q_{4c} q_3 - q_{3c} q_4\right) + \mu_6\left(-q_{3c} q_1 + q_{4c} q_2 + q_{1c} q_3 - q_{1c} q_4\right) \\
-\dot{\lambda}_{\omega_2} &= \tfrac{1}{2}\left[\lambda_{q_1} q_3 + \lambda_{q_2} q_4 + \lambda_{q_3} q_1 - \lambda_{q_4} q_2\right] + \lambda_{\omega_1}\omega_3\frac{J_2 - J_3}{J_1} + \lambda_{\omega_3}\omega_1\frac{J_1 - J_2}{J_3}\ldots \\
&\quad + \mu_4\left(q_{2c} q_1 - q_{1c} q_2 + q_{4c} q_3 - q_{3c} q_4\right) - \mu_6\left(q_{4c} q_1 + q_{3c} q_2 - q_{2c} q_3 - q_{1c} q_4\right) \\
-\dot{\lambda}_{\omega_3} &= \tfrac{1}{2}\left[\lambda_{q_1} q_1 - \lambda_{q_2} q_2 + \lambda_{q_3} q_3 - \lambda_{q_4} q_4\right] + \lambda_{\omega_1}\omega_2\frac{J_2 - J_3}{J_1} + \lambda_{\omega_2}\omega_1\frac{J_3 - J_1}{J_2}\ldots \\
&\quad - \mu_4\left(-q_{3c} q_1 + q_{4c} q_2 + q_{1c} q_3 - q_{1c} q_4\right) + \mu_5\left(q_{4c} q_1 + q_{3c} q_2 - q_{2c} q_3 - q_{1c} q_4\right)
\end{aligned} \tag{1.107}$$

Note that the complementarity condition adds following definitions of the last three control covectors:

$$\left.\begin{matrix}\mu_4\\ \mu_5\\ \mu_6\end{matrix}\right\} = \textit{unrestricted} \quad \text{because} \quad h_i^L = h_i^U \tag{1.108}$$

4. Evaluation of the Hamiltonian Value Condition

The Hamiltonian value condition (HVC) provides the value of the minimized Hamiltonian of the optimal solution at the final time. HVC is defined in equation (1.109) where $\mathcal{H}$ signifies the minimized Hamiltonian and $\overline{E}$ is the endpoint Lagrangian, which is defined in equation (1.110).

$$\mathcal{H}\left[@t_f\right] = -\frac{\partial \overline{E}}{\partial t_f} \tag{1.109}$$

with

$$\overline{E} = E + \vec{\upsilon}^T \bullet \vec{e} \tag{1.110}$$

The endpoint Lagrangian in this problem is shown in equation

$$\overline{E} = t_f + \upsilon_1 q_{1_f} + \upsilon_2 q_{2_f} + \upsilon_3 q_{3_f} + \upsilon_4 q_{4_f} + \upsilon_5 \omega_{1_f} + \upsilon_6 \omega_{2_f} + \upsilon_7 \omega_{3_f} \tag{1.111}$$

As with all minimum time optimization problems, the HVC simply yields

$$\mathcal{H}\left[@t_f\right] = -1 \tag{1.112}$$

5. Evaluation of the Hamiltonian Evolution Equation

The Hamiltonian must also satisfy the Hamiltonian evolution equation, which simply specifies that the time rate of change of the minimized Hamiltonian will equal the time rate of change of the Hamiltonian (i.e., $\frac{d\mathcal{H}}{dt} = \frac{\partial H}{\partial t}$). But examination of the Hamiltonian in this problem [equation (1.97)] shows that it is not explicitly a function of time. Therefore, the Hamiltonian evolution equation in

this problem reveals that the Hamiltonian of the optimal solution should be constant with respect to time.

$$\frac{d\mathcal{H}}{dt} = \frac{\partial H}{\partial t} = 0 \tag{1.113}$$

6. Evaluation of the Transversality Condition

Similar to the Hamiltonian value condition, the transversality condition specifies the value of the state covector, $\vec{\lambda}$, at the final time. The transversality condition is defined in equation (1.114).

$$\vec{\lambda}\left(t_f\right) = \frac{\partial \overline{E}}{\partial \vec{x}_f} \tag{1.114}$$

A cursory inspection of the endpoint Lagrangian [equation (1.111)] shows that the transversality condition in this problem is simply

$$\lambda_i\left(t_f\right) = \upsilon_i \tag{1.115}$$

Initially a condition that equates one unknown with another unknown may seem useless, but that is not so. While this condition cannot be used to determine the optimal control trajectory in this problem, it can be used to validate that a numerical solution is in fact optimal.

7. Time Optimal Solution to Open-Loop Eigenaxis Maneuver Problem

The problem definition for an optimal eigenaxis maneuver was coded into the DIDO optimal control software and yielded the results shown in Figures 68–74 for an N=64 node analysis.

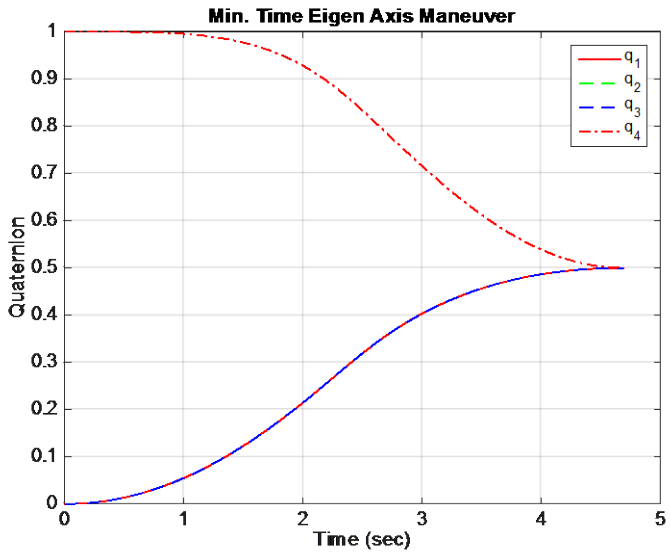

Figure 68. Quaternion trajectory of minimum time eigenaxis maneuver

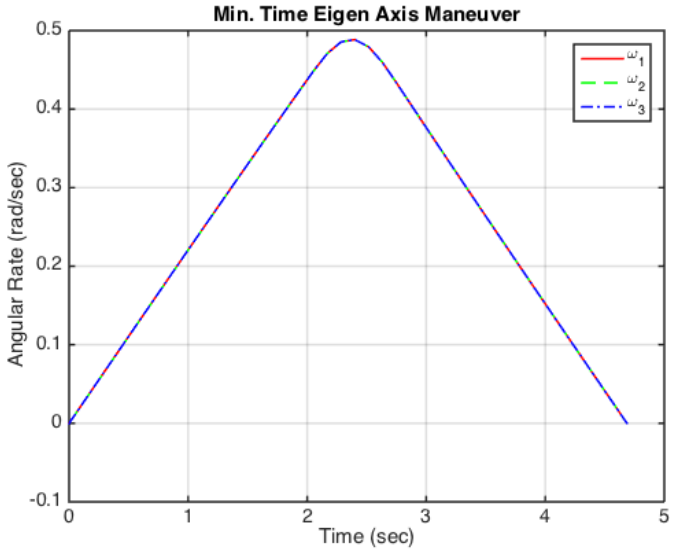

Figure 69. Angular rate trajectory in minimum time eigenaxis maneuver

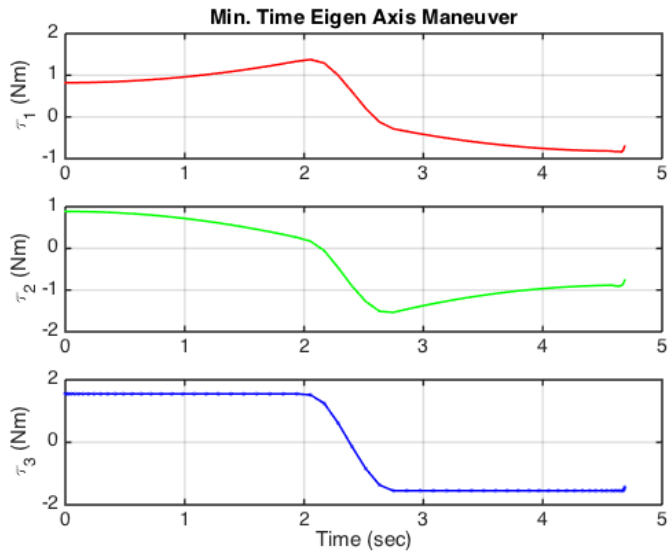

Figure 70. Torque trajectory in minimum time eigenaxis maneuver

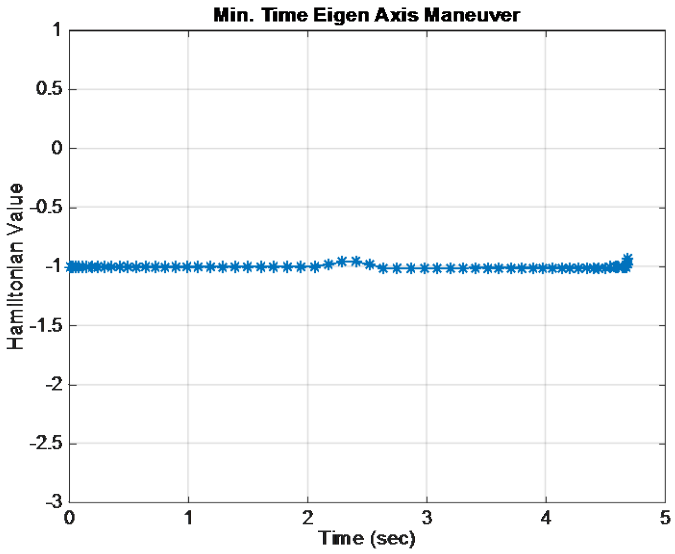

Figure 71. Hamiltonian trajectory in minimum time eigenaxis maneuver

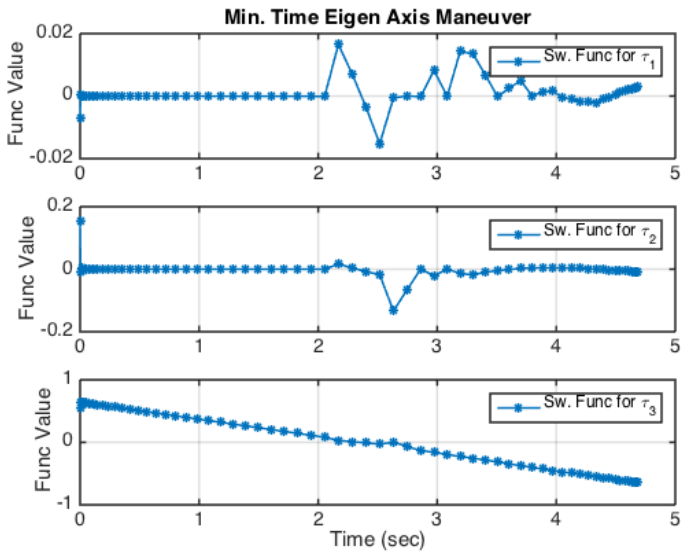

Figure 72. Switching functions in minimum time eigenaxis maneuver

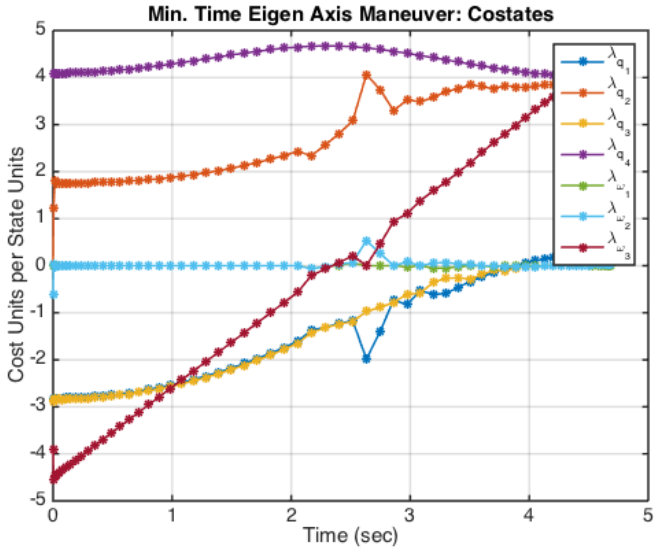

Figure 73. State covector trajectories in minimum time eigenaxis maneuver

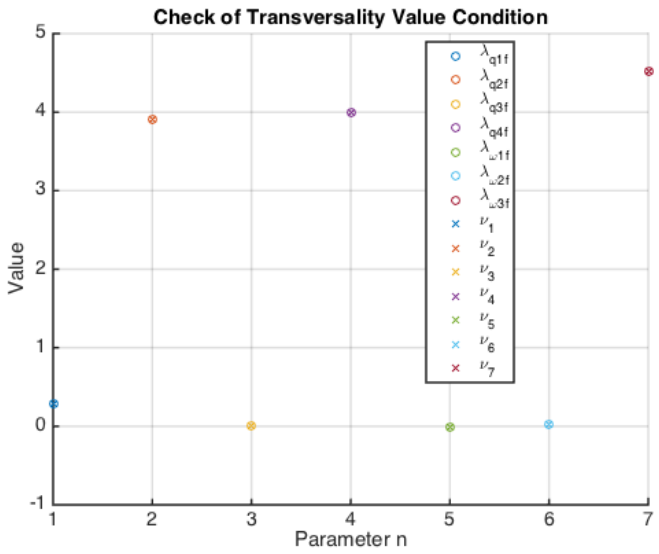

Figure 74. Transversality condition satisfaction in minimum time eigenaxis maneuver

The numerical solution indeed appears to be the time optimal eigenaxis solution. The control torque trajectories comply with the complementarity condition (compare Figure 70 with Figure 72). Observe that the component of the control torque in the z-direction appears to be the limiting factor; it is at either +1.55 Nm or -1.55 Nm throughout the maneuver. The Hamiltonian is approximately constant at a value of -1 throughout the maneuver (see Figure 71), demonstrating that the Hamiltonian Value Condition and Hamiltonian evolution equation are both satisfied. Finally, Figure 74 illustrates that the transversality condition is also satisfied by this solution.

Referring back to Figure 70, it is observed that the torque trajectory is not constant in all directions throughout the maneuver. A closer analysis of the control torque trajectory is instructive. Recall that in this simple eigenaxis maneuver problem, the control torque is composed of both the torque necessary to execute the maneuver's motion as well as the torque necessary to counter or prevent the gyroscopic motion. The torque necessary to prevent the gyroscopic motion is equal to the cross product in the rotational kinematics equation (i.e. $\vec{\omega} \times J\vec{\omega}$). This torque can be reconstructed based on the state trajectory from the

optimal control solution; subtracting that torque from the total control torque will reveal the torque trajectory that produces the motion of the spacecraft. These results are presented in Figures 75–77.

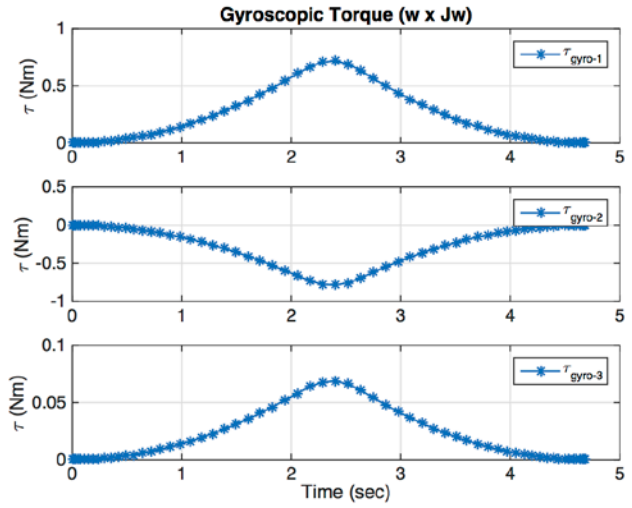

Figure 75. Reconstructed gyroscopic control torques

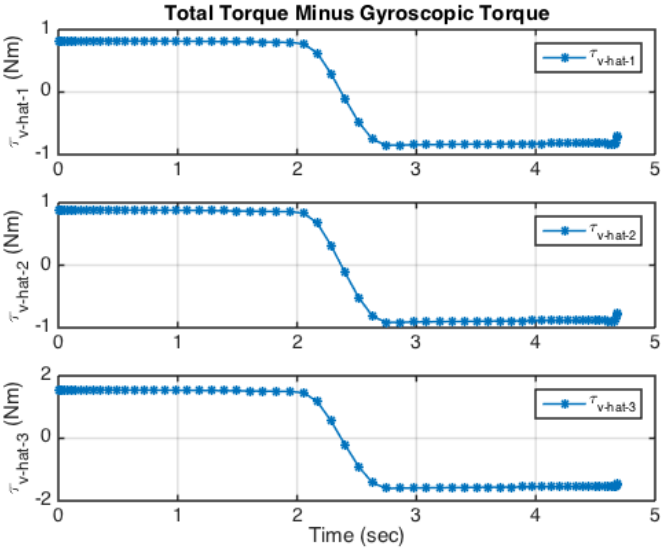

Figure 76. Reconstructed control torque in $\hat{v}$ direction

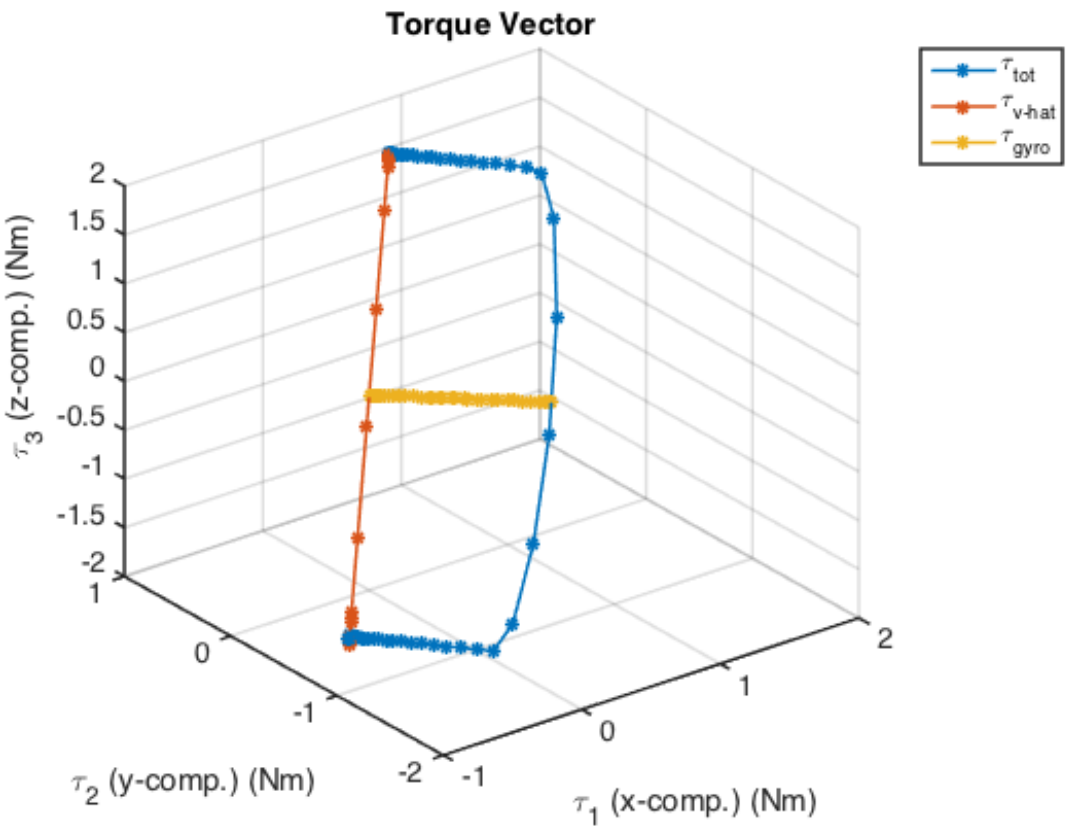

Figure 77. Three Dimensional Plot of Control Torque from DIDO Solution

The three dimensional plot in Figure 77 shows the trajectory of the control torque throughout the maneuver. In this spatial plot, time moves along the trajectory, starting at the top of the plot and ending at the bottom. The total control torque changes direction and magnitude throughout the maneuver in response to the growing gyroscopic torque, which is a function of velocity. However, the direction of the control torque in the $\hat{v}$ direction, shown in red, is constant through the maneuver, appearing to produce the “bang-bang” control pattern seen in the single degree of freedom optimal control.

The additional analyses shown in Figures 75 through 77 seem to confirm the expected response. The optimal control torque is composed of both the gyroscopic torque as well as torque aligned in the $\hat{\boldsymbol{v}}$ direction producing the actual motion. The torque along $\hat{\boldsymbol{v}}$ appears to follow the bang-bang pattern seen

in the SDOF optimal control solution, indicating that the RTOC methods developed in SDOF might be able to be transferred to the three dimensional problem. However, future analysis will reveal that these conclusions are flawed in a critical way, which was not immediately obvious by examining the numerical solution to the optimal control problem.

F. MINIMUM TIME EIGENAXIS MANEUVER WITH QUATERNION ERROR FEEDBACK AND FEED-FORWARD CONTROL TORQUE

The next step is to determine the solution for the optimal eigenaxis maneuver with a closed-loop control system, incorporating the quaternion error feedback loop and the feed-forward control torque. The optimal control problem formulation for a closed-loop system is surprisingly similar to the open-loop eigenaxis problem, with the addition of the quaternion error feedback torques in the dynamics of the velocity states and the expansion of the torque constraint to include both the quaternion error feedback torque as well as the control torque. This problem formulation is presented in equation (1.116), followed by the optimal control analysis. In this problem formulation, the counter gyroscopic torque is included in the feed-forward control torque, $\bar{u} = \left[\tau_1, \quad \tau_2, \quad \tau_3\right]^T$.

States: $\bar{x} = \begin{bmatrix} \bar{q} \\ \bar{\omega} \end{bmatrix}$ Controls: $\bar{u} = \begin{bmatrix} \tau_1 \\ \tau_2 \\ \tau_3 \end{bmatrix}$

minimize: $J\left[\bar{x}(\cdot), \bar{u}(\cdot), t_f\right] = t_f$

subject to:

$$\dot{q}_1 = \tfrac{1}{2}\left(\omega_3 q_2 - \omega_2 q_3 + \omega_1 q_4\right)$$

$$\dot{q}_2 = \tfrac{1}{2}\left(-\omega_3 q_1 + \omega_1 q_3 + \omega_2 q_4\right)$$

$$\dot{q}_3 = \tfrac{1}{2}\left(\omega_2 q_1 - \omega_1 q_2 + \omega_3 q_4\right)$$

$$\dot{q}_4 = \tfrac{1}{2}\left(-\omega_1 q_1 - \omega_2 q_2 - \omega_3 q_3\right)$$

$$\dot{\omega}_1 = \frac{J_2 - J_3}{J_1}\omega_2\omega_3 - k\left(q_{4c}q_1 + q_{3c}q_2 - q_{2c}q_3 - q_{1c}q_4\right) - c\omega_1 + \frac{\tau_1}{J_1}$$

$$\dot{\omega}_2 = \frac{J_3 - J_1}{J_2}\omega_1\omega_3 - k\left(-q_{3c}q_1 + q_{4c}q_2 + q_{1c}q_3 - q_{2c}q_4\right) - c\omega_2 + \frac{\tau_2}{J_2} \quad (1.116)$$

$$\dot{\omega}_3 = \frac{J_1 - J_2}{J_3}\omega_1\omega_2 - k\left(q_{2c}q_1 - q_{1c}q_2 + q_{4c}q_3 - q_{3c}q_4\right) - c\omega_3 + \frac{\tau_3}{J_3}$$

$$\bar{x}_0{}^T = \begin{bmatrix} 0, & 0, & 0, & 1, & 0, & 0, & 0 \end{bmatrix}^T$$

$$\bar{x}_f{}^T = \begin{bmatrix} 0.5, & 0.5, & 0.5, & 0.5, & 0, & 0, & 0 \end{bmatrix}^T$$

$$t_0 = 0$$

$$t_f = t^f$$

$$\begin{bmatrix} -1.55 \\ -1.55 \\ -1.55 \end{bmatrix} \le \left[-kJ\bar{q}_{error} - cJ\bar{\omega}_{error} + \begin{bmatrix} \tau_1 \\ \tau_2 \\ \tau_3 \end{bmatrix} \right] \le \begin{bmatrix} 1.55 \\ 1.55 \\ 1.55 \end{bmatrix}$$

$$\vec{\omega} \times \vec{q}_c = \vec{0}$$

1. The Hamiltonian

$$
\begin{aligned}
H\left(\bar{\lambda},\bar{x},\bar{u},t\right) &= F\left(\bar{x},\bar{u},t\right)+\bar{\lambda}^{T}\bullet\bar{f}\left(\bar{x},\bar{u},t\right)\\
&= \tfrac{1}{2}\lambda_{q_1}\left(\omega_3 q_2-\omega_2 q_3+\omega_1 q_4\right)\ldots\\
&+\tfrac{1}{2}\lambda_{q_2}\left(-\omega_3 q_1+\omega_1 q_3+\omega_2 q_4\right)\ldots\\
&+\tfrac{1}{2}\lambda_{q_3}\left(\omega_2 q_1-\omega_1 q_2+\omega_3 q_4\right)\ldots\\
&+\tfrac{1}{2}\lambda_{q_4}\left(-\omega_1 q_1-\omega_2 q_2-\omega_3 q_3\right)\ldots\\
&+\lambda_{\omega_1}\left(\frac{J_2-J_3}{J_1}\omega_2\omega_3-k\left(q_{4c}q_1+q_{3c}q_2-q_{2c}q_3-q_{1c}q_4\right)-c\omega_1+\frac{\tau_1}{J_1}\right)\ldots\\
&+\lambda_{\omega_2}\left(\frac{J_3-J_1}{J_2}\omega_1\omega_3-k\left(-q_{3c}q_1+q_{4c}q_2+q_{1c}q_3-q_{2c}q_4\right)-c\omega_2+\frac{\tau_2}{J_2}\right)\ldots\\
&+\lambda_{\omega_3}\left(\frac{J_1-J_2}{J_3}\omega_1\omega_2-k\left(q_{2c}q_1-q_{1c}q_2+q_{4c}q_3-q_{3c}q_4\right)-c\omega_3+\frac{\tau_3}{J_3}\right)
\end{aligned}
\tag{1.117}
$$

2. Evaluation of the Hamiltonian Minimization Condition

Because this problem formulation contains path constraints, the Hamiltonian minimization condition is satisfied through the minimization of the Lagrangian of the Hamiltonian.

$$
\begin{aligned}
\overline{H}\left(\bar{\mu},\bar{\lambda},\bar{x},\bar{u},t\right) &= H\left(\bar{\lambda},\bar{x},\bar{u},t\right)+\bar{\mu}^{T}\bullet\bar{h}\left(\bar{x},\bar{u},t\right)\\
&= H\left(\bar{\lambda},\bar{x},\bar{u},t\right)+\mu_1 h_1+\mu_2 h_2+\mu_3 h_3+\mu_4 h_4+\mu_5 h_5+\mu_6 h_6
\end{aligned}
\tag{1.118}
$$

where

$$
\begin{aligned}
h_1^{\,L} \le \left[-kJ_1\left(q_{4c}q_1+q_{3c}q_2-q_{2c}q_3-q_{1c}q_4\right)-cJ_1\omega_1+\tau_1\right] \le h_1^{\,U}\\
h_2^{\,L} \le \left[-kJ_2\left(-q_{3c}q_1+q_{4c}q_2+q_{1c}q_3-q_{2c}q_4\right)-cJ_2\omega_2+\tau_2\right] \le h_2^{\,U}\\
h_3^{\,L} \le \left[-kJ_3\left(q_{2c}q_1-q_{1c}q_2+q_{4c}q_3-q_{3c}q_4\right)-cJ_3\omega_3+\tau_3\right] \le h_3^{\,U}\\
h_4 = 0 = \left[\omega_2\left(q_{2c}q_1-q_{1c}q_2+q_{4c}q_3-q_{3c}q_4\right)-\omega_3\left(-q_{3c}q_1+q_{4c}q_2+q_{1c}q_3-q_{2c}q_4\right)\right]\\
h_5 = 0 = \left[-\omega_1\left(q_{2c}q_1-q_{1c}q_2+q_{4c}q_3-q_{3c}q_4\right)+\omega_3\left(q_{4c}q_1+q_{3c}q_2-q_{2c}q_3-q_{1c}q_4\right)\right]\\
h_6 = 0 = \left[\omega_1\left(-q_{3c}q_1+q_{4c}q_2+q_{1c}q_3-q_{2c}q_4\right)-\omega_2\left(q_{4c}q_1+q_{3c}q_2-q_{2c}q_3-q_{1c}q_4\right)\right]
\end{aligned}
\tag{1.119}
$$

The Hamiltonian Minimization Condition is given by

$$\frac{\partial \overline{H}}{\partial \bar{u}} = 0 \quad \text{and} \quad \bar{\mu} \dagger \bar{h} \tag{1.120}$$

Evaluating equation (1.120) reveals the following switching structure for the control toque.

$$\mu_1 = -\frac{\lambda_{\omega_1}}{J_1} \text{ and } \tau_1 \begin{cases} = h_1^L & \text{if } \mu_1 \le 0 \\ \in \left[h_1^L, h_1^U\right] & \text{if } \mu_1 = 0 \\ = h_1^U & \text{if } \mu_1 \ge 0 \end{cases}$$

$$\mu_2 = -\frac{\lambda_{\omega_2}}{J_2} \text{ and } \tau_2 \begin{cases} = h_2^L & \text{if } \mu_2 \le 0 \\ \in \left[h_2^L, h_2^U\right] & \text{if } \mu_2 = 0 \\ = h_2^U & \text{if } \mu_2 \ge 0 \end{cases} \tag{1.121}$$

$$\mu_3 = -\frac{\lambda_{\omega_3}}{J_3} \text{ and } \tau_3 \begin{cases} = h_3^L & \text{if } \mu_3 \le 0 \\ \in \left[h_3^L, h_3^U\right] & \text{if } \mu_3 = 0 \\ = h_3^U & \text{if } \mu_3 \ge 0 \end{cases}$$

As with the previous problem, μ_4, μ_5, and μ_6 will take arbitrary values.

3. The Adjoint Equations

Like the Hamiltonian minimization condition, the adjoint equations must also be defined in based on the Lagrangian of the Hamiltonian due to the presence of path constraints.

$$-\dot{\bar{\lambda}} = \frac{\partial \overline{H}}{\partial \bar{x}} \quad \left(\text{and } \bar{\mu} \dagger \bar{h}\right) \tag{1.122}$$

$$
\begin{aligned}
-\dot{\lambda}_{q_1} &= \tfrac{1}{2}\left[-\lambda_{q_2}\omega_3 + \lambda_{q_3}\omega_2 - \lambda_{q_4}\omega_1\right]\ldots \\
&\quad -\mu_1 kJ_1 q_{4c} + \mu_2 kJ_2 q_{3c} - \mu_3 kJ_3 q_{2c}\ldots \\
&\quad +\mu_4\left(\omega_2 q_{2c} + \omega_3 q_{3c}\right) + \mu_5\left(\omega_3 q_{4c} - \omega_1 q_{2c}\right) + \mu_6\left(-\omega_1 q_{3c} - \omega_2 q_{4c}\right) \\
-\dot{\lambda}_{q_2} &= \tfrac{1}{2}\left[\lambda_{q_1}\omega_3 - \lambda_{q_3}\omega_1 - \lambda_{q_4}\omega_2\right]\ldots \\
&\quad -\mu_1 kJ_1 q_{3c} - \mu_2 kJ_2 q_{4c} + \mu_3 kJ_3 q_{1c}\ldots \\
&\quad +\mu_4\left(-\omega_2 q_{1c} - \omega_3 q_{4c}\right) + \mu_5\left(\omega_1 q_{1c} + \omega_3 q_{3c}\right) + \mu_6\left(\omega_1 q_{4c} - \omega_2 q_{3c}\right) \\
-\dot{\lambda}_{q_3} &= \tfrac{1}{2}\left[-\lambda_{q_1}\omega_2 + \lambda_{q_2}\omega_1 - \lambda_{q_4}\omega_3\right]\ldots \\
&\quad +\mu_1 kJ_1 q_{2c} - \mu_2 kJ_2 q_{1c} - \mu_3 kJ_3 q_{4c}\ldots \\
&\quad +\mu_4\left(\omega_2 q_{4c} - \omega_3 q_{1c}\right) + \mu_5\left(-\omega_1 q_{4c} - \omega_3 q_{2c}\right) + \mu_6\left(\omega_1 q_{1c} + \omega_2 q_{2c}\right) \\
-\dot{\lambda}_{q_4} &= \tfrac{1}{2}\left[\lambda_{q_1}\omega_1 + \lambda_{q_2}\omega_2 + \lambda_{q_3}\omega_3\right]\ldots \\
&\quad +\mu_1 kJ_1 q_{1c} + \mu_2 kJ_2 q_{2c} + \mu_3 kJ_3 q_{3c}\ldots \\
&\quad +\mu_4\left(-\omega_2 q_{3c} + \omega_3 q_{2c}\right) + \mu_5\left(\omega_1 q_{3c} - \omega_3 q_{1c}\right) + \mu_6\left(-\omega_1 q_{2c} + \omega_2 q_{1c}\right) \\
-\dot{\lambda}_{\omega_1} &= \tfrac{1}{2}\left[\lambda_{q_1} q_4 + \lambda_{q_2} q_3 - \lambda_{q_3} q_2 - \lambda_{q_4} q_1\right]\ldots \\
&\quad +\lambda_{\omega_2}\omega_3\frac{J_3 - J_1}{J_2} + \lambda_{\omega_3}\omega_2\frac{J_1 - J_2}{J_3} - \lambda_{\omega_1} c - \mu_1 cJ_1\ldots \\
&\quad -\mu_5\left(q_{2c} q_1 - q_{1c} q_2 + q_{4c} q_3 - q_{3c} q_4\right) + \mu_6\left(-q_{3c} q_1 + q_{4c} q_2 + q_{1c} q_3 - q_{1c} q_4\right) \\
-\dot{\lambda}_{\omega_2} &= \tfrac{1}{2}\left[\lambda_{q_1} q_3 + \lambda_{q_2} q_4 + \lambda_{q_3} q_1 - \lambda_{q_4} q_2\right]\ldots \\
&\quad +\lambda_{\omega_1}\omega_3\frac{J_2 - J_3}{J_1} + \lambda_{\omega_3}\omega_1\frac{J_1 - J_2}{J_3} - \lambda_{\omega_2} c - \mu_2 cJ_2\ldots \\
&\quad +\mu_4\left(q_{2c} q_1 - q_{1c} q_2 + q_{4c} q_3 - q_{3c} q_4\right) - \mu_6\left(q_{4c} q_1 + q_{3c} q_2 - q_{2c} q_3 - q_{1c} q_4\right) \\
-\dot{\lambda}_{\omega_3} &= \tfrac{1}{2}\left[\lambda_{q_1} q_1 - \lambda_{q_2} q_2 + \lambda_{q_3} q_3 - \lambda_{q_4} q_4\right]\ldots \\
&\quad +\lambda_{\omega_1}\omega_2\frac{J_2 - J_3}{J_1} + \lambda_{\omega_2}\omega_1\frac{J_3 - J_1}{J_2} - \lambda_{\omega_3} c - \mu_3 cJ_3\ldots \\
&\quad -\mu_4\left(-q_{3c} q_1 + q_{4c} q_2 + q_{1c} q_3 - q_{1c} q_4\right) + \mu_5\left(q_{4c} q_1 + q_{3c} q_2 - q_{2c} q_3 - q_{1c} q_4\right)
\end{aligned}
\tag{1.123}
$$

Again, μ_4, μ_5, and μ_6 will take arbitrary values.

4. Evaluation of the Hamiltonian Value Condition

Evaluation of the Hamiltonian value condition for this problem reveals the same result as with the open-loop eigenaxis maneuver optimization.

$$\mathcal{H}\left[@t_f\right] = -1 \tag{1.124}$$

5. Evaluation of the Hamiltonian Evolution Equation

The Hamiltonian evolution equation in this problem formulation yields the same result as in the open-loop eigenaxis maneuver optimization.

$$\frac{d\mathcal{H}}{dt} = \frac{\partial H}{\partial t} = 0 \tag{1.125}$$

6. Evaluation of the Transversality Condition

Evaluation of the transversality condition in this problem, again, yields the same result as in the open-loop eigenaxis maneuver optimization.

$$\lambda_i\left(t_f\right) = \upsilon_i \tag{1.126}$$

7. Numerical Solution and Analysis

A N=100 node numerical solution to this problem formulation is presented in Figures 78–86.

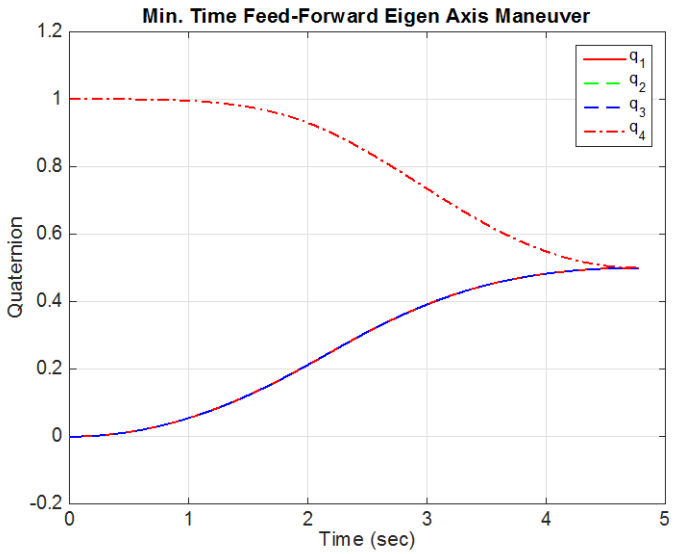

Figure 78. Quaternion trajectory for closed-loop eigenaxis solution

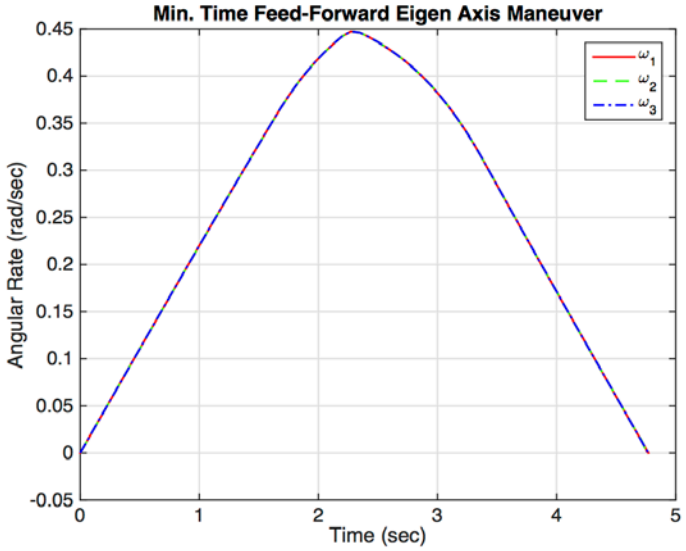

Figure 79. Rate trajectories for closed-loop eigenaxis solution

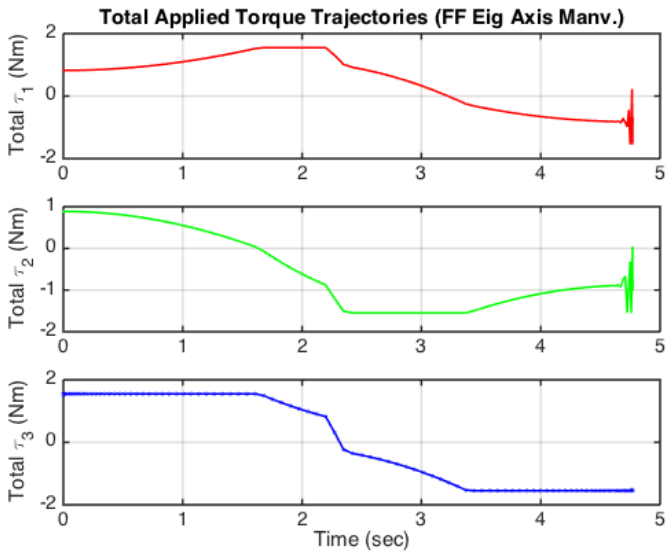

Figure 80. Total torque trajectories for closed-loop eigenaxis solution

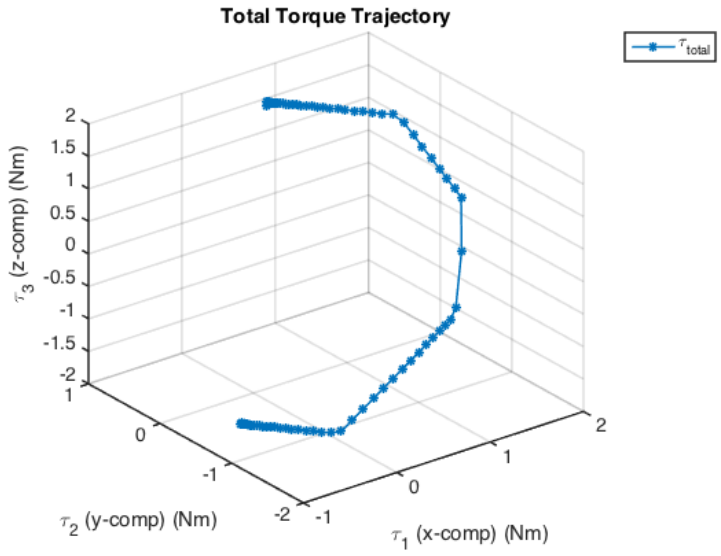

Figure 81. Spatial plot of the total torque trajectory for the closed-loop eigenaxis solution

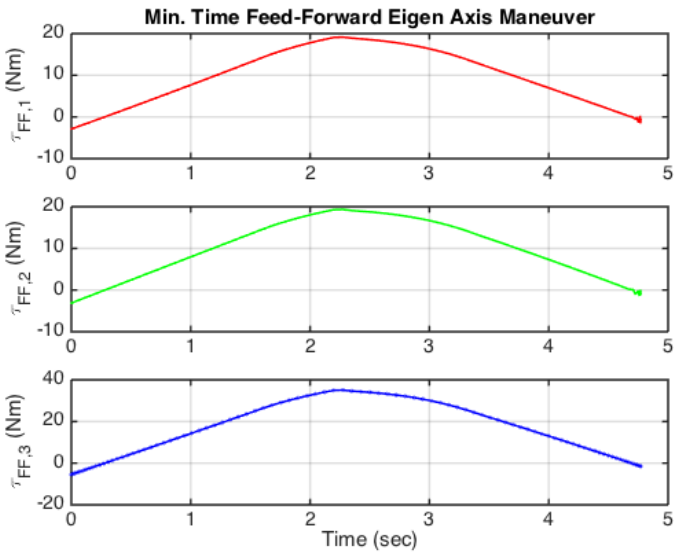

Figure 82. Feed-forward control torque trajectories for closed-loop eigenaxis solution

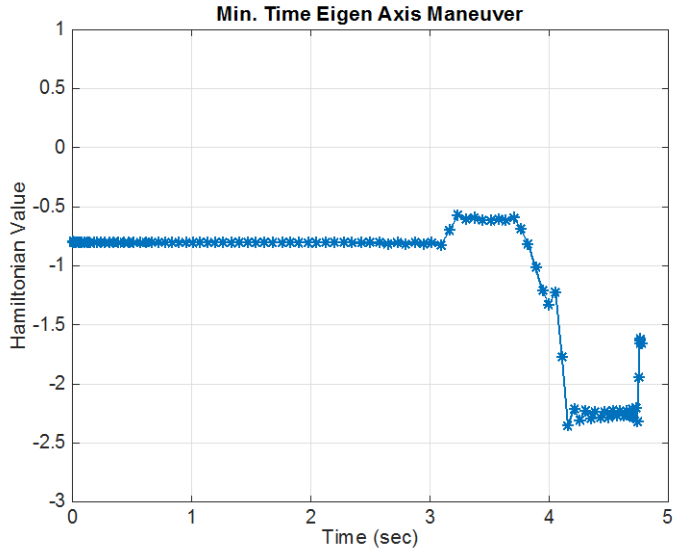

Figure 83. Hamiltonian Trajectory for Closed-Loop Eigenaxis Solution

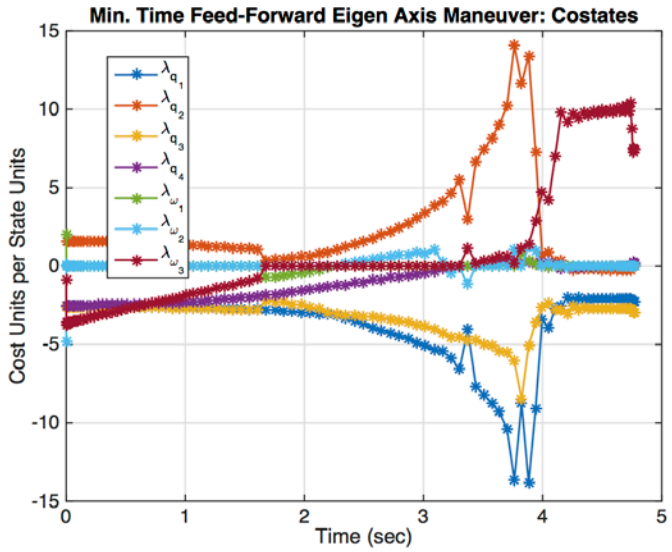

Figure 84. Costate Trajectories for Closed-Loop Eigenaxis Solution

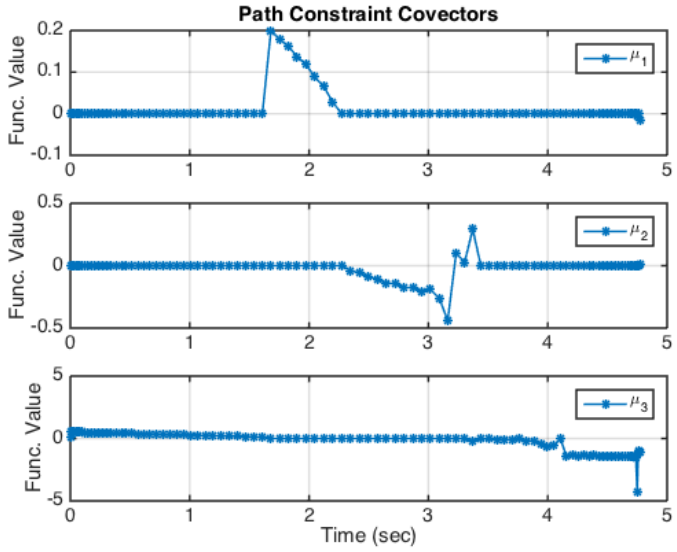

Figure 85. Path Covector Trajectories for Closed-Loop Eigenaxis Solution

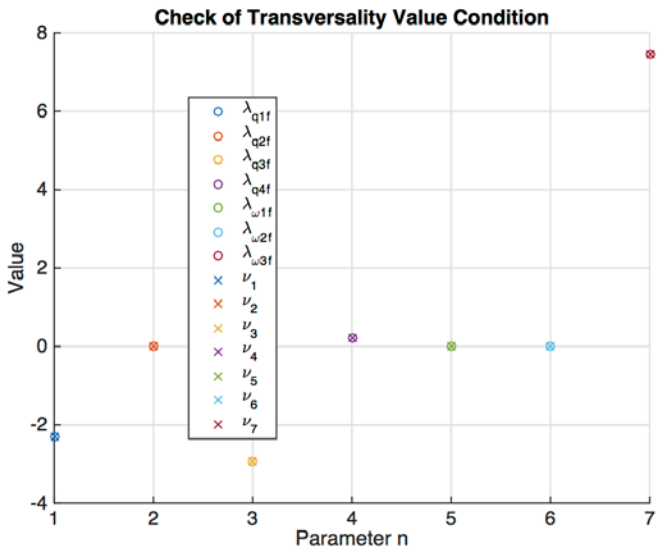

Figure 86. Transversality Value Condition Validation for Closed-Loop Eigenaxis Solution

These plots indicate that the necessary conditions for optimality have been met. The transversality value condition is met, as shown in Figure 86. The feed-forward control torque trajectories comply with the path constraint trajectories, demonstrating satisfaction of the complementarity condition. The Hamiltonian trajectory shown in Figure 83 only approximately satisfies the Hamiltonian value condition and the Hamiltonian evolution equation. A Hamiltonian that is more exactly constant at a value of -1 would be preferable; a comparison of the costate trajectories and the state trajectories indicates that this problem is suffering from a scaling challenge. But, the solution presented is sufficiently accurate to provide a great deal of information for the development of a real-time optimal eigenaxis controller.

Some additional analysis of these results will be instructive. Figure 87 contains a plot of the reconstructed gyroscopic torque; this torque is computed based on the solution's angular rates (i.e. $\tau_{gyro} = \bar{\omega} \times J\bar{\omega}$). Recall that the gyroscopic torque is incorporated into the feed-forward control torque. Figure 88 is a plot of the total torque in the $\hat{\nu}$ direction and Figure 89 is a separate plot of

its magnitude; this torque is computed by subtracting the gyroscopic torque from the sum of the quaternion error feedback torque and the feed-forward control torque.

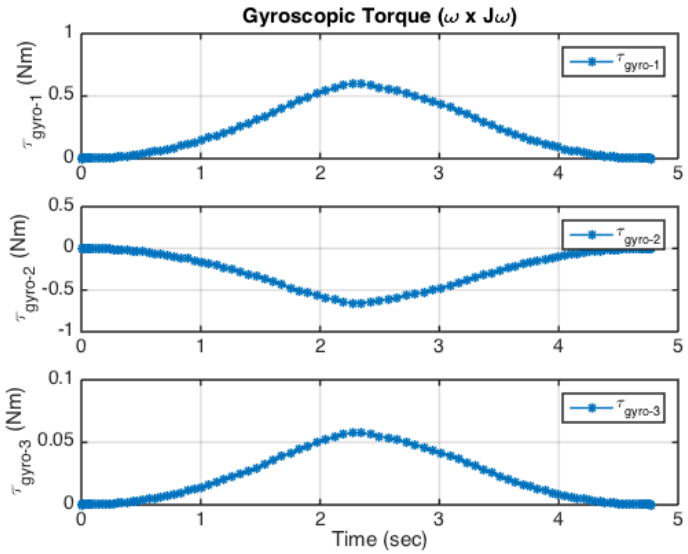

Figure 87. Gyroscopic torque for feed-forward solution

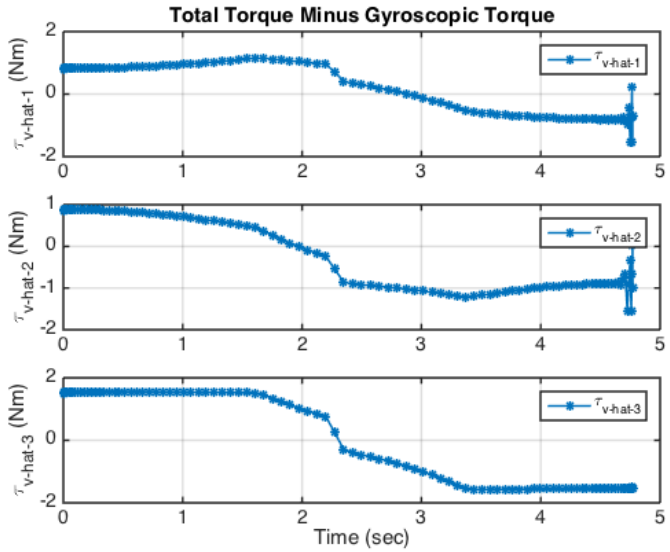

Figure 88. Torque in the $\hat{\boldsymbol{\nu}}$ direction from the feed-forward solution

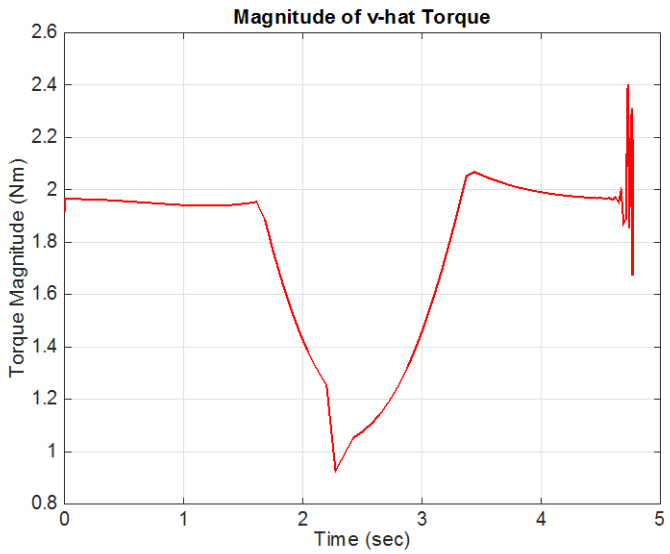

Figure 89. Magnitude of torque in the $\hat{\boldsymbol{v}}$ direction from the feed-forward solution

One of the most interesting insights revealed by this solution is the impact of the gyroscopic torque on the overall total torque trajectory and the torque in the $\hat{\boldsymbol{v}}$ direction in particular. The torque envelope constrains the total torque, which is the sum of both the quaternion error feedback and the feed-forward control torque. The open-loop solution demonstrated that the optimal solution for an eigenaxis maneuver is achieved when the torque in the $\hat{\boldsymbol{v}}$direction is maximized throughout the maneuver. Thus, the total torque can be written as follows:

$$\begin{aligned} \bar{\tau}_{tot} &= \bar{\tau}_{QEF} + \bar{\tau}_{FF} \\ &= \tau_{v-\max}\hat{v} + \bar{\tau}_{gyro} \end{aligned} \tag{1.127}$$

where $\bar{\tau}_{QEF}$ is the quaternion error feedback torque; $\bar{\tau}_{FF}$ is the feed forward control torque; $\bar{\tau}_{v-\max}$ is the maximum torque in the $\hat{\boldsymbol{v}}$ direction; and $\bar{\tau}_{gyro}$ is the counter gyroscopic torque.

Figures 80, 81 and 88 show that the z-component is dominant in the $\hat{\boldsymbol{v}}$ torque, but the x- and y-components are dominant in the gyroscopic torques. As

the maneuver progresses, and the body gains velocity, the gyroscopic torque increases. The minor increase in the z-component of the gyroscopic torque results in a corresponding decrease in $\bar{\tau}_{v-\max}$. The reduction in torque is most apparent in Figure 88. But, approximately 1.6 seconds into the maneuver, the growing x-component of the gyroscopic torque becomes the dominant component of the total torque. From start to approximately 1.6 seconds, the z-component of total torque is at its maximum (1.55 Nm); but at 1.6 seconds, the x-component is maxed at 1.55 Nm and the z-component begins to decrease dramatically. This decrease in the z-component of the total torque is due to the fact that the gyroscopic torque is continuing to increase as the body continues to accelerate about the eigenaxis. Because the counter gyroscopic torque must be maintained to sustain the eigenaxis motion, the only way to contain total torque within the torque envelope is to reduce the torque in the $\hat{\boldsymbol{v}}$ direction. This is most apparent in Figure 88, the plot of the magnitude of torque in the $\hat{\boldsymbol{v}}$ direction. After the switch at 2.27 seconds, the limiting component becomes the y-component. The y-component is saturated at -1.55 Nm until approximately 3.4 seconds when the gyroscopic torque has been sufficiently reduced to return the z-component to dominance. This variation is also apparent in the angular velocity trajectories shown in Figure 79; the slope of these curves is fairly constant at the beginning and toward the end of the maneuver, but the rate of change of the angular velocity is clearly not constant near the middle of the maneuver.

Even more intriguing than the fact that the torque in the $\hat{\boldsymbol{v}}$ direction varies in response to the variation of the gyroscopic torque is the asymmetry of the variation. Examine Figure 89. The difference between the shapes of the torque trajectory on either side of the switch at 2.27 seconds is dramatic. More remarkable still, the magnitude of torque in the $\hat{\boldsymbol{v}}$ direction at 3.44 seconds is 2.07 Nm, greater than 1.97 Nm, which would be predicted by the torque envelope. This is possible because only the total torque is limited to the envelope; in this case, the direction of the gyroscopic torque shifts the direction

of the total torque vector and allows greater torque to be produced in the $\hat{\nu}$ direction.

8. Implications for a Real-Time Optimal Controller

The natural consequence of the asymmetry of the torque in the $\hat{\nu}$ direction is that the acceleration is also asymmetric. Consequently, even for this rest-to-rest maneuver, the switch from acceleration torque to deceleration torque is not in the middle of the maneuver. In this case, the total maneuver is complete in 4.77 seconds, but the switch occurs at 2.27 seconds, slightly earlier than the half-way mark. Recall that the core of the one-dimensional RTOC controller was a kinematic algorithm that calculated the maneuver switch and final times based on constant acceleration. This algorithm will not work if the acceleration along the eigenaxis is not constant.

G. A FLAWED REAL-TIME OPTIMAL EIGENAXIS CONTROLLER

The significance of the $\tau_{v-\max}$ variation on a potential RTOC controller was not initially obvious. Indeed, due to an oversight in the analysis, the variation was not initially detected at all.[2] But this mistake proved to be very instructive and is worth presenting.

1. Introduction to the Eigenaxis RTOC Algorithm

The algorithm for this RTOC controller is very similar to the algorithm in the SDOF optimal control algorithm with a couple modest modifications necessary for implementation in three-dimensions. One modification accounts for the variation of the maximum torque as a function of the eigenaxis. This RTOC algorithm employs the same method of computing the switch and final maneuver times, based on θ_{error} extracted from the quaternion, the magnitude of velocity

[2] An early version of the closed-loop eigenaxis optimization analysis incorrectly defined the total torque constraint, essentially neglecting the gyroscopic torque. Without the need to modify $\tau\hat{\nu}$ in response to increasing τ_{gyro}, the optimal solution included a constant $\tau\hat{\nu}$ on either side of the switch. Of course, the total torque exceeded the torque envelope at certain points, but these minor breeches were not detected until much later, after erroneous conclusions had been drawn.

along the eigenaxis and the maximum acceleration possible about the eigenaxis. There is, however, one significant modification. The analysis leading up to the SDOF RTOC controller included the development of an analytical solution to the feed-forward torque using Laplace transforms and other linear control techniques. Any hopes of a simple conversion of that formula to a three-dimensional formula were likely dashed on the rocks of mathematical reality during the discussion of the three dimensional rotational kinematics.

But there is a deceptively simple solution to this problem. The nonlinearities of Euler's rotational kinematic equations, the quaternion definition and quaternion error feedback formula preclude the use of Laplace transforms as a method of control analysis. However, knowledge of the optimal control trajectory (i.e., the bang-bang total torque) enables the use of a state space model of the system and a standard ordinary differential equation propagator to develop the feed-forward control torque trajectory. In other words, the feedback torque can be computed numerically using a sample-and-propagate technique, allowing the computation of feed-forward torque based on predicted system states.

Because the trajectory of the total torque vector is known, from the optimal control solution analysis, and the current quaternion and angular rate vector are known, the complete quaternion and angular rate trajectories can be predicted simply by propagating the quaternion and angular rate dynamics with an ODE propagator. This is analogous (but with zero error) to the use of a state estimator to compute unmeasured states [7]. A related implementation of sample-and-propagate optimal control trajectory generation is also described in [10]. The quaternion and angular rate dynamics are given by:

$$\dot{\bar{q}} = \frac{1}{2}\begin{bmatrix} 0 & \omega_3 & -\omega_2 & \omega_1 \\ -\omega_3 & 0 & \omega_1 & \omega_2 \\ \omega_2 & -\omega_1 & 0 & \omega_3 \\ -\omega_1 & -\omega_2 & -\omega_3 & 0 \end{bmatrix}\begin{bmatrix} q_1 \\ q_2 \\ q_3 \\ q_4 \end{bmatrix} \qquad (1.128)$$
$$\dot{\vec{\omega}} = J^{-1} \cdot \vec{\tau}_{\hat{v}-\max}$$

Further, the fact that an eigenaxis maneuver is essentially a one-dimensional rotation in the plane defined by the eigenaxis vector allows a further simplification of this ODE propagation estimator. The commanded position is known, and the current position is known, therefore, $\hat{\boldsymbol{v}}$ is known. Because the gyroscopic motion is zeroed, the dynamics of the system simplify to (1.86). This knowledge can be used to construct the euler angle and angular rate trajectories in the following simple state space model.

$$\begin{aligned} \dot{\theta}_{error} &= \omega_{\hat{e}} \\ \dot{\omega}_{\hat{e}} &= \frac{1}{J_{eff}}\left|\left|\vec{\tau}_{tot}\right|\right|(t) \end{aligned} \qquad (1.129)$$

In (1.129) θ_{error} is the Euler angle, used in the quaternion error feedback, and $\omega_{\hat{e}}$ is the magnitude of the angular velocity in the eigenaxis direction. It is helpful to note that because the eigenaxis by definition has a magnitude of 1, $\omega_{\hat{e}}$ can be calculated by

$$\omega_{\hat{e}} = \left|\left|\vec{\omega}\right|\right| = \vec{\omega} \bullet \hat{e} \qquad (1.130)$$

which also means

$$\vec{\omega} = \omega_{\hat{e}}\hat{e} \qquad (1.131)$$

Once the states trajectories are calculated in (1.129), the quaternion error feedback and control torque trajectories can be computed with the simple formulas given in (1.132).

$$\vec{\tau}_{QEF}(t) = -k \cdot J \cdot \hat{e} \cdot \sin\left(\frac{\theta_{error}(t)}{2}\right) - c \cdot J \cdot \omega_{\hat{e}}(t) \cdot \hat{e} + \left(\left(\omega_{\hat{e}}(t) \cdot \hat{e}\right) \times J\left(\omega_{\hat{e}}(t) \cdot \hat{e}\right)\right) \quad (1.132)$$
$$\vec{\tau}_{ctrl}(t) = \vec{\tau}_{tot}(t) - \vec{\tau}_{QEF}(t)$$

Alternatively, and even more simply, the quaternion error feedback torque or system states could be measured directly and the control torque could be computed in real time. The particular implementation would depend on the existing system architecture, processing power and sampling frequency.

The simplicity of this solution stems from the fact that the RTOC controller can measure the quaternion error feedback torque directly *in real-time* and modulate the feed-forward control torque accordingly. While this is fairly straightforward, some complications remain.

The feed-forward control torque contains the gyroscopic torque; thus the control torque formula can be written as

$$\tau_{ctrl}(t)\hat{v} = \vec{\tau}_{tot}(t) + k \cdot J \cdot \vec{q}_{error}(t) + c \cdot J \cdot \vec{\omega}_{error}(t) - \vec{\tau}_{gyro}(t) \quad (1.133)$$

where $\tau_{ctrl}\hat{v}$ is the portion of the control torque in the $\hat{v}$ direction. τ_{ctrl} is a scalar quantity that scales $\hat{v}$ such that the total torque vector, $\vec{\tau}_{tot}$, is maximized within the available torque envelope. Solving for $\tau_{ctrl}$is the principle challenge.

Equation (1.133) contains several known quantities; because the system's states can be measured in real time, the quaternion error torque and the gyroscopic torque terms are known. The direction of $\tau_{ctrl}\hat{v}$ is known, but its magnitude is not. Neither the exact direction nor the magnitude of the total torque, $\vec{\tau}_{tot}$, is known, but what is known is that at least one of the components (i.e., the x-, y- or z-components of total torque vector) will be at the torque limit.

Equation (1.133) can be solved by populating each of the components of $\vec{\tau}_{tot}$with the properly signed torque limit and creating a vector of scalar variables

in place of τ_{ctrl}. Each of these scalar variables is the value that maximizes $\bar{\tau}_{tot}$ in its respective direction. The correct value of τ_{ctrl} is the minimum of these variables. See the example in Equation (1.134); this example is based on the state of the system at $t = 1.008\,\text{sec}$ in the closed-loop eigenaxis solution presented in Figures 78–89.

$$\tau_{ctrl}(t)\cdot\hat{v}\cdot I = \bar{\tau}_{tot}(t) + k\cdot J\cdot\bar{q}_{error}(t) + c\cdot J\cdot\bar{\omega}_{error}(t) - \bar{\tau}_{gyro}(t)$$

$$\begin{bmatrix} a \\ b \\ c \end{bmatrix}\begin{bmatrix} -0.42 & 0 & 0 \\ 0 & -0.45 & 0 \\ 0 & 0 & -0.79 \end{bmatrix} = \begin{bmatrix} 1.55 \\ 1.55 \\ 1.55 \end{bmatrix} + \begin{bmatrix} -3.49 \\ -3.76 \\ -6.58 \end{bmatrix} + \begin{bmatrix} 10.3 \\ 11.1 \\ 19.4 \end{bmatrix} - \begin{bmatrix} 0.15 \\ -0.16 \\ 0.01 \end{bmatrix}$$

$$\begin{bmatrix} a \\ b \\ c \end{bmatrix}\begin{bmatrix} -0.42 & 0 & 0 \\ 0 & -0.45 & 0 \\ 0 & 0 & -0.79 \end{bmatrix} = \begin{bmatrix} 8.20 \\ 9.04 \\ 14.36 \end{bmatrix}$$

$$\begin{bmatrix} a \\ b \\ c \end{bmatrix} = \begin{bmatrix} -19.5918 \\ -19.9693 \\ -18.2404 \end{bmatrix}$$

$$\tau_{ctrl} = signed\min\left(\begin{vmatrix} a \\ b \\ c \end{vmatrix}\right) \qquad (1.134)$$

$$\tau_{ctrl} = -18.2404$$

$$\bar{\tau}_{FF} = \tau_{ctrl}\hat{v} + \bar{\tau}_{gyro} = \begin{bmatrix} 7.7829 \\ 8.0939 \\ 14.3748 \end{bmatrix}$$

$$\bar{\tau}_{tot} = -k\cdot J\cdot\bar{q}_{error} - c\cdot J\cdot\bar{\omega}_{error} + \bar{\tau}_{FF} = \begin{bmatrix} 0.9843 \\ 0.7675 \\ 1.5500 \end{bmatrix}$$

In this example *a, b* and *c* are the candidate scalar's that must be evaluated. They are evaluated on a per component basis (i.e., scalar *a* is evaluated along the x-component, etc.). This can be accomplished by solving

each of the three equations individually; or, *a, b* and *c* can be treated as components of a vector, and the a-b-c vector can be determined with standard linear algebra techniques if $\hat{\boldsymbol{v}}$ is converted to a diagonal square matrix by multiplying by the identity matrix, I , as was done in (1.134).

Note that τ_{ctrl} is set equal to the component of the a-b-c matrix with the smallest magnitude, but the sign of that component must be retained; this is the meaning of $signed\min(|\ |)$.

One nuance in the eigenaxis RTOC algorithm is worth mentioning. The switch and final times are computed in the same manner as the one-dimensional RTOC controller using θ_{error}, which is computed from the fourth component of the error quaternion [equation (1.85)]. Arccosine is a dual-valued function but the positive value is preferentially chosen in this algorithm; this sign ambiguity is complimented by the sign of the eigenaxis vector, which is also computed from the error quaternion. As such, θ is always positive and θ_{cmd} is always zero; hence, from the perspective of the maneuver time algorithm, all maneuvers are reverse maneuvers, regardless of the direction of rotation.

2. The Eigenaxis Algorithm

The eigenaxis algorithm is summarized in the following steps. References to the relevant calculations are included.

1. Check the Update Time Interval and Dead-Band
2. Compute error quaternion, $\bar{q}_e$ [equation (1.84)]
3. Compute $\hat{\boldsymbol{v}}$ [equation (1.88)]
4. Compute θ_{error} and ω_{error} [equations (1.85) and (1.93)]
5. Compute $\alpha_{\max}$ [algorithm (1.94) and equation (1.95)]
6. Compute t_{sw} and t_f based on θ_{error}, ω_{error} and $\alpha_{\max}$
7. Check for Overspeed Condition; re-compute t_{sw} and t_f if necessary

8. Determine torque direction based on maneuver phase (i.e., acceleration or deceleration)

9. Compute Feed-Forward control torque (equation (1.133))

3. Results from a Flawed Eigenaxis RTOC Controller Maneuver

The results of a maneuver conducted with a flawed RTOC controller are presented in Figures 90–95; this is the same maneuver analyzed in the preceding optimal control analyses. Recall that the flaw in this algorithm is the assumption that the magnitude of the torque in the $\hat{v}$ direction is constant throughout the maneuver, which it is not.

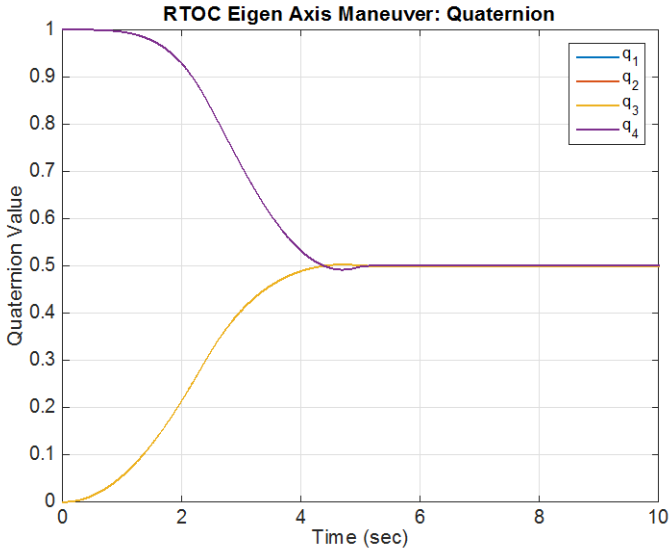

Figure 90. Quaternion trajectory with flawed RTOC controller

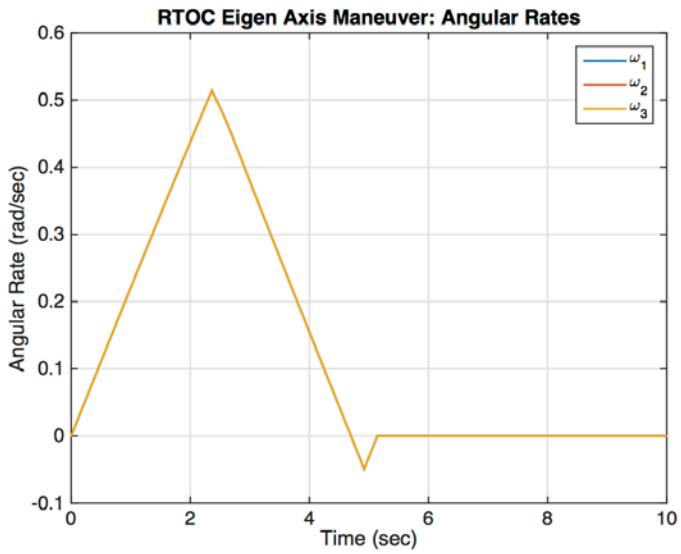

Figure 91. Angular rate trajectory with flawed RTOC controller

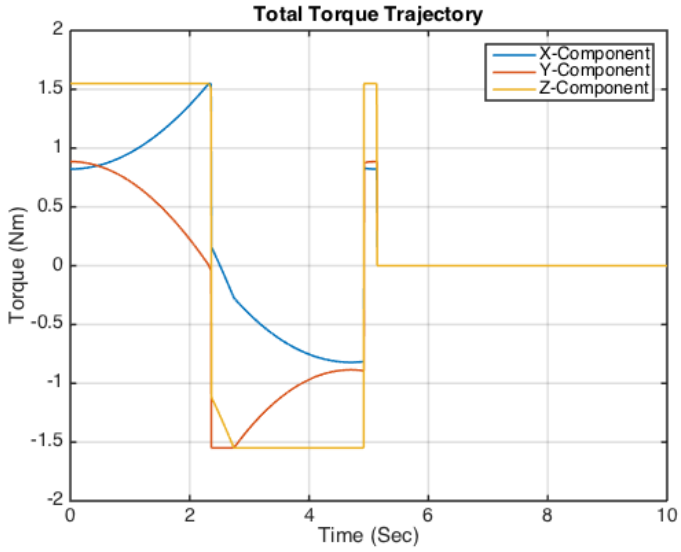

Figure 92. Total torque trajectory by component with flawed RTOC controller

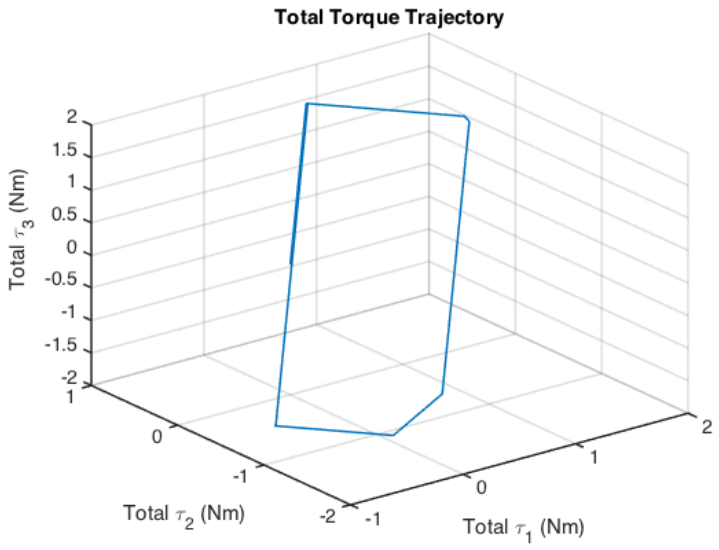

Figure 93. Spatial plot of total torque trajectory with flawed RTOC controller

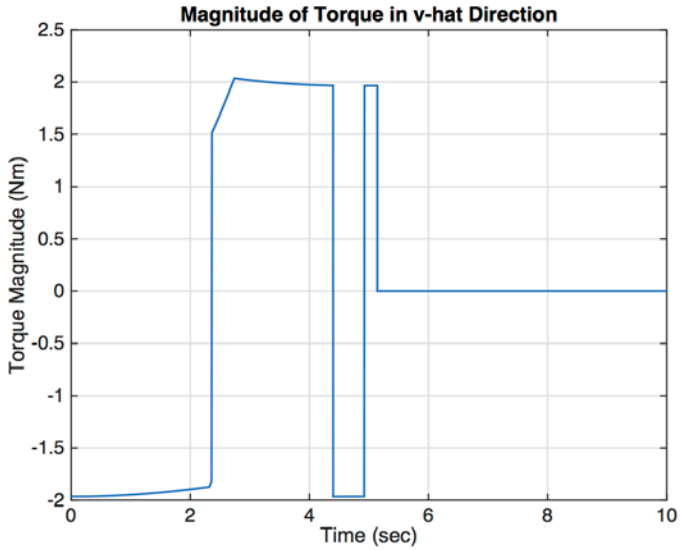

Figure 94. Magnitude of torque applied in the $\hat{\boldsymbol{v}}$ direction during maneuver with flawed RTOC controller

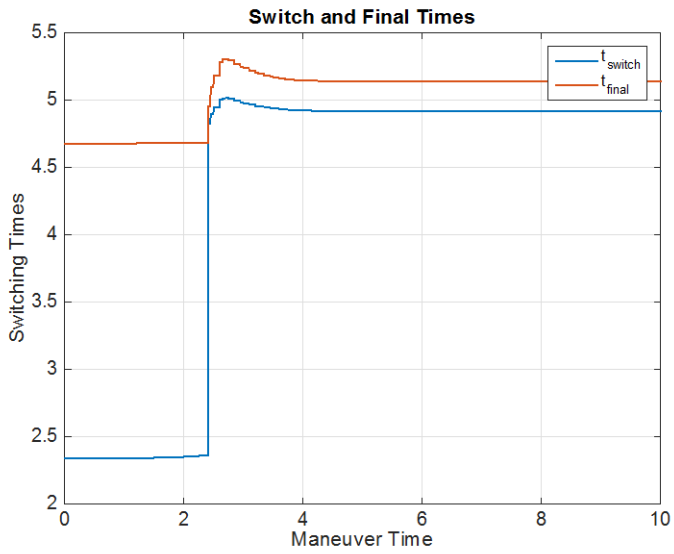

Figure 95. Switch and final times computed during maneuver with flawed RTOC controller

Figure 94 shows the magnitude of torque applied in the $\hat{\boldsymbol{v}}$ direction throughout the maneuver. It has more switches than the torque plots (see Figure 92), but that is due to the change in the eigenaxis direction as a consequence of the overshoot. The switch at 4.4 seconds corresponds to the attitude crossing the commanded quaternion; at that time, the sign of the eigenaxis changes, and consequently, so does the sign of $\hat{\boldsymbol{v}}$ (see the discussion of the sign of θ_{error} at the end of section G.1). This plot is produced by computing the dot product of total torque with $\hat{\boldsymbol{v}}$ at each increment throughout the maneuver.

4. Analysis of the Results from Flawed Eigenaxis RTOC Controller

Given that the implemented maneuver is intended to be a minimum time maneuver, the most relevant parameter to check is the final maneuver time. The flawed RTOC controller completed the maneuver in 5.14 seconds. Yet, the numerical solution produced with DIDO took only 4.77 seconds. Clearly there is a discrepancy. A review of the state trajectories indicates that overshoot occurred.

However, given that this simulation is a maneuver of the nominal system with no uncertainties or disturbances, overshoot should not have occurred.

The problem, of course, is the variation of torque in the $\hat{\nu}$ direction though out the maneuver. The results plotted in Figures 90–95 illustrate the challenge in high fidelity. Figure 92 is particularly interesting because it depicts the trajectory of each of the components of total torque on the same plot. In this plot, it is clear that the total torque vector is touching the maximum torque envelope throughout the maneuver; but it is equally clear that the limiting component changes throughout the maneuver. It is interesting to compare this plot with Figure 94, the plot of the magnitude of torque in the $\hat{\nu}$ direction and Figure 95, the plot of switch and final times. The magnitude of torque along $\hat{\nu}$ decreases only mildly through most of the first half of the maneuver; a very subtle corresponding increase in switch and final time also occurs at this time. During this time, the x-component of total torque has been growing dramatically in response to the gyroscopic torque, and just as the switch occurs, the x-component becomes the limiting component (see Figure 92). But, immediately following the switch, the y-component is now the limiting factor in the total torque vector, and the magnitude of torque along $\hat{\nu}$ is severely limited due to the cubic torque envelope. This unanticipated limitation in torque results in the system not decelerating as quickly as expected and creates an over-speed condition.

The trajectory of the switch and final times following the switch is interesting. The limited deceleration torque results in dramatic increases in the switch and final times. Once the gyroscopic torque has been reduced sufficiently such that the z-component is once again the limiting factor, the magnitude of torque along $\hat{\nu}$ is restored to approximately 2Nm; indeed, at that point, torque along $\hat{\nu}$ exceeds the torque envelope in the $\hat{\nu}$ direction, outpacing the expected torque. There is a corresponding reduction in the switch and final times, but this is not enough to recover from the over-speed condition, which ultimately leads to the overshoot of the targeted position.

5. Alternative RTOC Approaches

The root of the flaw in the preceding RTOC controller is the improper accounting of the variation of the acceleration about the eigenaxis and the resulting miscalculation of switch and final times. There are several potential remedies to resolve this issue. One alternative would be to incorporate optimal control solution software such as DIDO in a closed-loop to constantly update the feed-forward control torque, essentially performing the function of a real time optimal controller. But, this approach could demand a significant computational burden.

Another approach would be to develop a new method of computing the switch and final time. The $\hat{\boldsymbol{v}}$ and $\vec{\tau}_{gyro}$ vectors form a plane; the intersection of that plane with the torque envelope defines the potential trajectory of total torque, and, correspondingly, the trajectory of torque along $\hat{\boldsymbol{v}}$. While some new approach that exploits this fact is conceivable, it is beyond the scope of this thesis.

Fortunately, many spacecraft operate in a manner that precludes such complicated alternatives. Spacecraft that employ zero-net bias control systems do not produce a significant gyroscopic disturbance and therefore would not require counter gyroscopic torque to achieve eigenaxis maneuvers. As such, the torque along $\hat{\boldsymbol{v}}$ would be fairly constant for these systems, and the current method of computing switch and final maneuver times will be accurate and practically implementable.

H. MINIMUM TIME EIGENAXIS MANEUVER OF ZERO-NET BIAS CONTROL SYSTEM WITH QUATERNION ERROR FEEDBACK

Before embarking on the development of an RTOC eigenaxis controller for zero-net biased control system, it is prudent to conduct a new optimal control analysis. While the solution may seem obvious based on the analysis of other control systems, minor changes in an optimal control problem formulation can produce unanticipated and sometimes significant changes in the optimal control solution. The problem formulation is presented in equation (1.135). It is

remarkably similar to the previous closed-loop optimal control problem, except that there are no gyroscopic terms in the angular rate dynamics.

$$
\begin{aligned}
&\underline{\text{States}}: \quad \bar{x} = \begin{bmatrix} \bar{q} \\ \bar{\omega} \end{bmatrix} \qquad\qquad \underline{\text{Controls}}: \quad \bar{u} = \begin{bmatrix} \tau_1 \\ \tau_2 \\ \tau_3 \end{bmatrix} \\
&\underline{\text{minimize}}: \quad J\left[\bar{x}(\cdot), \bar{u}(\cdot), t_f\right] = t_f \\
&\underline{\text{subject to}}: \quad \dot{q}_1 = \tfrac{1}{2}\left(\omega_3 q_2 - \omega_2 q_3 + \omega_1 q_4\right) \\
&\qquad \dot{q}_2 = \tfrac{1}{2}\left(-\omega_3 q_1 + \omega_1 q_3 + \omega_2 q_4\right) \\
&\qquad \dot{q}_3 = \tfrac{1}{2}\left(\omega_2 q_1 - \omega_1 q_2 + \omega_3 q_4\right) \\
&\qquad \dot{q}_4 = \tfrac{1}{2}\left(-\omega_1 q_1 - \omega_2 q_2 - \omega_3 q_3\right) \\
&\qquad \dot{\omega}_1 = -k\left(q_{4c} q_1 + q_{3c} q_2 - q_{2c} q_3 - q_{1c} q_4\right) - c\omega_1 + \frac{\tau_1}{J_1} \\
&\qquad \dot{\omega}_2 = -k\left(-q_{3c} q_1 + q_{4c} q_2 + q_{1c} q_3 - q_{2c} q_4\right) - c\omega_2 + \frac{\tau_2}{J_2} \qquad (1.135) \\
&\qquad \dot{\omega}_3 = -k\left(q_{2c} q_1 - q_{1c} q_2 + q_{4c} q_3 - q_{3c} q_4\right) - c\omega_3 + \frac{\tau_3}{J_3} \\
&\qquad \bar{x}_0{}^T = \begin{bmatrix} 0, & 0, & 0, & 1, & 0, & 0, & 0 \end{bmatrix}^T \\
&\qquad \bar{x}_f{}^T = \begin{bmatrix} 0.5, & 0.5, & 0.5, & 0.5, & 0, & 0, & 0 \end{bmatrix}^T \\
&\qquad t_0 = 0 \\
&\qquad t_f = t^f \\
&\qquad \begin{bmatrix} -1.55 \\ -1.55 \\ -1.55 \end{bmatrix} \le \left[-kJ\bar{q}_{error} - cJ\bar{\omega}_{error} + \begin{bmatrix} \tau_1 \\ \tau_2 \\ \tau_3 \end{bmatrix} \right] \le \begin{bmatrix} 1.55 \\ 1.55 \\ 1.55 \end{bmatrix} \\
&\qquad \bar{\omega} \times \bar{q}_c = \bar{0}
\end{aligned}
$$

1. The Hamiltonian

The Hamiltonian for this problem is given in (1.136)

$$
\begin{aligned}
H\left(\vec{\lambda},\vec{x},\vec{u},t\right) &= F\left(\vec{x},\vec{u},t\right)+\vec{\lambda}^{T}\bullet\vec{f}\left(\vec{x},\vec{u},t\right)\\
&= \tfrac{1}{2}\lambda_{q_1}\left(\omega_3 q_2-\omega_2 q_3+\omega_1 q_4\right)\ldots\\
&+\tfrac{1}{2}\lambda_{q_2}\left(-\omega_3 q_1+\omega_1 q_3+\omega_2 q_4\right)\ldots\\
&+\tfrac{1}{2}\lambda_{q_3}\left(\omega_2 q_1-\omega_1 q_2+\omega_3 q_4\right)\ldots\\
&+\tfrac{1}{2}\lambda_{q_4}\left(-\omega_1 q_1-\omega_2 q_2-\omega_3 q_3\right)\ldots\\
&+\lambda_{\omega_1}\left(-k\left(q_{4c}q_1+q_{3c}q_2-q_{2c}q_3-q_{1c}q_4\right)-c\omega_1+\frac{\tau_1}{J_1}\right)\ldots\\
&+\lambda_{\omega_2}\left(-k\left(-q_{3c}q_1+q_{4c}q_2+q_{1c}q_3-q_{2c}q_4\right)-c\omega_2+\frac{\tau_2}{J_2}\right)\ldots\\
&+\lambda_{\omega_3}\left(-k\left(q_{2c}q_1-q_{1c}q_2+q_{4c}q_3-q_{3c}q_4\right)-c\omega_3+\frac{\tau_3}{J_3}\right)
\end{aligned}
\tag{1.136}
$$

2. Evaluation of the Hamiltonian Minimization Condition

Due to the path constraints, the Hamiltonian minimization condition is satisfied when the Lagrangian of the Hamiltonian is minimized with respect to the control variable. The Lagrangian of the Hamiltonian is given in the following equation.

$$
\begin{aligned}
\overline{H}\left(\vec{\mu},\vec{\lambda},\vec{x},\vec{u},t\right) &= H\left(\vec{\lambda},\vec{x},\vec{u},t\right)+\vec{\mu}^{T}\bullet\vec{h}\left(\vec{x},\vec{u},t\right)\\
&= H\left(\vec{\lambda},\vec{x},\vec{u},t\right)+\mu_1 h_1+\mu_2 h_2+\mu_3 h_3+\mu_4 h_4+\mu_5 h_5+\mu_6 h_6
\end{aligned}
\tag{1.137}
$$

where the path constraints are given by

$$
\begin{aligned}
h_1^{\,L} &\le \left[-kJ_1\left(q_{4c}q_1+q_{3c}q_2-q_{2c}q_3-q_{1c}q_4\right)-cJ_1\omega_1+\tau_1\right] \le h_1^{\,U}\\
h_2^{\,L} &\le \left[-kJ_2\left(-q_{3c}q_1+q_{4c}q_2+q_{1c}q_3-q_{2c}q_4\right)-cJ_2\omega_2+\tau_2\right] \le h_2^{\,U}\\
h_3^{\,L} &\le \left[-kJ_3\left(q_{2c}q_1-q_{1c}q_2+q_{4c}q_3-q_{3c}q_4\right)-cJ_3\omega_3+\tau_3\right] \le h_3^{\,U}\\
h_4^{\,L} &\le \left[\omega_2\left(q_{2c}q_1-q_{1c}q_2+q_{4c}q_3-q_{3c}q_4\right)-\omega_3\left(-q_{3c}q_1+q_{4c}q_2+q_{1c}q_3-q_{2c}q_4\right)\right] \le h_4^{\,U}\\
h_5^{\,L} &\le \left[-\omega_1\left(q_{2c}q_1-q_{1c}q_2+q_{4c}q_3-q_{3c}q_4\right)+\omega_3\left(q_{4c}q_1+q_{3c}q_2-q_{2c}q_3-q_{1c}q_4\right)\right] \le h_5^{\,U}\\
h_6^{\,L} &\le \left[\omega_1\left(-q_{3c}q_1+q_{4c}q_2+q_{1c}q_3-q_{2c}q_4\right)-\omega_2\left(q_{4c}q_1+q_{3c}q_2-q_{2c}q_3-q_{1c}q_4\right)\right] \le h_6^{\,U}
\end{aligned}
\tag{1.138}
$$

The Hamiltonian minimization condition is now given by

$$\frac{\partial \overline{H}}{\partial \bar{u}} = 0 \quad \text{and} \quad \bar{\mu} \dagger \bar{h} \tag{1.139}$$

Evaluation of the Hamiltonian minimization condition reveals the following switching structure.

$$\begin{aligned}
\mu_1 = -\frac{\lambda_{\omega_1}}{J_1} \ \text{and} \ \tau_1 &\begin{cases} = h_1^L & \text{if} \quad \mu_1 \le 0 \\ \in \left[h_1^L, h_1^U \right] & \text{if} \quad \mu_1 = 0 \\ = h_1^U & \text{if} \quad \mu_1 \ge 0 \end{cases} \\
\mu_2 = -\frac{\lambda_{\omega_2}}{J_2} \ \text{and} \ \tau_2 &\begin{cases} = h_2^L & \text{if} \quad \mu_2 \le 0 \\ \in \left[h_2^L, h_2^U \right] & \text{if} \quad \mu_2 = 0 \\ = h_2^U & \text{if} \quad \mu_2 \ge 0 \end{cases} \\
\mu_3 = -\frac{\lambda_{\omega_3}}{J_3} \ \text{and} \ \tau_3 &\begin{cases} = h_3^L & \text{if} \quad \mu_3 \le 0 \\ \in \left[h_3^L, h_3^U \right] & \text{if} \quad \mu_3 = 0 \\ = h_3^U & \text{if} \quad \mu_3 \ge 0 \end{cases}
\end{aligned} \tag{1.140}$$

As before, because $h_{4,5,6}^L = h_{4,5,6}^U$, the path multipliers μ_4, μ_5, and μ_6 take arbitrary values.

3. Adjoint Equations

The adjoint equations are given in (1.141).

$$
\begin{aligned}
-\dot{\lambda}_{q_1} &= \tfrac{1}{2}\left[-\lambda_{q_2}\omega_3 + \lambda_{q_3}\omega_2 - \lambda_{q_4}\omega_1\right] - \mu_1 kJ_1 q_{4c} + \mu_2 kJ_2 q_{3c} - \mu_3 kJ_3 q_{2c} \ldots \\
&\quad + \mu_4\left(\omega_2 q_{2c} + \omega_3 q_{3c}\right) + \mu_5\left(\omega_3 q_{4c} - \omega_1 q_{2c}\right) + \mu_6\left(-\omega_1 q_{3c} - \omega_2 q_{4c}\right) \\
-\dot{\lambda}_{q_2} &= \tfrac{1}{2}\left[\lambda_{q_1}\omega_3 - \lambda_{q_3}\omega_1 - \lambda_{q_4}\omega_2\right] - \mu_1 kJ_1 q_{3c} - \mu_2 kJ_2 q_{4c} + \mu_3 kJ_3 q_{1c} \ldots \\
&\quad + \mu_4\left(-\omega_2 q_{1c} - \omega_3 q_{4c}\right) + \mu_5\left(\omega_1 q_{1c} + \omega_3 q_{3c}\right) + \mu_6\left(\omega_1 q_{4c} - \omega_2 q_{3c}\right) \\
-\dot{\lambda}_{q_3} &= \tfrac{1}{2}\left[-\lambda_{q_1}\omega_2 + \lambda_{q_2}\omega_1 - \lambda_{q_4}\omega_3\right] + \mu_1 kJ_1 q_{2c} - \mu_2 kJ_2 q_{1c} - \mu_3 kJ_3 q_{4c} \ldots \\
&\quad + \mu_4\left(\omega_2 q_{4c} - \omega_3 q_{1c}\right) + \mu_5\left(-\omega_1 q_{4c} - \omega_3 q_{2c}\right) + \mu_6\left(\omega_1 q_{1c} + \omega_2 q_{2c}\right) \\
-\dot{\lambda}_{q_4} &= \tfrac{1}{2}\left[\lambda_{q_1}\omega_1 + \lambda_{q_2}\omega_2 + \lambda_{q_3}\omega_3\right] + \mu_1 kJ_1 q_{1c} + \mu_2 kJ_2 q_{2c} + \mu_3 kJ_3 q_{3c} \ldots \\
&\quad + \mu_4\left(-\omega_2 q_{3c} + \omega_3 q_{2c}\right) + \mu_5\left(\omega_1 q_{3c} - \omega_3 q_{1c}\right) + \mu_6\left(-\omega_1 q_{2c} + \omega_2 q_{1c}\right) \\
-\dot{\lambda}_{\omega_1} &= \tfrac{1}{2}\left[\lambda_{q_1} q_4 + \lambda_{q_2} q_3 - \lambda_{q_3} q_2 - \lambda_{q_4} q_1\right] - \lambda_{\omega_1} c - \mu_1 cJ_1 \ldots \\
&\quad - \mu_5\left(q_{2c} q_1 - q_{1c} q_2 + q_{4c} q_3 - q_{3c} q_4\right) + \mu_6\left(-q_{3c} q_1 + q_{4c} q_2 + q_{1c} q_3 - q_{1c} q_4\right) \\
-\dot{\lambda}_{\omega_2} &= \tfrac{1}{2}\left[\lambda_{q_1} q_3 + \lambda_{q_2} q_4 + \lambda_{q_3} q_1 - \lambda_{q_4} q_2\right] - \lambda_{\omega_2} c - \mu_2 cJ_2 \ldots \\
&\quad + \mu_4\left(q_{2c} q_1 - q_{1c} q_2 + q_{4c} q_3 - q_{3c} q_4\right) - \mu_6\left(q_{4c} q_1 + q_{3c} q_2 - q_{2c} q_3 - q_{1c} q_4\right) \\
-\dot{\lambda}_{\omega_3} &= \tfrac{1}{2}\left[\lambda_{q_1} q_1 - \lambda_{q_2} q_2 + \lambda_{q_3} q_3 - \lambda_{q_4} q_4\right] - \lambda_{\omega_3} c - \mu_3 cJ_3 \ldots \\
&\quad - \mu_4\left(-q_{3c} q_1 + q_{4c} q_2 + q_{1c} q_3 - q_{1c} q_4\right) + \mu_5\left(q_{4c} q_1 + q_{3c} q_2 - q_{2c} q_3 - q_{1c} q_4\right)
\end{aligned}
\tag{1.141}
$$

4. Evaluation of the Hamiltonian Value Condition

As with the previous problems, as a minimum time problem, the Hamiltonian value condition is given by

$$
\mathcal{H}\left[@t_f\right] = -1 \tag{1.142}
$$

5. Evaluation of the Hamiltonian Evolution Equation

The Hamiltonian evolution equation in this problem formulation yields the same result as in the previous optimizations.

$$
\frac{d\mathcal{H}}{dt} = \frac{\partial H}{\partial t} = 0 \tag{1.143}
$$

6. Evaluation of the Transversality Condition

Evaluation of the transversality condition in this problem, again, yields the same result as in the previous optimizations.

$$\lambda_i\left(t_f\right)=\upsilon_i \tag{1.144}$$

7. DIDO Solution and Analysis

The numerical solution to the zero-net bias optimal control problem is presented in Figures 96–104.

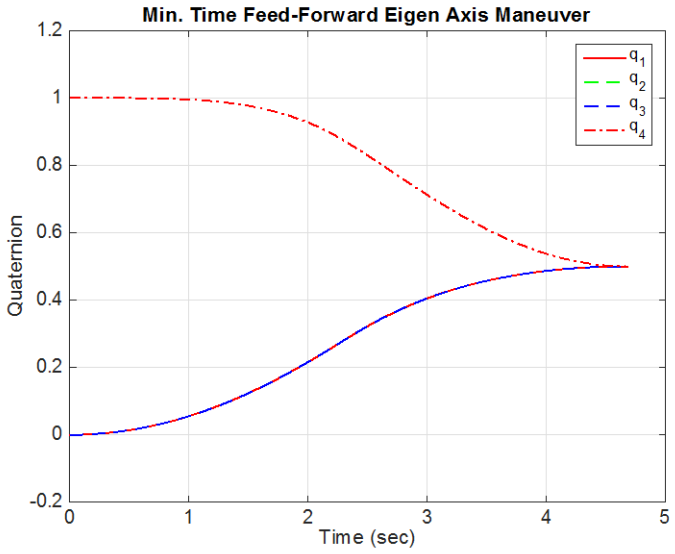

Figure 96. Quaternion trajectory of a maneuver with a zero-net bias system

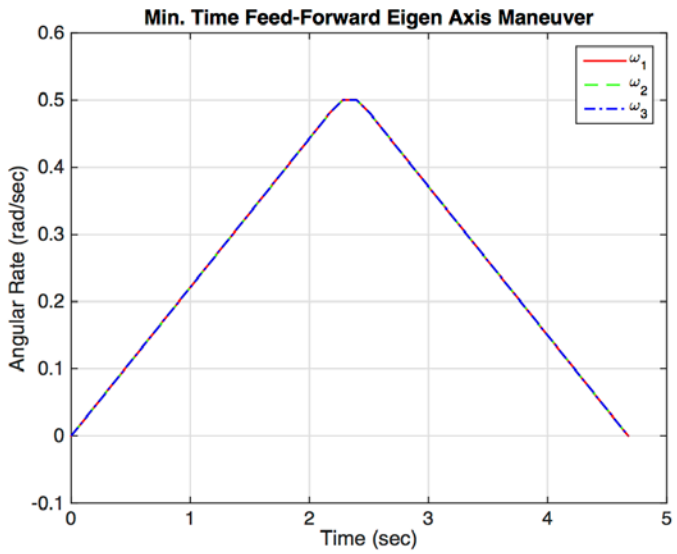

Figure 97. Angular rate trajectories of a maneuver with a zero-net bias system

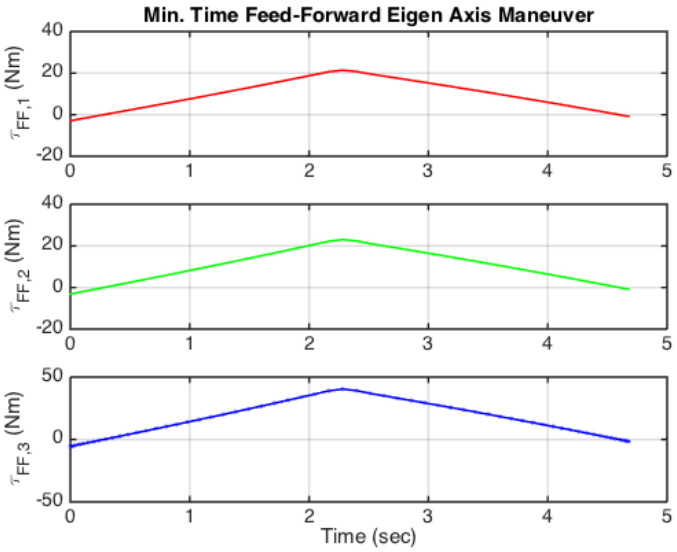

Figure 98. Feed-forward control torque trajectories of a maneuver with a zero-net bias system

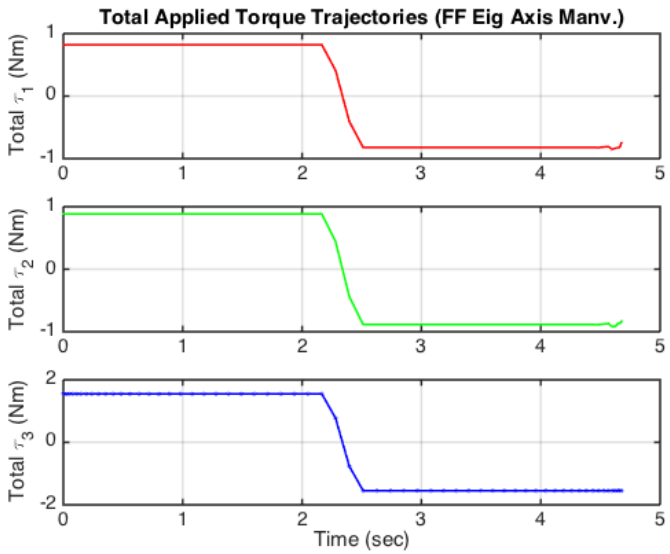

Figure 99. Total torque trajectory of a maneuver with a zero-net bias system

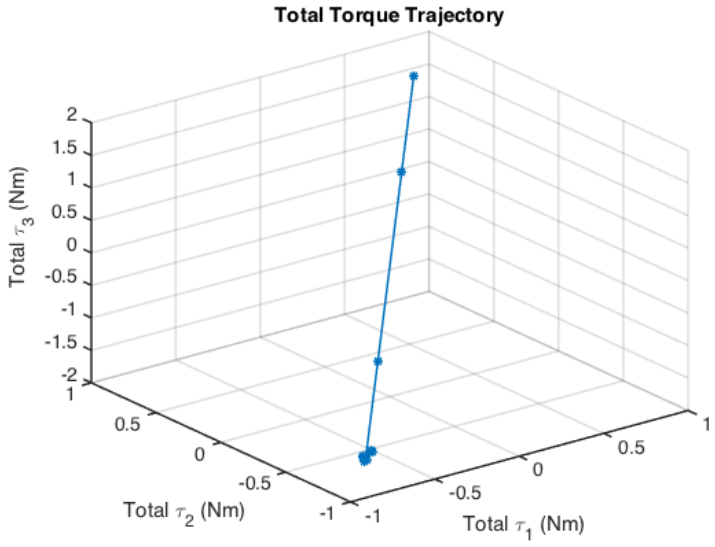

Figure 100. Spatial plot of total torque trajectory of a maneuver with a zero-net bias system

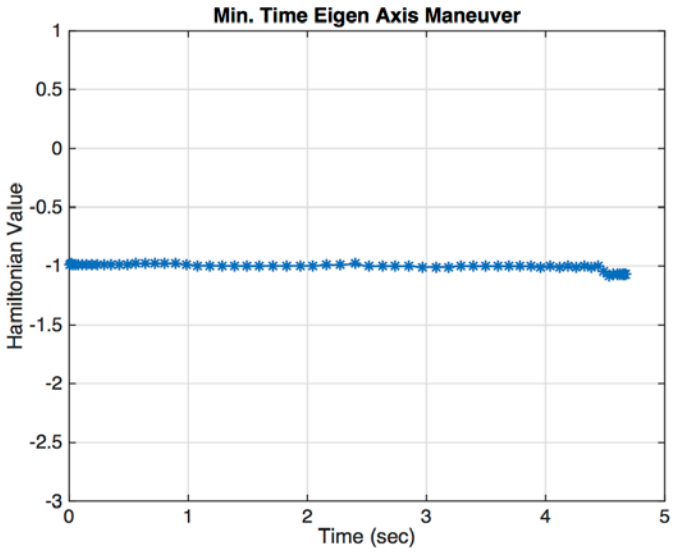

Figure 101. Hamiltonian trajectory of a maneuver with a zero-net bias system

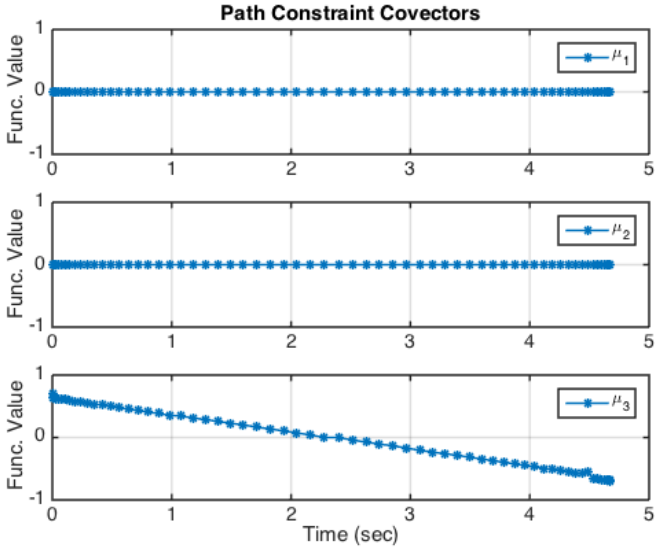

Figure 102. Switching structures of a maneuver with a zero-net bias system

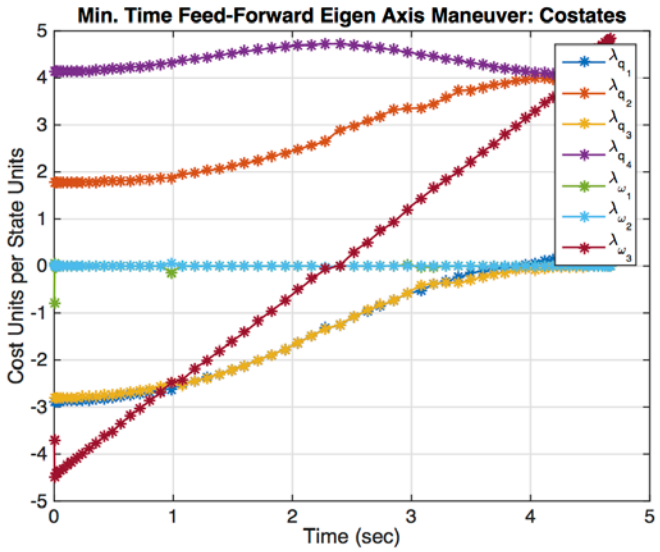

Figure 103. Costate trajectories of a maneuver with a zero-net bias system

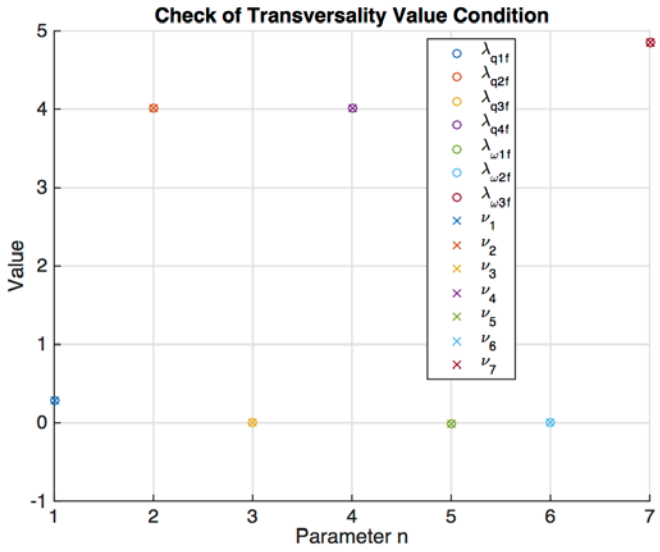

Figure 104. Transversality condition satisfaction of a maneuver with a zero-net bias system

The results of the numerical solution confirm that in a zero-net bias control system, the optimal total torque trajectory follows a more traditional bang-bang pattern. The total torque is aligned along $\hat{\nu}$ throughout the maneuver, due to the absence of the gyroscopic torque. The control torque is modulated to compliment

the quaternion error feedback torque to produce the bang-bang control. At 4.67 seconds, the optimal maneuver time is just slightly faster than the optimal maneuver time for a system gyroscopic torque, reflecting a real cost of the gyroscopic torque on system performance.

I. RTOC CONTROLLER FOR ZERO-NET BIAS CONTROLLER SYSTEMS WITH QUATERNION ERROR FEEDBACK

The flawed RTOC control algorithm can be modified to be effective for systems with zero-net bias control systems. But, before making the adjustments indicated by the preceding optimal control analysis, one last complication will be introduced. Although not explicitly stated, the previous method for calculating the magnitude of torque in the $\hat{\nu}$ direction is predicated on the assumption that the quaternion error feedback torque is also in the $\hat{\nu}$ direction [see equation (1.133)]. For maneuvers that start with the system at rest, or with an initial velocity that is already parallel to the eigenaxis, this will be true; but, if the initial velocity is not in the eigenaxis direction, the velocity error portion of the feedback torque will not be in the $\hat{\nu}$ direction. In such a case, the previous method for computing feed-forward control torque produces undesirable results.

1. New RTOC Algorithm

A new method for computing the feedback torque is now developed. This new method reflects the simpler bang-bang control necessary for zero-net bias systems and includes a remedy for the complication of off-axis velocity.

First, the off-axis quaternion error feedback torque must be mathematically defined. The component of quaternion error feedback torque due to velocity error[3] can be written as

$$\vec{\tau}_{\omega} = cJ\left(\vec{\omega}_{cmd} - \vec{\omega}\right) \tag{1.145}$$

[3] Up to this point, some liberty has been taken with the definition of the quaternion error feedback torque in that the commanded velocity, $\vec{\omega}_{cmd}$, has been omitted; this treatment is also employed by Wie [7]. However, a more complete definition should include $\vec{\omega}_{cmd}$ allowing for the possibility that a non-zero velocity state is desired.

As with any vector, $\vec{\tau}_{\omega}$ can also be written as the sum of the component aligned with $\hat{\boldsymbol{v}}$ and the component not aligned with $\hat{\boldsymbol{v}}$.

$$\vec{\tau}_{\omega} = \left(\vec{\tau}_{\omega} \bullet \hat{v}\right)\hat{v} + \vec{\phi} \tag{1.146}$$

where $\vec{\phi} = \left(\vec{\tau}_{\omega} - \left(\vec{\tau}_{\omega} \bullet \hat{v}\right)\hat{v}\right)$ is the component of quaternion error feedback torque that is not aligned in the $\hat{\boldsymbol{v}}$ direction.

The off-axis feedback torque is necessary to zero out motion that is not in the eigenaxis direction, but, unlike the gyroscopic torque, it is not critical to the maneuver that it be produced precisely as defined by the quaternion error feedback equation. In other words, the counter-gyroscopic torque must be exactly equal in magnitude and opposite in direction to the gyroscopic torque to satisfy an eigenaxis constraint; in contrast, the direction of the off-axis feedback torque must be accurate, but the magnitude need not be exact. This fact enables a simpler approach to computing the feed-forward torque than is necessary in the systems with gyroscopic torque. In this algorithm, the total torque will be calculated based on the sum of $\vec{\tau}_{\hat{v}-\max}$, the maximum torque in the $\hat{\boldsymbol{v}}$ direction allowed by the torque envelope, and $\vec{\phi}$, the off-axis feedback torque. This vector sum must also be scaled to ensure that it does not exceed the torque envelope. This algorithm is presented in (1.147), where $\boldsymbol{\tau_{max}}$ is the scalar limit of the torque envelope (1.55 Nm in these examples) and $\vec{\tau}_{QEF}$ is the full quaternion error feedback torque.

$$a = \frac{\tau_{\max}}{\max\left(\left|\vec{\phi} + S \cdot \vec{\tau}_{\hat{v}-\max}\right|\right)}$$

$$\vec{\tau}_{tot} = a\left(\vec{\phi} + S \cdot \vec{\tau}_{\hat{v}-\max}\right) \tag{1.147}$$

$$\vec{\tau}_{FF} = \vec{\tau}_{tot} - \vec{\tau}_{QEF}$$

As with the one-dimensional RTOC controller, the variable S is used as a sign variable to ensure that the total torque is directed commensurately with the given phase of the maneuver (i.e., accelerating or decelerating).

With the minor change of equation (1.147) incorporated into the RTOC controller, it is now ready for testing. All other steps for computing the control torque previously described are still applicable.

2. RTOC Controller in Closed-Loop Zero-Net Bias System, Example 1: Rest-to-Rest Maneuver

Figures 105–108 contain plots of the results of the RTOC controller in a zero-net bias system performing the same rest-to-rest maneuver that the previous discussions have addressed.

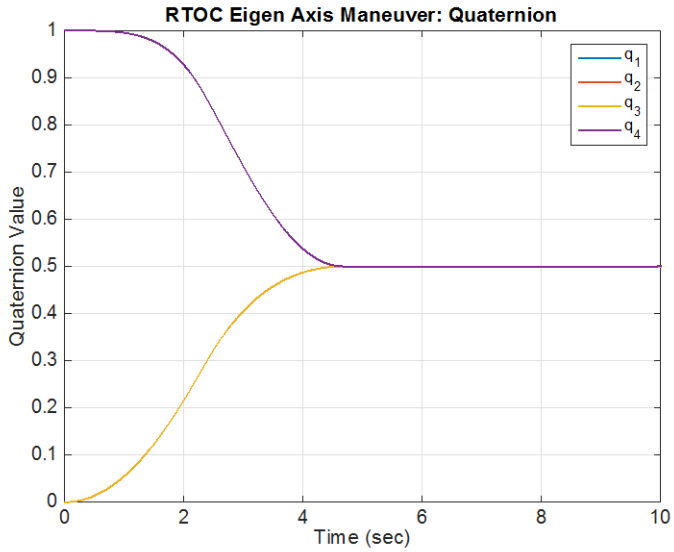

Figure 105. Quaternion trajectory of closed-loop RTOC controller in zero-net bias system

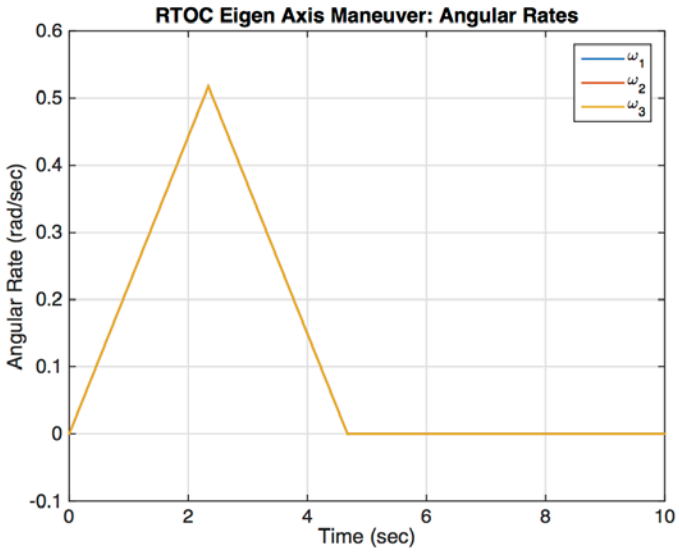

Figure 106. Angular rate trajectories of closed-loop RTOC controller in zero-net bias system

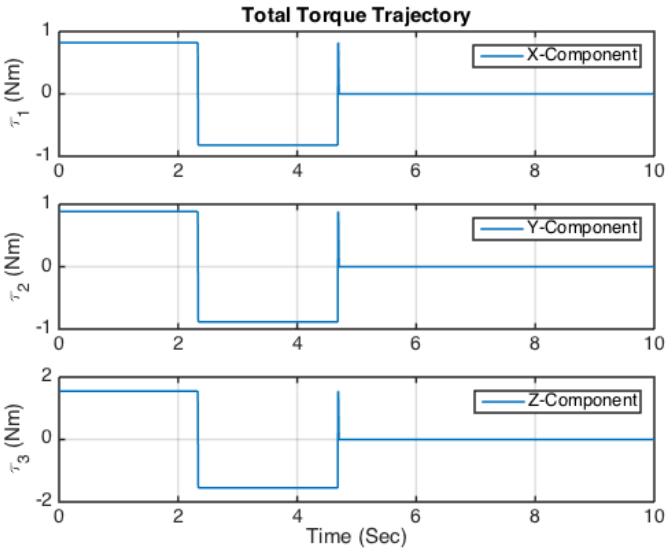

Figure 107. Total torque trajectory of closed-loop RTOC controller in zero-net bias system

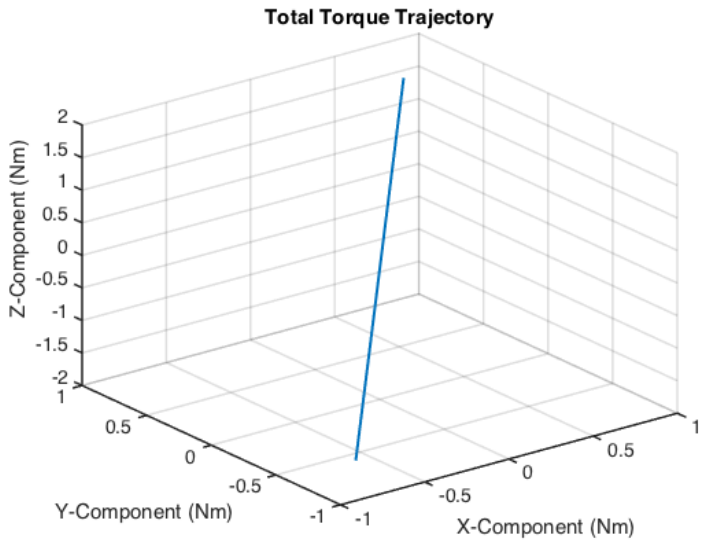

Figure 108. Spatial plot of total torque trajectory of closed-loop RTOC controller in zero-net bias system

The results plotted in Figures 105–108 indicate that the RTOC controller is effective in a zero-net bias control system. The state trajectories plotted in Figures 105 and 106 follow the expected patterns, without the overshoot observed in the previous RTOC results (discussed in section G). The maneuver is completed in 4.70 seconds, on par with the numerical solution of 4.67 seconds. The total torque is maximized, touching the boundary of the torque envelope, throughout the maneuver. Similar to the one-dimensional RTOC simulations, this simulation suffers from the numerical accumulation of error common in fixed step differential equation propagators; this is the cause for the brief torque application at the very end of the maneuver most notable in Figure 107.

3. RTOC Controller in Closed-Loop Zero-Net Bias System, Example 2: Off-Axis Initial Velocity

Figures 109—112 illustrate the performance of the RTOC controller when the initial velocity not aligned with the eigenaxis.

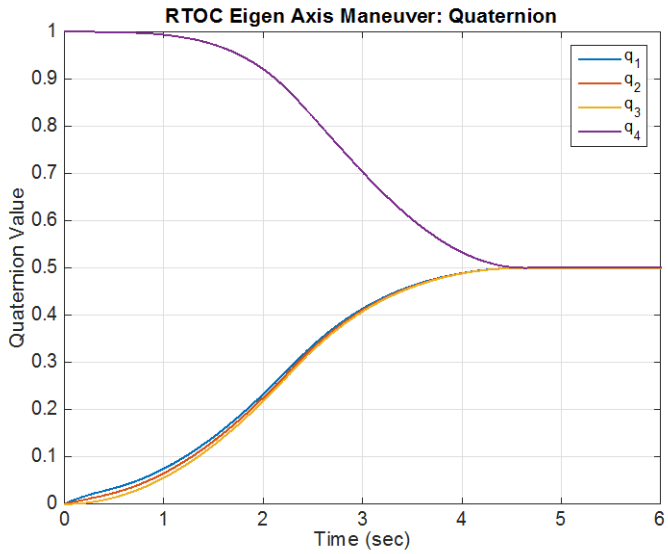

Figure 109. Quaternion trajectory of RTOC controller with zero-net bias system and off-axis initial velocity

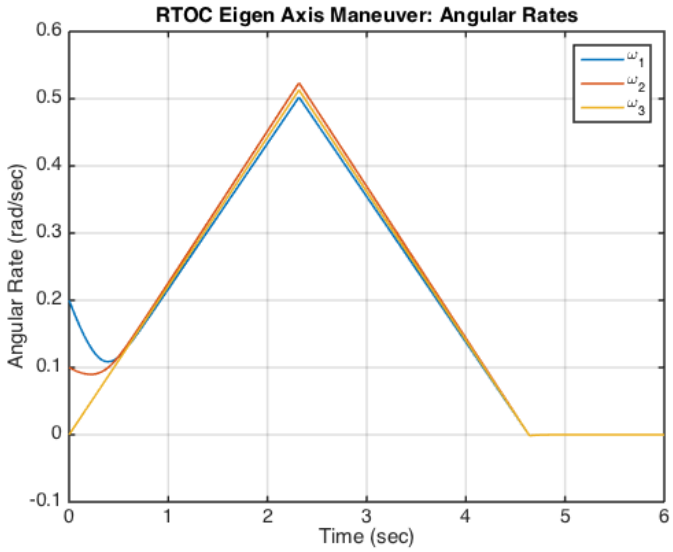

Figure 110. Angular rate trajectories of RTOC controller with zero-net bias system and off-axis initial velocity

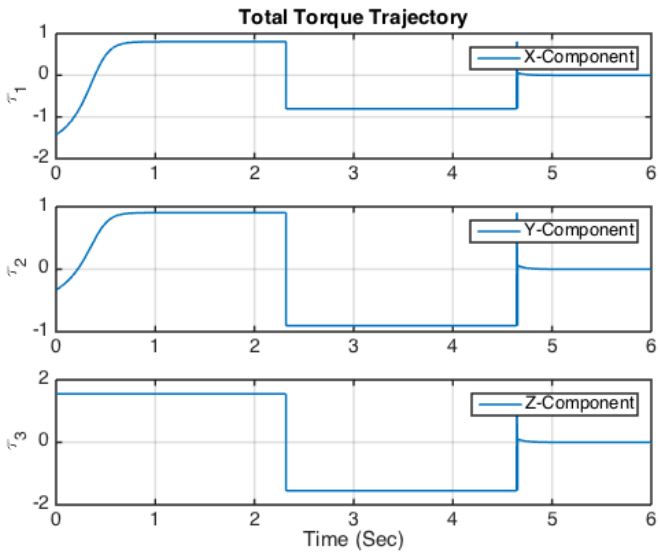

Figure 111. Total torque trajectory of RTOC controller with zero-net bias system and off-axis initial velocity

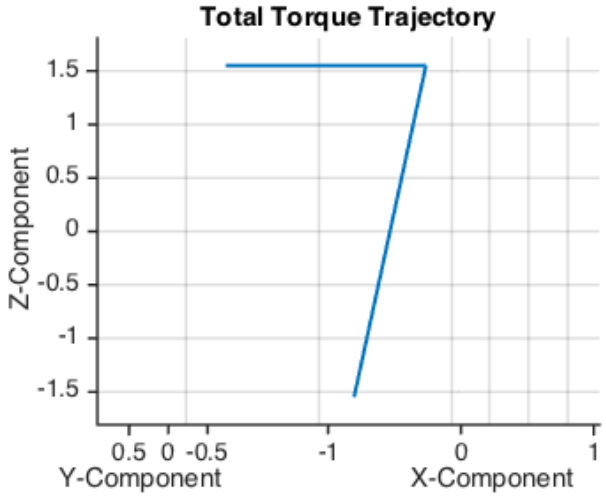

Figure 112. Spatial plot of total torque of RTOC controller with zero-net bias system and off-axis initial velocity

The results plotted in Figures 109–112 demonstrate that the RTOC controller can compensate for off-axis angular velocity and still produce a maneuver very closely resembling an optimal eigenaxis maneuver. The streak of

total torque trajectory across the top of the spatial total torque plot, Figure 112, correlates to the portion of the maneuver with off-axis velocity. (Illustrating this effect is the purpose of the peculiar point of view chosen in Figure 112.) But, within 0.5 seconds, the off-axis velocity has largely been zeroed out, and the maneuver resumes a more typical bang-bang control sequence. After the elimination of off-axis velocity, the state trajectories plotted in Figures 109 and 110 follow the expected trajectory for a bang-bang maneuver. Moreover, Figures 111 and 112 indicate that the total torque does follow the prescribed bang-bang profile. Thus, the RTOC controller can accommodate some off-eigenaxis velocity. This aspect can be useful when switching direction of motion without stopping, as in a dog-leg maneuver

J. SUMMARY

The results presented in this chapter show that it is possible to translate the real-time optimal control methods developed for one-dimensional rotational maneuvers to three-dimensional eigenaxis maneuvers for zero-net biased control systems using a closed-loop feed-forward control architecture. The underlying principles that govern the one-dimensional RTOC controller are applied in the eigenaxis controller, specifically that the optimal control torque signal is updated based on feedback from the system states. However, these control torque updates are accomplished differently in the eigenaxis RTOC controller than in the one-dimensional RTOC controller. Because the dynamics of three-dimensional rotations are non-linear, the control torque is updated by sampling the current system states and numerically predicting the future states in order to predict the feedback torque rather than developing an analytical solution for control torque. Knowledge of the optimal total torque profile, which is also updated based on system response feedback, enables prediction of future states simply by numerically propagating the system dynamics. The control torque is modulated in response to the predicted feedback torque to produce the optimal total torque application at the plant.

There is no fundamental reason that the same methodology could not be applied to control systems that do not have zero-net bias. However, the key ingredient is knowledge of the optimal total torque profile throughout the maneuver, and the simple bang-bang torque profile algorithm employed in the one-dimensional RTOC controller and the eigenaxis RTOC controller for zero-net bias systems may not be accurate in systems with significant gyroscopic torque, unless an appropriate margin is retained to null the effect.

THIS PAGE INTENTIONALLY LEFT BLANK

VII. CONCLUSIONS

The primary goal of this thesis was to address optimal control implementation in the presence of feedback loops for the double integrator problem. The most effective implementation was determined to be through a feed-forward signal that is modulated in response to the feedback signal produced by the underlying, pre-existing, feedback system. When combined with the PD controller, a feed-forward control torque to produce a total torque that follows the expected “bang-bang” optimal torque trajectory can be computed analytically. In the case of three-dimensional eigenaxis rotations, the feed-forward torque is produced through the direct measurement or prediction of the quaternion error feedback.

The employment of a numerical solution and lack of an analytical solution for the eigenaxis maneuver may seem to be inferior to the one-dimensional solution, but it is in fact a more powerful approach and illustrates the broader application of this methodology. Many systems involve non-linear dynamics which cannot be solved analytically. However, the results of this thesis have demonstrated that in spite of those nonlinearities, there are multiple paths to producing an optimal total control trajectory in the presence of typically ignored feedback signals. The developed approach allows adjustment through the course of the maneuver to compensate for unanticipated control action. The examples examined in this thesis introduced unanticipated control action through the introduction of rotational inertia error which caused unexpected state changes. In this scenario, the optimal total torque trajectory was recalculated to improve maneuver performance; the control torque signal was adjusted in real time based on the feedback signals to conform to the correct (but unanticipated) optimal total torque trajectory.

An alternative example would be a minimum time optimal maneuver of a CMG actuated spacecraft using feed-forward CMG gimbal angles as the control. Such an architecture would be very similar to those considered in this thesis with

the addition of a CMG steering law that translates torque commands to CMG gimbal commands; the feed-forward control signal, rather than being a torque command, would be gimbal rate commands that when combined with the steering law's feedback gimbal commands achieve the desired overall gimbal trajectory. The designer could develop an optimal trajectory for the CMG gimbals to achieve the minimum time maneuver. But due to the underlying mathematics of most CMG steering laws, small uncertainties can produce large, unanticipated feedback gimbal angles, particularly as the gimbals approach singular states. If the closed-loop optimal control implementation approach developed in this paper were employed, the feed-forward gimbal angle trajectory could be adjusted in real time, allowing the control system to follow the optimal gimbal angle trajectories in spite of the unanticipated feedback gimbal commands. Such an implementation is a straightforward extension of the concepts herein and is recommended for future work.

This thesis also proposes two RTOC controllers, one for one-dimensional rotations and another for three-dimensional eigenaxis maneuvers for use with systems under zero-net bias. These controllers demonstrate the ability to adjust the duration and sequence of bang-bang total torque trajectory in response to system errors and uncertainties. They demonstrate improved performance over preconceived, static optimal control torque solutions, both in terms of maneuver time as well as compliance with torque limits. The additional computational burden is minor and is well within the capability of modern space systems.

APPENDIX A. MINIMUM EFFORT SOLUTIONS

In this appendix, the two basic control architectures of Chapter 2, the state guidance and feed-forward, are evaluated to minimize the control effort necessary to accomplish the same rest-to-rest maneuver. Because the amount of control effort required in any control configuration varies based on the amount of time allowed for the maneuver, the minimum effort maneuvers are required to be completed in one second. Additionally, control effort will be defined using the traditional quadratic cost, the integration of squared applied torque over time; this is mathematically defined in the cost function in equation (1.148). This definition of control effort does not equate to the traditional definitions of work, power or energy. Therefore, its units will be referred to as “units of effort.”

A. MINIMUM EFFORT GUIDED CONTROL

The problem formulation for the minimum effort control problem in the state-guided control architecture presented in equation (1.148), and the problem statement is as follows:

> Problem Statement—Minimum Effort w/ State Guidance: Perform a minimum effort rotation of a rigid body with a pre-existing PD controller using state guidance as the control. The initial system state will be in a position of zero radians at zero velocity, and the final state will be at a position of one radian and zero velocity. See Figure 6 for control system diagram.

$$\underline{\text{States:}} \qquad \vec{x} = \begin{bmatrix} \theta \\ \omega \\ \theta_{cmd} \end{bmatrix} \qquad\qquad \underline{\text{Controls:}} \;\; \vec{u} = \begin{bmatrix} \omega_{cmd} \end{bmatrix}$$

$$\underline{\text{minimize:}} \qquad J\left[\vec{x}(\bullet), \vec{u}(\bullet), t_f\right] = \int_{t_0}^{t_f} \frac{1}{2} \tau_{tot}^2 \, dt$$

$$= \int_{t_0}^{t_f} \frac{1}{2} \left[k_p \theta_{cmd} - k_p \theta + k_v \omega_{cmd} - k_v \omega \right]^2 dt$$

$$\underline{\text{subject to:}} \qquad \dot{\theta} = \omega \tag{1.148}$$

$$\dot{\omega} = \frac{1}{J_e} \left[k_p \theta_{cmd} - k_p \theta + k_v \omega_{cmd} - k_v \omega \right]$$

$$\dot{\theta}_{cmd} = \omega_{cmd}$$

$$t_0 = 0$$

$$t_f = 1 \text{ sec}$$

$$\vec{x}_0^T = \left[0, 0, 0\right]^T$$

$$\vec{x}_f^T = \left[1, 0, 1\right]^T$$

This problem formulation differs from the previous formulations in several important ways. First, the final time is definitively set to 1 sec; second, the cost function is significantly different. Another difference is that no path constraints are placed on the problem. The same system is being optimized and it is still only capable of producing $\pm 60 \; Nm$ of torque. But as a minimum effort problem, this is unlikely to be a limiting factor. If the solution did attempt greater amounts of torque, then a problem formulation with the torque constraints included would be analyzed.

Without the path constraints, the HMC simplifies to that described in equation (1.15). Evaluating the HMC yields the following:

$$\omega_{cmd} = \frac{1}{k_v} \left(k_p \theta + k_v \omega - k_p \theta_{cmd} - \frac{\lambda_\omega}{J_e} - \frac{\lambda_{\theta_{cmd}}}{k_v} \right) \tag{1.149}$$

Rather than providing a switching function, the Hamiltonian minimization condition in the minimum effort problem yields an expression solvable for the optimal control variable trajectory, ω_{cmd}. This and the transversality condition, which follows the same pattern as the previous problems, are the most significant conditions and will be evaluated with the solution results, which are presented in Figures 113–116.

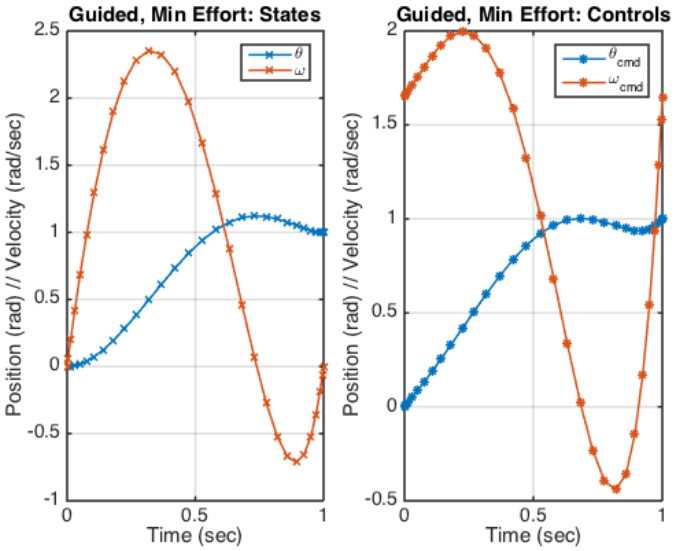

Figure 113. State and control trajectories in minimum effort optimization of state-guided architecture

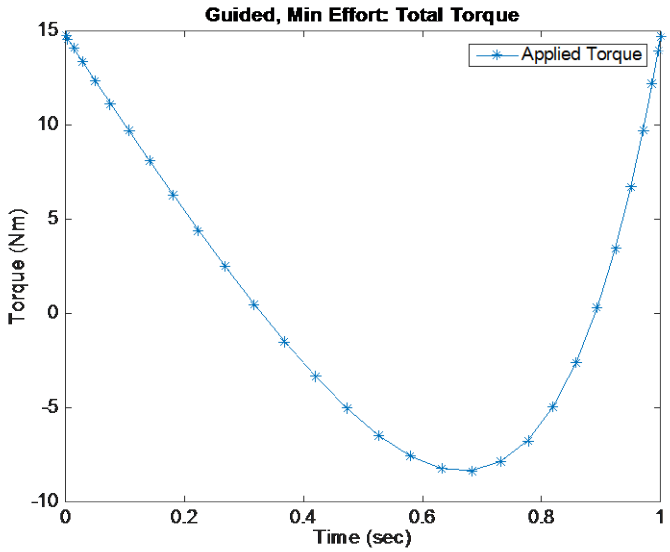

Figure 114. Total torque trajectory in minimum effort optimization of state-guided architecture

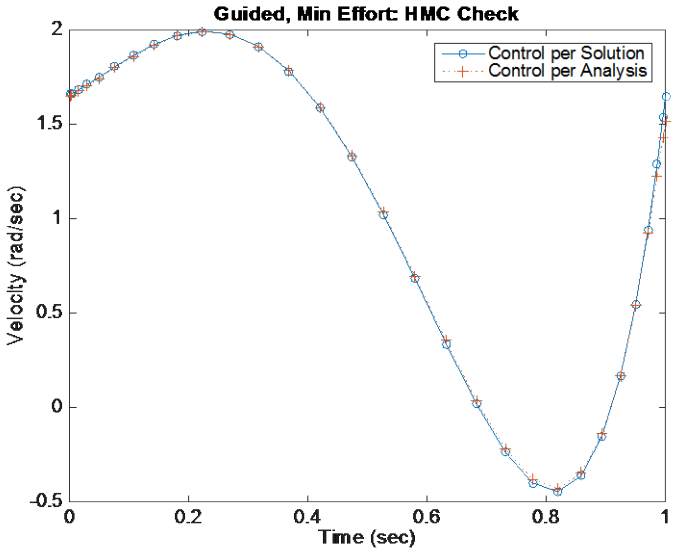

Figure 115. Control trajectory in minimum effort optimization of state-guided architecture

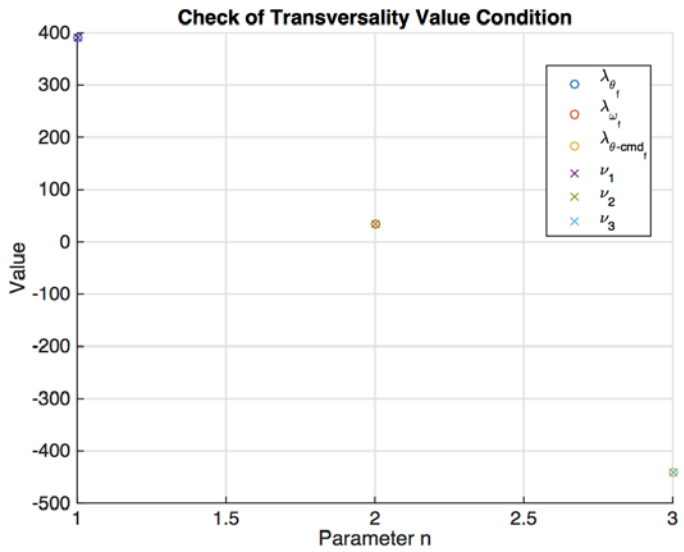

Figure 116. Transversality condition in minimum effort optimization of state-guided architecture

Figure 115 contains a plot of both control trajectory offered in the DIDO solution as well as the control trajectory based on the preceding analysis (1.149) of the Hamiltonian minimization condition. In other words, Figure 115 contains both the DIDO control trajectory and a control trajectory reconstructed with the values of each of the states and costates that comprise the formula for the optimal control found in equation (1.149). The fact that the two plots are consistent corroborates the optimality of the DIDO solution. Satisfaction of the transversality condition, shown in Figure 116, provides further confidence that this solution is optimal.

This maneuver required 25.0 units of effort; that is dramatically lower than the cost of the baseline system with PD control, which requires 48.5 units of effort. The reduction in energy has, however, come at the cost of an increased transfer time.

B. MINIMUM EFFORT FEED-FORWARD CONTROL

The problem formulation for the minimum effort control problem in the feed-forward control architecture presented in equation (1.150) and the problem statement is as follows:

> Problem Statement—Min. Effort w/ Feed-Forward Control: Perform a minimum effort rotation of a rigid body with a pre-existing PD controller using feed-forward torque control. The initial system state will be in a position of zero radians at zero velocity, and the final state will be at a position of one radian and zero velocity. See Figure 12 for control system diagram.

$$
\begin{aligned}
&\underline{\text{States}}: && \vec{x} = \begin{bmatrix} \theta \\ \omega \end{bmatrix} && \underline{\text{Controls}}: \ \vec{u} = [\tau] \\
&\underline{\text{minimize}}: && J\left[\vec{x}(\bullet), \vec{u}(\bullet), t_f\right] = \int_{t_0}^{t_f} \frac{1}{2} \tau_{tot}^2 \, dt \\
& && \quad = \int_{t_0}^{t_f} \frac{1}{2} \left[\tau + k_p \theta_{cmd} - k_p \theta - k_v \omega\right]^2 dt \\
&\underline{\text{subject to}}: && \dot{\theta} = \omega \\
& && \dot{\omega} = \frac{1}{J_e}\left[\tau + k_p \theta_{cmd} - k_p \theta - k_v \omega\right] \\
& && t_0 = 0 \\
& && t_f = 1 \ \text{sec} \\
& && \vec{x}_0^T = [0,0]^T \\
& && \vec{x}_f^T = [1,0]^T
\end{aligned}
\tag{1.150}
$$

Analyis of this problem formulation follows a similar pattern as the previous minimum effort problem. Like the problem in section A, this formulation also neglects the total torque constraint. Analysis of the HMC yields the following:

$$\tau = -k_p \theta_{cmd} + k_p \theta + k_v \omega - \frac{\lambda_\omega}{J_e} \tag{1.151}$$

Again, the HMC yields a formula for the optimal trajectory of the control variable. The solution results are presented in the Figures 117–120.

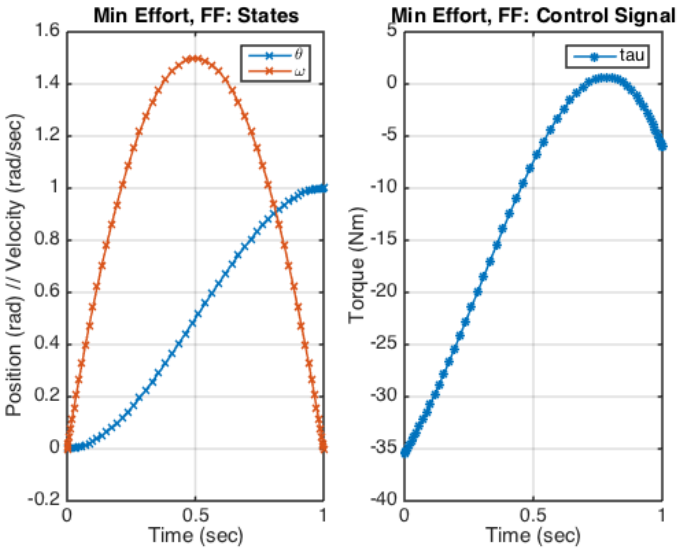

Figure 117. State and control trajectories in minimum effort optimization of feed-forward architecture

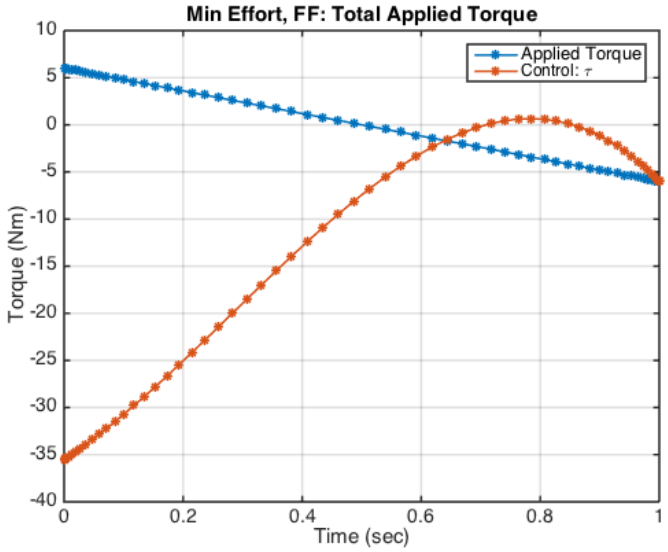

Figure 118. Control torque and total torque trajectories in minimum effort optimization of feed-forward architecture

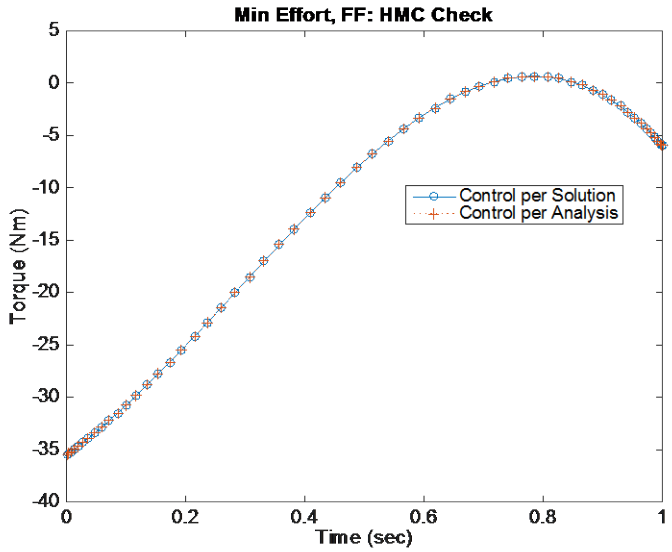

Figure 119. Control trajectory in minimum effort optimization of feed-forward architecture

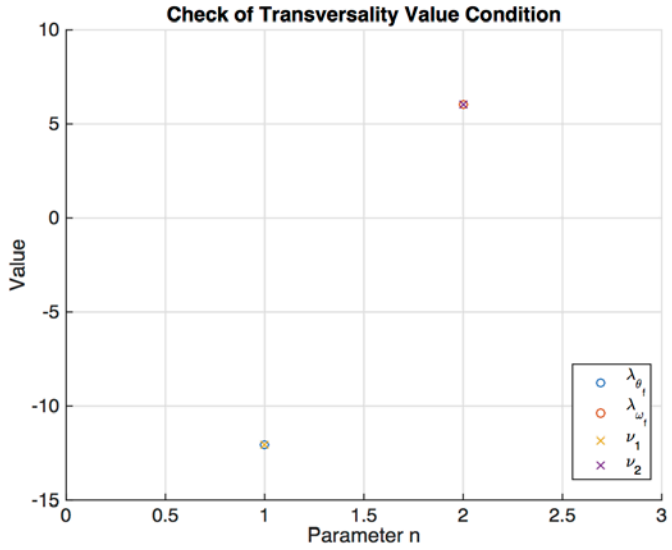

Figure 120. Transversality condition in minimum effort optimization of feed-forward architecture

Figure 119 contains a plot of the control torque contained in the DIDO solution as well as the reconstructed control torque trajectory based on the analysis of the Hamiltonian minimization condition (1.151). The two plots align

perfectly indicating that the HMC has been satisfied in this solution. These results are also noteworthy in that the trajectory of total applied torque is the same solution to the open-loop minimum effort maneuver, which follows the same characteristic as the minimum time solution for the feed-forward control architecture, namely that in the later case a bang-bang solution was recovered using the feed-forward control architecture.

The total “effort” required for this maneuver with the feed-forward architecture is 8.1 units of effort, which is lower than the optimal solution for the guided-control architecture and much lower than the baseline system with PD control.

C. SUMMARY

A comparison of the minimum effort optimization of a feed-forward control architecture and the state-guided architecture indicates that the feed-forward architecture is superior. That control architecture is able to complete a one radian rotation with less than one third of the control effort required in a state-guided architecture.

THIS PAGE INTENTIONALLY LEFT BLANK

APPENDIX B. IMPACTS OF INERTIA UNCERTAINTY

The plots contained in this appendix are combination scatter-histogram plots presenting the data of numerous (10,000) simulations each illustrating the impact of inertia uncertainty on the control architectures studied in Chapter 2. The central plot is a scatter plot of settling time or control effort (depending on the plot) versus the actual inertia for each simulation, and the bars along the x and y axes are histograms depicting the relative number of occurrences of each data point. The data contained in this analyzed and discussed in Chapter 4.

A. BASELINE SYSTEM (CLASSICAL CONTROLS)

Figure 121 depicts the variation of settling time in response to variations in the actual system inertia of the baseline system with a standard PD controller with a step input command. The settling time of the nominal system is 0.93 seconds. Figure 122 illustrates the impact of inertia uncertainty on the control effort required in a system with the baseline PD controller and no optimization. The nominal control effort is 48.5 units of effort.

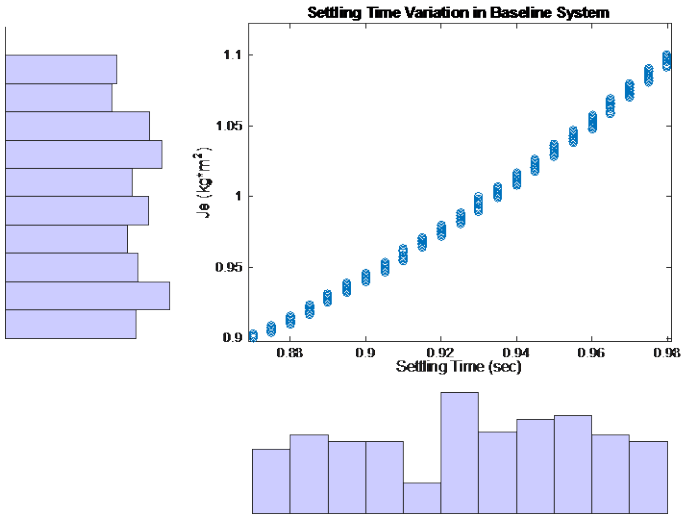

Figure 121. Impact of uncertainty on settling time in baseline system

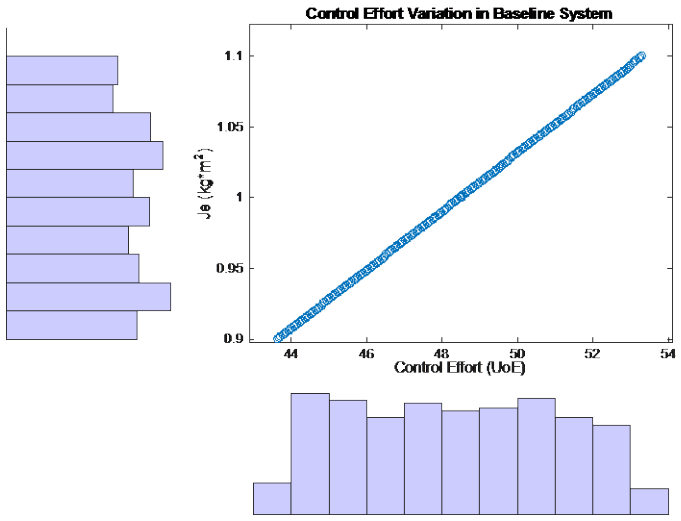

Figure 122. Impact of uncertainty on control effort in baseline system

B. GUIDED OPTIMAL CONTROL ARCHITECTURE

The settling time of the nominal system using optimal state-guidance is 0.47 seconds and requires 808.5 units of effort.

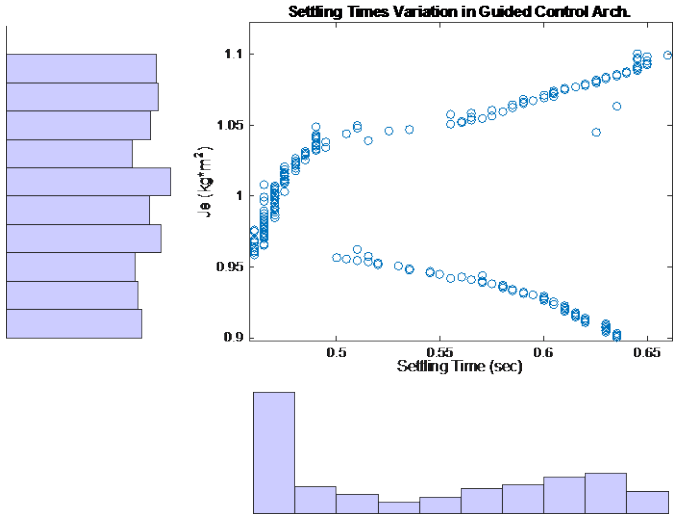

Figure 123. Impact of uncertainty on optimal state-guided architecture

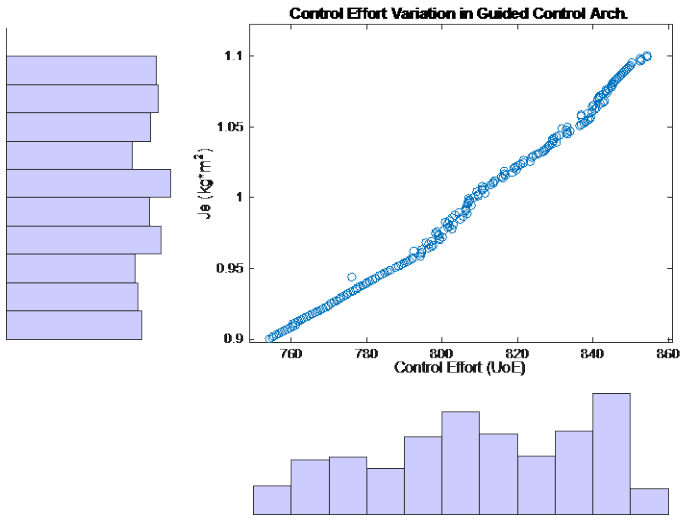

Figure 124. Impact of uncertainty on optimal state-guided architecture

C. FEED-FORWARD OPTIMAL CONTROL ARCHITECTURE

The settling time of the optimal feed-forward control with nominal inertia is 0.23 sec and requires 420.5 units of effort.

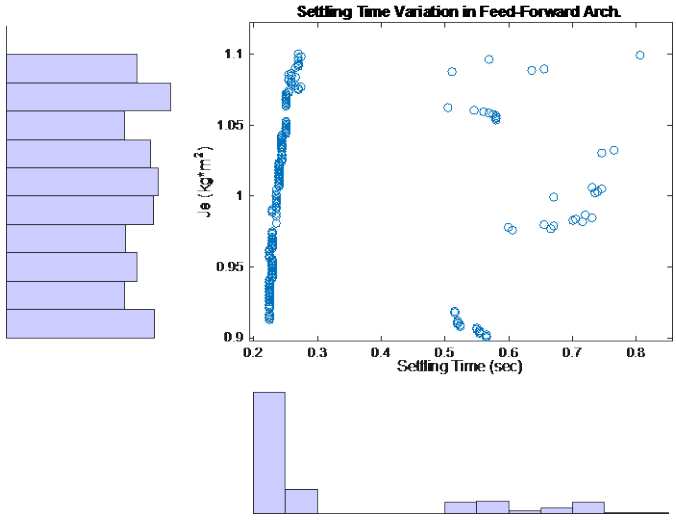

Figure 125. Impact of uncertainty on optimal feed-forward architecture

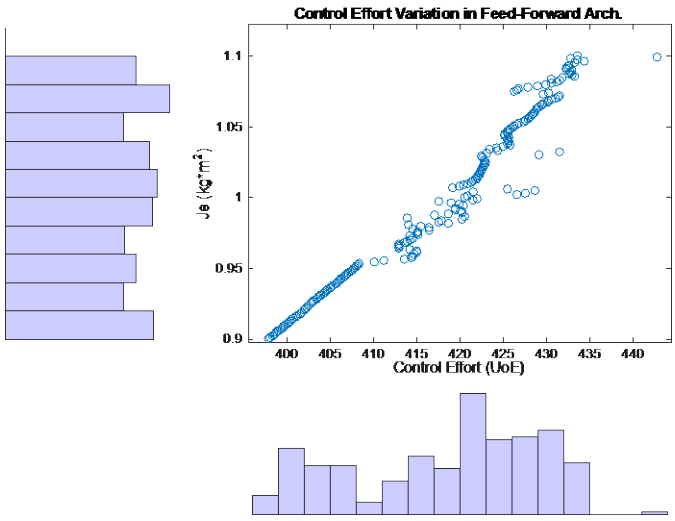

Figure 126. Impact of uncertainty on optimal feed-forward architecture

D. ACCELERATION FEED-FORWARD OPTIMAL CONTROL ARCHITECTURE

The settling time of the nominal acceleration feed-forward optimal control system is 0.23 sec and requires 450.7 units of effort.

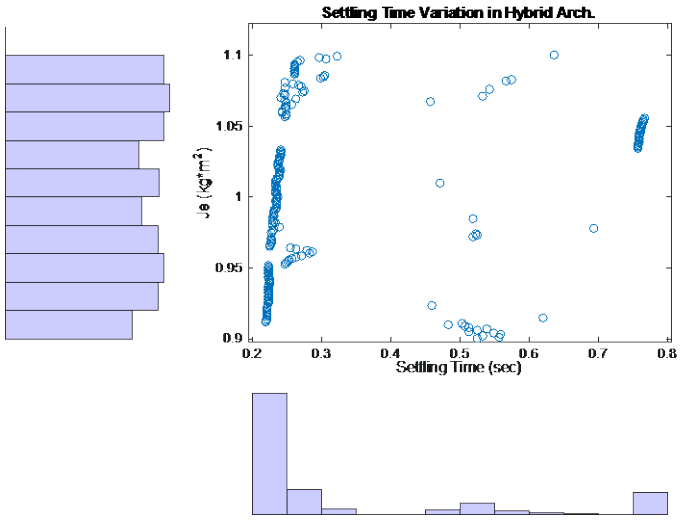

Figure 127. Impact of uncertainty on optimal acceleration feed-forward architecture

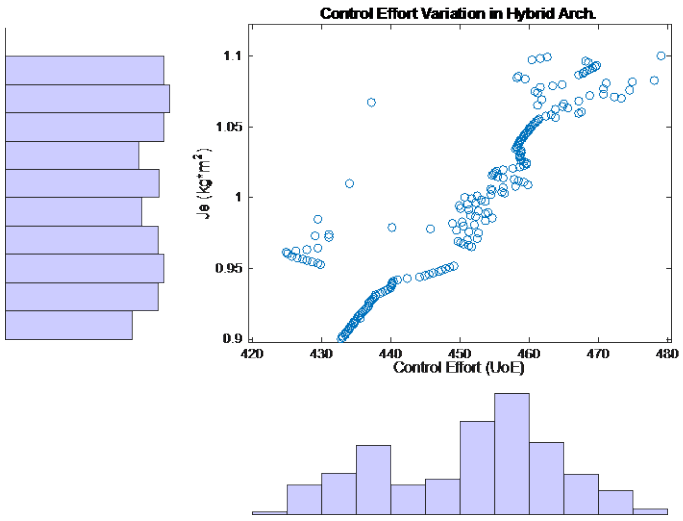

Figure 128. Impact of uncertainty on optimal acceleration feed-forward architecture

E. HIGH-BANDWIDTH GUIDED CONTROL ARCHITECTURE

The settling time of the nominal system with high-bandwidth state-guided control is 0.231 sec and requires 480.1 units of effort.

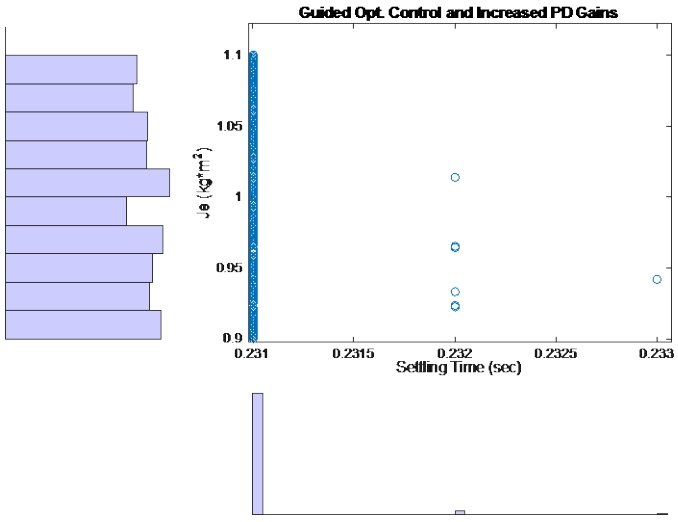

Figure 129. Impact of uncertainty on high-bandwidth state-guided architecture

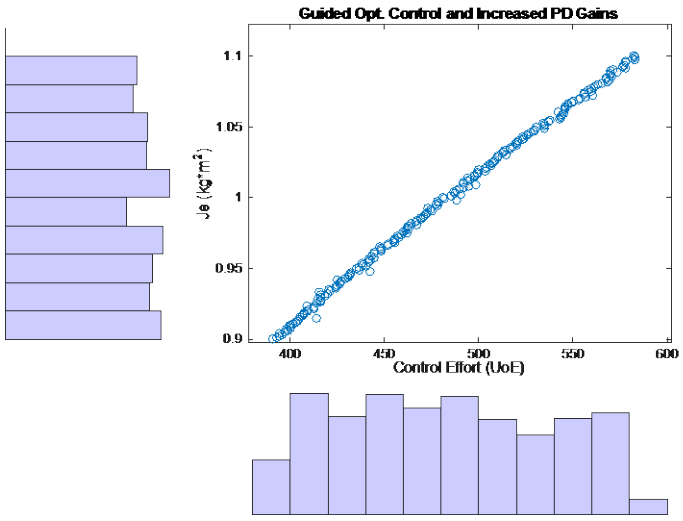

Figure 130. Impact of uncertainty on high-bandwidth state guided architecture

F. FEED-FORWARD ARCHITECTURE WITH INCREASED PD GAINS

The settling time of the nominal system with a high-bandwidth feed-forward control architecture is 0.231 seconds and requires 456.1 units of effort.

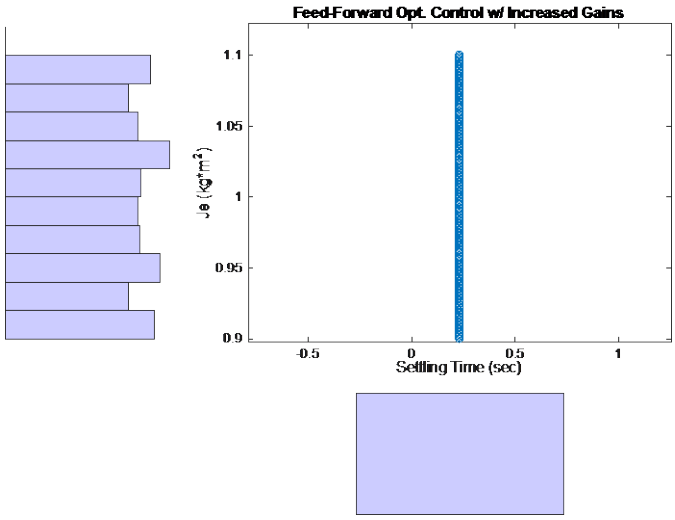

Figure 131. Impact of uncertainty on high-bandwidth feed-forward architecture

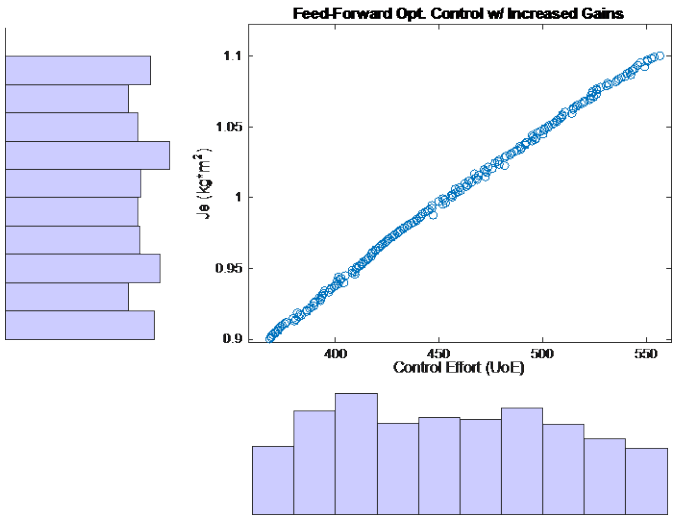

Figure 132. Impact of uncertainty on high-bandwidth feed-forward architecture

G. ACCELERATION GUIDED OPTIMAL CONTROL WITH INCREASED PD GAINS

The nominal system with high control bandwidth and acceleration guided control has a settling time of 0.231 seconds and requires 472.8 units of effort.

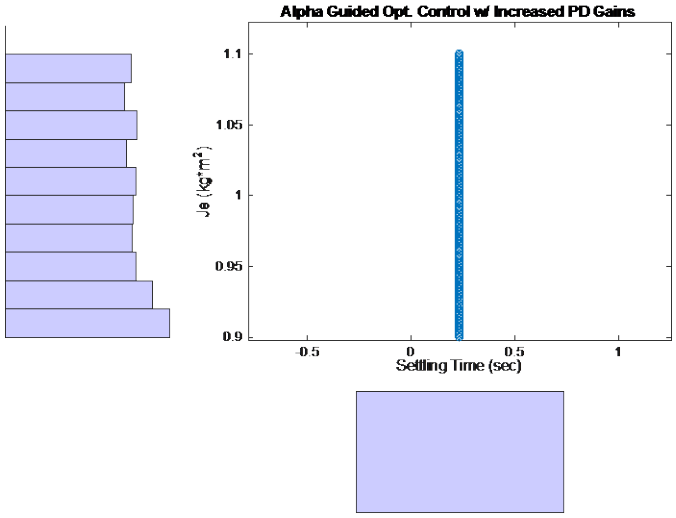

Figure 133. Acceleration Guidance: Settling Time Variation

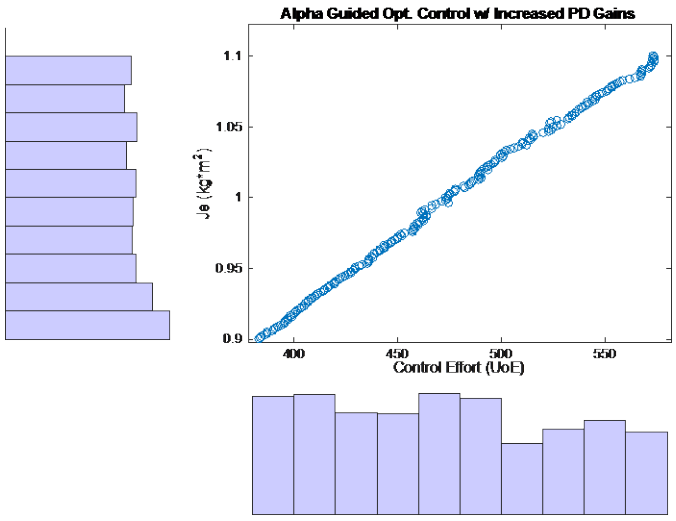

Figure 134. Acceleration Guidance: Control Effort Variation

LIST OF REFERENCES

[1] C. T. Chen, *Analog and Digital Control System Design: Transfer-Function, State-Space, and Algebraic Methods*. New York: Saunders College Publishing, 1993.

[2] I. M. Ross, *A Primer on Pontryagin's Principle in Optimal Control*, 2nd ed. San Francisco, CA: Collegiate Publishers, 2015.

[3] I. M. Ross and M. Karpenko, "A review of pseudospectral optimal control: From theory to flight," *Annual Reviews in Control*, vol. 36, no. 2, pp 182–197, Dec. 2012.

[4] Elissar-Global (2015). DIDO, version 7.5.0. [Online.] Available: http://www.elissarglobal.com/. Accessed Apr. 10, 2016.

[5] M. Athans and P. L. Falb, *Optimal Control: An Introduction to the Theory and Its Applications.* New York: McGraw-Hill, 1966.

[6] K. D. Bilimoria and B. Wie, "Time-optimal three-axis reorientation of a rigid spacecraft," *Journal of Guidance, Control, and Dynamics,* vol. 16, no. 3, pp. 446–452. May—Jun. 1993

[7] B. Wie, *Space Vehicle Dynamics and Control*, 2nd ed. Reston, VA: American Institute of Aeronautics and Astronautics, Inc., 2008.

[8] M. Karpenko, J. T. King and I. M. Ross, "Agilitoid-based design analysis of next generation attitude control systems," presented at 38th Annual AAS Guidance & Control Conference, January 30 to February, 4, 2015, Breckenridge, CO. Paper number: AAS 15–047

[9] B. C. Fields, S. M. Kocis, K. L. Williams and M. Karpenko, "Hardware-in-the-loop simulator for rapid prototyping of CMG-based attitude control systems," presented at 39th Annual AAS Guidance & Control Conference, February 5 to February 10, 2016, Breckenridge, CO. Paper number: AAS 16–014.

[10] I. M. Ross, P. Sekhavat, A. Fleming, and Q. Gong, "Optimal feedback control: Foundations, examples, and experimental results for a new approach," *Journal of Guidance, Control, and Dynamics*, vol. 31, no. 2, Mar.—Apr. 2008

THIS PAGE INTENTIONALLY LEFT BLANK

INITIAL DISTRIBUTION LIST

1. Defense Technical Information Center
   Ft. Belvoir, Virginia

2. Dudley Knox Library
   Naval Postgraduate School
   Monterey, California